FOREWORD

Since most programs of the Metals and Ceramics Division report progress on a quarterly or semiannual schedule, the need for an annual report has diminished. However, work supported by the Office of Materials Science, Division of Physical Research, is usually published in the open literature. In order to give a view of this program in the Metals and Ceramics Division, an annual report has been prepared. It consists of abstracts of papers published or presented during the year ending June 30, 1977, and summaries of work in progress.

During this reporting period a number of new programs have been started and others phased out in order to reflect the broadened responsibilities of the Division of Physical Research to the Energy Research and Development Administration compared with the Atomic Energy Commission. During this reporting period our effort supported fission (24%), fusion (24%), other nonnuclear technologies (28%), and multidirectional base research (24%).

A special note is made that D. S. Billington's retirement from full-time research coincides with the date of this report. Doug has had an important impact on the materials science community through his research and his service as Director of the Solid State Division. I will particularly miss his advice and services freely given these years as a member of this section.

Following the reports of our technical progress is an appendix listing (1) assignments of our staff in other organizations, (2) guest assignments in our section, (3) staff changes, (4) joint appointments of our staff with the University of Tennessee for the academic year 1976–1977, (5) papers presented at technical meetings, and (6) publications.

C. J. McHargue

CONTENTS

SUMMARY

1. STRUCTURE OF MATERIALS

1.1 Theoretical Research

In the area of surface physics we developed a cluster technique that permits us to treat quite general surface complexes, particularly in the low coverage limit. This approach has been complemented by a new method for calculating the energy band structure of thin film systems. This new approach allows us to treat the high-coverage chemisorption limit for ordered overlayers. Studies with this method elucidated differences in s, p, and d bonding of oxygen on aluminum and copper surfaces. Factors effective in surface molecular bond breaking were studied for O_2 dissociatively chemisorbed on aluminum.

In the area of physics of transition metals and alloys we extended our Korringa-Kohn-Rostocker programs to treat hexagonal close-packed systems and applied these programs to a study of the Fermi surface of technetium. In collaboration with members of the theory group at the University of Bristol, England, we also developed methods that allow solution of the coherent potential approximation equations for a muffin-tin potential model of substitutional alloys. We performed calculations on the binary systems Cu-Ni and Nb-Mo for various alloy compositions.

In collaboration with an experimental group at the University of Birmingham, England, we measured angle-resolved photoemission spectra from a (100) surface of a single crystal Cu-23 at. % Ni alloy and have interpreted the results in terms of our calculations on this system. We have also been able to interpret results of soft x-ray emission experiments on a number of Cu-Ni alloys.

We calculated the electron-phonon coupling parameter, which determines the superconducting transition temperature, for the entire 4d transition metal series. The agreement with experiment is quite good, and the results are amenable to a simple interpretation. We have also calculated the phonon linewidth due to electron-phonon coupling in niobium. The calculations show strong coupling arising from longitudinal phonons in the [110] direction. This strong coupling was subsequently verified experimentally by inelastic neutron scattering experiments performed at ORNL. Our calculations may necessitate a reassessment of present theories of lattice dynamics for the transition metals and tunneling experiments on niobium.

In the area of defect migration in irradiated materials we have developed a generalized rate theory model of dislocation loop growth and void swelling in metals and alloys under irradiation. This model has been used to interpret some of the results of neutron and charged-particle damage experiments performed at ORNL.

1.2 X-Ray Diffraction Research

An experiment in which inner-shell atomic x-ray spectra were excited by energy-tuned synchrotron radiation was performed in a search for superheavy elements. Though these elements were not found, detectability limits of about 5×10^9 atoms of an element were demonstrated for target particles containing only 10^{15} to 10^{16} other atoms.

Careful diffraction measurements on monoclinic europia crystals grown and maintained in controlled chemical environments have indicated subtle structural changes associated with chemical interactions of the oxide with ambient laboratory atmospheres. In particular, a degradation of symmetry from monoclinic to triclinic was suggested for crystals exposed to water.

The differential equations governing interactions of incident and diffracted x-ray beams in imperfect crystals have, for the first time, been solved without approximations. The solution promises important progress in our understanding of secondary extinction and in our ability to make meaningful corrections for this effect in diffracted intensity data sets.

Applications of small-angle x-ray scattering to structural problems in a wide variety of materials have been extensively broadened and intensively sharpened by the 10-m scattering camera recently constructed in our laboratories. Important results for irradiated metals, coals and pyrocarbons, catalysts, polymers, and biological materials have been demonstrated; these advances suggest new experiments utilizing the unique capabilities of the instrument.

1.3 Fundamental Ceramics Studies

The study of erosion of ceramics has continued, and to date samples of nine different ceramic compositions have been tested. We are analyzing the eroded samples by scanning and transmission electron microscopy. The application of metallurgical techniques to the analysis of coals has continued with the demonstration of a variety of such techniques to analyze coal constituents. Further data have been collected on the mineral contents and porosity of coals. Thermal conductivities of advanced nuclear fuels have been measured. The stability of selected transition metal tellurides was determined by vapor pressure measurements using the Knudsen effusion weight-loss technique.

1.4. Preparation and Synthesis of High-Temperature and Special Service Materials

Calculations to predict the oxygen partial pressure, P_{O_2}, required for equilibrium of the eutectic systems Cr_2O_3-Cr and Cr_2O_3-Mo were extended to predict equilibrium P_{O_2} for off-eutectic compositions and superheated melts. Eutectic-like structures were observed

for the new systems $LaCrO_3$-W, $LaCrO_3$-Mo, $LaCrO_3$-Cr, $YCrO_3$-W, $YCrO_3$-Mo, and $YCrO_3$-Cr. Since heat flow can partially unmix chemical components in a liquid phase (the Soret effect) and large thermal gradients are believed to exist at the solid-liquid interface of metal oxide-metal systems during internal zone growth, the eutectic constitutional supercooling criterion of Mollard and Flemmings was rederived to include thermally induced mass flow. Directional solidification studies have been initiated for the ternary system W-C-Co and a number of other complex metal carbide and metal boride systems. Hydrothermal growth studies of SiO_2 and CdS have continued. Czochralski growth of single-crystal fayalite, Fe_2SiO_4, has been accomplished. The effect of die-top geometry (planer, convex, or concave) on solidification interface shape and eutectic morphology was investigated for the edge-defined, film-fed growth of Mn_2SiO_4-MnO.

1.5 Stabilities of Microphases in High-Temperature Structural Materials

Examination of type 316 stainless steel weld metal showed large variations in the amount of δ-ferrite within a weld zone, large variations within a given heat of material, and large heat-to-heat variations. Aging of the weld caused $M_{23}C_6$ to precipitate around the ferrite, thus removing carbon from solution and causing more ferrite and martensite to form. The transformation of ferrite to σ phase was examined by x-ray fluorescence analysis of electron microscopy samples. Variations in Cr/Fe ratios were found in both the ferrite and sigma. Studies on the activity of carbon in iron- and nickel-base alloys were started. The composition of the carbide phase precipitated in nickel-base alloys was determined as a function of the kind and amount of alloying elements.

2. DEFORMATION AND MECHANICAL PROPERTIES

2.1 Physical Metallurgy

A metastable phase diagram was determined for near-monotectoid compositions of uranium-niobium binary alloys. Shape memory effects were identified, and the effect of tensile prestrain on thermally induced shape recovery was measured. The recrystallization behavior of a rolled $(110)[1\bar{1}0]$ tantalum single crystal was characterized and the role of deformation bands and subgrain structure ascertained. The geometry of the zone of deformation in rolling was found to importantly affect the formation of texture gradients in niobium. Residual resistivity ratio, (RRR), microhardness, and transmission electron microscopy (TEM) were used to follow the precipitation process in aluminum-gold alloys; relationships between hardness and RRR were established.

2.2 Grain Boundary Segregation and Embrittlement

A theoretical model was developed to treat the temperature dependence of solute segregation to grain boundaries. An experimental program was initiated to study the mechanism of grain boundary embrittlement by impurity segregation in Fe–3% Si doped with phosphorus.

3. PHYSICAL PROPERTIES AND TRANSPORT PHENOMENA

3.1 Mechanisms of Surface and Solid State Reactions

Apparatuses were built and test methods perfected to study the reaction kinetics of iron-base alloys and their components in sulfur and oxygen-sulfur environments at accurately measured sulfur pressures and to characterize the defect structures of the reaction products in terms of magnetic, electrical, and Hall-effect measurements. An x-ray study of vacancy ordering in FeS is also in progress. The chromia matrix of Cr_2O_3–W composites was shown to be stable in sulfur at about 0.1 Pa, and MgO was unattacked at 1000°C in sulfur at about 0.1 MPa (1 atm). We completed theoretical studies relating to the correlation of tracer diffusion for both solute and solvent atoms in alloys for which interstitial-vacancy interactions are responsible for the diffusion process. Vacancy correlation in dilute alloys showed general applicability to diffusion theory. Two modes of diffusion of tritium in rutile were identified on the basis of direct diffusion profile measurements and infrared spectral studies. The diffusion coefficient for oxygen in Nb–Zr alloys was determined in the range 550 to 1100°C, and the binding entropy, $\Delta S/k$, of O–Zr clusters was found to be −3.3. Oxygen diffusion in α-zirconium and α-Zircaloy-4 was measured at 1050, 1300, and 1450°C. To evaluate the binding energy of titanium-vacancy complexes formed during the diffusion of Ti^{4+} in NiO, the tracer diffusivity of Ti^{4+} was measured from 1000 to 1300°C. Investigations of the dissociative mechanism of diffusion centered on the Pb–Cd system, where the cadmium diffusion rate went through a minimum as a function of cadmium concentration. An investigation of possible fast diffusion phenomena in refractory metals began, and short-circuit diffusion processes were considered as a possible cause of otherwise anomalous diffusion behavior observed in several metals.

3.2 Physical Properties Research

The thermal conductivity of single-crystal and polycrystalline specimens of CsI and CsBr revealed that impurity differences and phonon scattering by grain boundaries and voids were negligible. The lattice thermal resistance of hot-pressed Cr_2O_3 decreased near the Néel temperature. Data on chromium alloys show that phonon conduction is quite important in chromium. Data on iron alloys were

used to define the phonon thermal conductivity of pure iron and indicated that lattice strain scattering of phonons is only about 20% of that predicted by theory. A correlation describing the interaction of phonons with conduction electrons was developed and shows that electron-phonon scattering may be significant in some metals. The resistivity ratio of several superconducting niobium-base alloys was measured. Measurements of the Ettingshausen-Nernst coefficient of Alumel showed some literature values to be in error by a factor of 1100. The thermal expansion coefficient of nickel was measured through its Curie temperature, and the results correlate with scaling laws of critical phenomena.

3.3 Superconducting Materials

Fluxoid pinning by radiation-induced voids was studied experimentally, and the results were compared with expressions for void pinning by use of the statistical theory of Labusch. Lithium-titanite specimens were prepared by several methods and their superconducting properties have been measured. Measurements indicate that significant heat is generated when a multifilamentary composite conductor is stressed in tension to levels expected in large, high-field magnets, and that the properties of the matrix material largely determine the size of the effect. Mechanical behavior and stress effects in high-field superconductors was reviewed, and the effects of stress on critical current density have been measured in several commercial conductors. We observed that a portion of the critical current degradation that occurs under stress is recovered upon relief of load in multifilamentary Nb_3Sn conductors; study of this phenomenon is under way. A long-range study of flux pinning by crystal boundaries has begun with extensive measurements of the critical current in cylindrical bicrystals of niobium.

4. RADIATION EFFECTS

The Radiation Effects Program is directed at understanding the effects of composition and microstructure on the structure and properties of materials irradiated at elevated temperatures. Activities supported by the Division of Physical Research complement and support work sponsored by Breeder Reactor and Magnetic Fusion Energy programs by examining relatively simple systems and by conducting studies aimed at identifying mechanisms that control damage.

A survey of the effects of alloying elements on evolution of damage in aluminum showed that undersize solutes suppressed the development of both a dislocation structure and voids. Swelling could not be correlated with partial diffusion coefficients.****Analytical electron microscopy studies of low-swelling stainless steel showed segregation of silicon to the interstitial dislocation loops. In addition, growth of the loops was retarded relative to those in a high swelling (low silicon) steel.****A new phase, not previously found in thermally treated

specimens, was discovered in a Ni–20 at. % Mo alloy irradiated with nickel ions and electrons. Order in this alloy was affected by the type of irradiation; short-range order was stable under ion bombardment, but long-range order was stable under electron irradiation. The difference was attributed to the mixing effect of cascades produced by the ions but not by the electrons. Voids were not formed in this alloy at exposures up to 100 displacements per atom (dpa); other nickel-molybdenum alloys that showed no evidence of order exhibited significant amounts of void swelling for equivalent irradiation exposures.****Analysis of helium profiles in metals produced by injection from a ^{244}Cm oxide surface source showed depth distributions in agreement with theory.

Work began on a generalized rate theory model of void swelling and dislocation loop growth that takes into account temporal and spatial effects. The latter is particularly important for electron and ion bombardment work, where surface effects alter defect profiles. The model was applied to the growth of Frank loops in nickel by electron irradiation to give values for the vacancy migration energy and the preference factor of dislocations for interstitials.****Interstitials implanted during ion bombardment reduced swelling, but the amount of reduction depended on temperature except when fixed sinks were the predominant annihilation mechanism.****The status of the theory of void growth was critically assessed, and items were identified where improvements are required to use low-dose neutron data and high-dose particle data to estimate high-dose neutron behavior.****A surface coating that changes elastic properties in the vicinity of a void increased significantly the rate of nucleation of voids. Such coatings, which could arise from impurity segregation to void surfaces, may also influence nucleation rates through changes in the specific surface energy.

The heavy-ion bombardment facility was upgraded during the year by adding a second beam line connected to a 0.4-MeV Van de Graaff. This permits simultaneous bombardment with 4-MeV heavy ions to create displacement damage and 0.2 to 0.4-MeV alpha particles to simulate helium production that occurs during neutron irradiation by (n,α) reactions. Development of a nuclear microanalysis capability as part of the facility began. A new damage chamber that permits more efficient operation and improved diagnostic capabilities was installed, and the vacuum system was improved. Experiments to study effects of He-to-dpa ratio and to examine the influence of method of helium injection on void formation were undertaken.****The facility for simulating neutron irradiation creep was completed and performed satisfactorily. Precision measurements demonstrated that bulk creep properties can be duplicated in vacuum or helium in specimens only 25 μm thick.****A systematic investigation was completed to define the optimum operating modes in an analytical electron microscope. Procedures were developed for performing energy-dispersive x-ray analyses in the analytical electron microscope.****The addition of cryopumps to the vacuum system in high-voltage electron microscope achieved a vacuum of 11 μPa (3×10^{-8} torr) in the specimen chamber. A side-entry specimen stage was added to the microscope during the year. Several cooperative studies with universities and other research organizations are listed.

1. STRUCTURE OF MATERIALS

1.1 THEORETICAL RESEARCH — J. S. Faulkner

The Theory group is primarily concerned with four major areas of research. These are: (1) electronic structure of metal surfaces and metal-adsorbate bonding; (2) electronic structure of transition metals and alloys; (3) electron-phonon interaction, superconductivity, and transport in transition metals; and (4) migration of radiation-induced defects in metals. In addition, members of the Theory Group are available to other groups in the Division and Laboratory for informal consultation and collaboration or theoretical and experimental problems of mutual interest.

1.1.1 Bonding Properties of Stepped Transition Metal Surfaces[1] — G. S. Painter, R. O. Jones,[2] and P. J. Jennings[3]

Electronic structures for small metallic clusters are analyzed to determine (1) how electrons are distributed spatially and energetically in small crystallites and at surfaces, (2) how electrons respond to surface disorder (kinks, steps, reduced coordination number), and (3) how electronic characteristics are related to chemically active surface sites.

1.1.2 Surface Studies of Chemisorptive Bonding[4] — G. S. Painter

A primary objective of surface studies of chemisorbed species is to obtain an understanding of the bonding mechanism between substrate and adsorbate. With this basic knowledge, one can approach problems that deal with chemisorption and molecular dissociation and with the influence of substrate characteristics on these processes. Some first-principles linear variational calculations in cluster and thin film energy band models are summarized. These provide some insight into the nature of adsorbate-substrate bonding. Progress toward calculating dissociation energies for molecular adsorbates will be reported.

---

[1]Abstract of pp. 136–49 in *The Electron Factor in Catalysis on Metals, Nat. Bur. Stand. Spec. Publ.* 475, U.S. National Bureau of Standards, Washington, D.C., 1977.

[2]Institut für Festkörperforschung, Kernforschungsanlage, Jülich, West Germany.

[3]School of Physical Sciences, Murdoch University, Murdoch, Australia.

[4]Abstract of paper presented at the Spring Meeting of the American Physical Society, San Diego, Calif., Mar. 21–24, 1977.

1.1.3 The Theory of Surfaces: The State of the Art[5] — G. S. Painter

Recent advances in electronic structure theory are providing a detailed fundamental understanding of atomic phenomena at surfaces. These developments are reviewed and their connections with basic surface experiments and applied materials science problems are discussed.

1.1.4 Theoretical Studies of the Electronic Structure and Bonding Properties of Surfaces[6] — G. S. Painter

Theoretical models and techniques for the description of the electronic structure and associated properties of atom configurations representative of the surface and chemisorbed species are discussed. An important objective of these studies is to relate calculated local densities of states to surface probe experiments, to extend our understanding of bonding mechanisms in chemisorption, and to establish how properties depend on surface atom coordination. A uniting of solid state and molecular theoretical concepts to study surface interactions is a principal consideration in this work.

1.1.5 Local Densities of States and Bonding Properties of 3d Transition Metal Clusters[7] — P. J. Jennings,[3] G. S. Painter, and R. O. Jones[2]

Electronic structures have been calculated for 13-atom clusters of 3d transition metal atoms. The cluster geometry has features of both stepped and flat surfaces and the results demonstrate certain trends that parallel those of the bulk: (1) d-bands are broader and d-orbitals more extended for lighter elements, (2) states near the top of the band are anti-bonding and more contracted than the bonding states near the bottom of the band, (3) gross features of the densities of states of clusters and bulk are similar. However, cluster energy distributions are more complex because of the lower symmetry at the surface, and edge and corner atoms show pronounced charge redistributions as a result of interactions among neighboring d-orbitals. Some consequences of the results are discussed, and the scattered-wave cluster technique for chemisorption studies is assessed.

---

[5]Abstract of paper presented at the DPR Surface Science Workshop, Mar. 16–18, 1977, Berkeley, Calif.

[6]Abstract of paper presented to in-house Surface Science and Heterogeneous Catalysis Seminar, Oak Ridge, Nov. 8–9, 1976.

[7]Abstract of *Surf. Sci.* 60: 225–71 (1976).

1.1.6 Bonding of Oxygen on Aluminum: Relation Between Energy Band and Cluster Models[8] — G. S. Painter

A study of some factors that influence the position and shape of resonance bands for adsorbates on surfaces is presented with particular emphasis upon the case of oxygen chemisorption on aluminum. A twofold approach has been taken to determine the relative roles of local and delocalized electron effects: the energy band structure for a thin film geometry is correlated with eigenvalue spectra from a "surface molecule" cluster model. Oxygen resonance features are found to originate from a bond mechanism involving orbitals directed parallel to the surface plane, such that the local bonding surface molecule model provides a reasonable description of the resonance position. Delocalization of the substrate electrons in the plane provides a bulklike background against which the localized resonance is observed. The bond mode provides an interpretation of how the theoretical results are related to experimental data for systems that depart from the ideal structures assumed in the models.

1.1.7 Angle-Resolved Photoemission from a (001) Surface of Single-Crystal Cu–23 at. % Ni Random Substitutional Alloy[9] — B. L. Gyorffy,[10] G. M. Stocks, W. E. Temmerman,[10] R. Jordan,[11] D. R. Lloyd,[12] C. M. Quinn,[12] and N. V. Richardson[12]

We have studied the angular distribution of photoemitted electrons from a (001) surface of single-crystal Cu–23 at. % Ni random substitutional alloy. A number of alloying effects were observed. We have interpreted these in terms of calculations based on the Coherent Potential Approximation for nonoverlapping muffin-tin potentials (KKR-CPA).

1.1.8 The Coherent Potential Approximation for Nonoverlapping Muffin-Tin Potentials: Paramagnetic Ni_cCu_{1-c} (ref. 13) — G. M. Stocks, B. L. Gyorffy,[10] E. S. Guiliano,[14] and R. Ruggeri[14]

We present a method for solving the CPA equations for a random substitutional alloy crystal potential, which consists of nonoverlapping

---

[8]Abstract of paper submitted to *Physical Review.*

[9]Abstract of paper submitted to *Physical Review Letters.*

[10]H. H. Wills Physics Laboratory, University of Bristol, U.K.

[11]Center for material Science, University of Birmingham, U.K.

[12]Department of Chemistry, University of Birmingham, U.K.

[13]Abstract of paper to be published in *Journal of Physics F.*

[14]Instituto di Fisica della Università di Messina and Gruppo Nazionale Struttura della Materia, Messina, Italy.

"muffin-tin" potential wells. As an example we consider the case of paramagnetic nickel-copper alloys.

1.1.9 Angle-Resolved Photoemission Spectra from a Disordered Cu-Ni Alloy[5] — D. R. Lloyd,[12] C. M. Quinn,[12] N. V. Richardson,[12] R. Jordan,[11] G. M. Stocks, B. L. Gyorffy,[10] and W. E. Temmerman[10]

Angle-resolved photoemission spectra from the (100) surface of a single crystal of a substitutionally disordered Cu-23 at. % Ni alloy have been measured. The electron distribution curves for electrons emitted from the surface after excitation with helium-I photons incident 20° from the surface normal are presented for analyzer positions projecting onto the ΓX, ΓK, and ΓL directions. The data are analyzed in terms of one-dimensional densities of states calculated for the ΓX, ΓK, and ΓL directions, based on the solution of the coherent potential approximation for an array of nonoverlapping muffin-tin potentials. Structures in the one-dimensional densities of states resulting from host and impurity states correlate well with structures observed in the experiments, with differences between the various directions in the Brillouin zone being evident.

1.1.10 The Coherent Potential Approximation for Nonoverlapping Muffin-Tin Potentials: Applications to Disordered Cu-Ni and Mo-Nb Alloys[5] — G. M. Stocks, B. L. Gyorffy,[10] W. E. Temmerman,[10] E. S. Guiliano,[14] and R. Ruggeri[14]

The CPA equations for a random substitutional alloy in which the alloy potential is described by a nonoverlapping muffin-tin model are solved. Computational procedures based both on real-space methods, in terms of clusters of effective scattering centers, and on reciprocal-space Brillouin zone integration are presented. The results from the two methods agree well. The necessity for solving the CPA equations and not stopping short with the average t-matrix approximation is stressed. Electronic densities of states and Bloch spectral densities (to be defined) will be presented for Ni-Cu and Mo-Nb. The qualitatively different alloying effects evident in the two systems and the extent to which the results are verifiable by experiment will be discussed.

1.1.11 Electronic States in Random Substitutional Alloys: The CPA and Beyond[15] — G. M. Stocks and B. L. Gyorffy[10]

We develop the "band" theory of disordered substitutional alloys. The discussion summarizes early theories of the electronic states in

---

[15]Lecture notes to be published as part of a NATO Advanced Studies Institute, Ghent, Belgium, 1976, in book form by Plenum Press in 1977.

disordered alloys, and we introduce the coherent potential approximation (CPA). The CPA is first discussed in terms of a simple tight binding model. Within the framework of the CPA we develop a new theory in terms of a nonoverlapping muffin-tin potential model of disordered alloys. The theory may be regarded as a generalization of the KKR band theory method to disordered substitutional alloys; we call the method the KKR-CPA. We show how the resulting equations may be solved numerically for transition metal alloys. Some of the physical "observables" that may be calculated are discussed, with particular emphasis placed on a new quantity, which we call a Bloch spectral density and which gives us information concerning the energies and lifetimes of Bloch states in alloys.

1.1.12 Solution of the KKR-CPA Equations for Paramagnetic Cu_cNi_{1-c} Alloys[16] — W. E. Temmerman,[10] G. M. Stocks, and B. L. Gyorffy[10]

We have implemented the coherent potential idea (CPA) for a regular array of nonoverlapping muffin-tin potentials that represent Ni and Cu atoms in a random fashion. We have solved the KKR-CPA equations for the effective scattering amplitude that describes the averaged behavior of the random lattice by making use of a simplification of the KKR structure constants first suggested by O. K. Andersen. We shall discuss the energy "bands" for five different concentrations in terms of the averaged Bloch spectral functions.

1.1.13 Fermi Surfaces of Concentrated Cu_cNi_{1-c} Alloys[16] — W. E. Temmerman,[10] G. M. Stocks, and B. L. Gyorffy[10]

The de Haas-van Alphen signal in alloys disappears if the impurity broadening, $\Delta\varepsilon$, of the states at the Fermi surface becomes 5 K or so. This means that in Cu_cNi_{1-c} alloys there is no Fermi surface in the conventional sense beyond c or $1-c$ greater than a few hundred parts per million. However, on the scale of the separation of the various d bands, about 1.0 eV, the states at the Fermi energy ε_F can be still quite well defined at much greater concentrations. Using the results of KKR-CPA calculations we show that this is indeed the case all through the concentrations $0 < c < 1$. We discuss in detail the shape of the Fermi surface, the lifetimes of the states at the Fermi surface, the density of states at ε_F, and the electron-phonon mass enhancement for concentrations $c = 0.87$, 0.77, 0.62, 0.38, and 0.19.

---

[16]Abstract of a talk to be presented at the International Conference on Physics of Transition Metals, Toronto, Canada, Aug. 15–19, 1977.

1.1.14 On the Band Structure of Nb_cMo_{1-c} Alloys[16] — S. Guiliano,[14] B. L. Gyorffy,[10] R. Ruggeri,[14] and G. M. Stocks

These alloys are considered as the best examples of random substitutional alloys that follow the predictions of the rigid band model. To examine the extent to which this hypothesis is correct we studied the band structure of Nb_cMo_{1-c} at a number of concentrations using the KKR-CPA theory. We solved for the effective scattering amplitudes that describe the average behavior of the random lattice by the recently developed cluster method. In the energy range of the bonding part of the d-band the effective bands were sharp and, except for more or less constant shifts due to changes in the lattice parameter, behaved as required by the rigid band model. However, in the antibonding empty part of the d-band we found a number of non-rigid-band effects. We discuss the experimental optical spectra of Nb_cMo_{1-c} in the light of this result. We also suggest some new experiments that could check the theory. In conclusion, we consider the Fermi Surface of $Nb_{0.5}Mo_{0.5}$ and the superconducting transition temperature T_c as a function of concentration.

1.1.15 Angle-Resolved Photoemission from Cu_cNi_{1-c} Random Alloys[16] — B. L. Gyorffy,[10] R. Jordan,[11] D. R. Lloyd,[12] C. M. Quinn,[12] N. V. Richardson,[12] G. M. Stocks, and W. E. Temmerman[10]

To gain more information about their band structure than afforded by the usual photoemission experiments, we have studied the angle-resolved photoemission spectra of various Cu_cNi_{1-c} random substitutional alloys. Single-crystal samples were grown by the Bridgeman technique, and we took special care to monitor surface enrichment. For the Cu-rich samples, in the energy range of the Cu d-band, the spectrum and its variations with the direction of analyzer are remarkably similar to those from pure Cu. Above the Cu-related d-band but below the Fermi energy we find a Ni impurity peak whose shape is different for electrons emitted in different directions. We interpret this variation in terms of one-dimensional densities of states calculated by the KKR-CPA method for describing the energy bands in random alloys.

1.1.16 Soft X-Ray Emission Spectra of Cu_cNi_{1-c} Alloys[16] — P. Durham,[10] B. L. Gyorffy,[10] C. Hague,[17] G. M. Stocks, and W. E. Temmerman[10]

We will present calculations and measurements of the $L_{II,III}$ soft x-ray emission spectra from various Cu-Ni alloys. The calculations are based on the solution of the KKR-CPA equations using the Andersen simplification of the structure constants. The matrix elements are

[17]Laboratoire de Chimie Physique, Université Pierre et Marie Curie, Paris, France.

evaluated without further approximations. The results show striking non-rigid-band behaviour. When plotted with respect to the Fermi energy the maxima of the Ni spectra lie about 2 eV above those of Cu. This is confirmed by the experiment in which we used ESCA to determine the relative position of the core states.

1.1.17 The Fermi Surface of Technetium from a Constant-Energy-Search KKR Band Theory Calculation[18] — J. S. Faulkner

We generate two muffin-tin potentials for technetium using Slater exchange and calculate the Fermi energies and Fermi surfaces very accurately using the constant-energy-search KKR method. An explanation is proposed for experimental de Haas-van Alphen frequencies that were not previously understood. The bare band theory contribution to the low-temperature specific heat is $\gamma_o = 2.12$ mJ/mol K^2 for the better potential. We demonstrate the feasibility of using the methods outlined in this paper for carrying out highly detailed calculations on hcp metals.

1.1.18 Electronic Contribution to the Phonon Linewidth in Nb[4] — W. H. Butler and P. B. Allen[19]

Phonons have a finite lifetime and energy width because of the electron-phonon interaction. We have calculated this linewidth, $\gamma^{\lambda}(\vec{q})$, as a function of crystal momentum, $\vec{q}$, and mode index, λ. Our calculations employ the rigid muffin-tin approximation. Preliminary results show a great deal of structure. The most prominent peak is in the longitudinal mode for $\vec{q} = (0.7,0,0)2\pi/a$. This peak coincides with a pronounced dip in the longitudinal phonon frequency. We also discuss the peculiar behavior of the electron-phonon interaction when viewed in real space.

1.1.19 Electron-Phonon Coupling in the Transition Metals: Electronic Aspects[18] — W. H. Butler

The electron-phonon parameter λ may be written as the product of three factors: the Fermi energy density of states, $N(E_F)$; the Fermi surface average of the electron-phonon interaction, $\langle I^2 \rangle$; and an effective inverse lattice force constant, Φ. We have calculated $\langle I^2 \rangle$

---

[18]Abstract of *Phys. Rev. B* 15: 5267 (1977).

[19]Department of Physics, State University of New York, Stony Brook.

and $N(E_F)$ for eleven $4d$ transition metal systems using the rigid muffin-tin approximation. We find a large but understandable variation in $\langle I^2 \rangle$, which is in good agreement with the empirical variation in $\langle I^2 \rangle$. It varies approximately as the inverse second power of the atomic volume and as the first power of the fraction of $\ell = 3$ Fermi energy state density within the Wigner-Seitz cell. We discuss the implications of our findings in regard to the search for systems with higher superconducting transition temperatures.

1.1.20 Electron-Phonon Contribution to the Phonon Linewidth in Niobium: Theory and Experiment[20] — W. H. Butler, H. G. Smith,[21] and N. Wakabayashi[21]

Phonons have a finite lifetime and energy width due to the electron-phonon interaction. In this paper we present theoretical calculations and experimental measurements of this linewidth. The calculations employ the rigid muffin-tin approximation and a realistic band structure. The measurements are done at low temperature to minimize the anharmonic contribution to the linewidth. The calculations show a narrow peak in the longitudinal mode at $\vec{q} = (0.7,0,0)2\pi/a$, which coincides with a pronounced dip in the longitudinal phonon frequency. The most prominent peak in both the calculated and measured linewidths is for the longitudinal mode near the N point. Our results indicate stronger electron-phonon coupling for the longitudinal modes than is observed in tunneling experiments.

1.1.21 The Rigid Muffin-Tin Approximation for the Electron-Phonon Interaction in Transition Metals[16] — W. H. Butler

The rigid muffin-tin approximation (RMTA) is a simple and widely used ad hoc prescription for calculating electron-phonon matrix elements. According to the RMTA the change in crystal potential due to the displacement of a single atom is proportional to the spatial derivative of the ordinary band theory potential. We will present evidence that the RMTA works quite well for the transition metals, both in a global sense, yielding electron-phonon coupling constants, λ, which are in reasonable agreement with experiment, and in a microscopic sense since it predicts phonon linewidths that are also in reasonable agreement with the experiment. The RMTA fails for the simple metals, however, indicating that the basis of its success for the transition metals lies in the fact that transition metal atoms are "compact" scatterers.

---

[20] Abstract of paper submitted to *Physical Review Letters*.

[21] Solid State Division.

1.1.22 Dislocation Loop Growth and Void Swelling in Bounded Media by Charged Particle Damage[22] — M. H. Yoo

A system of partial differential rate equations for the growth of dislocation loops and voids in one-dimensionally bounded media, such as the semiinfinite medium and the foil, under charged particle irradiation has been formulated in terms of the diffusion-controlled kinetics of defect annealing and clustering. Both time and space dependences of the point defect generation rate, the concentrations of free point defects, and the sizes of fixed internal sinks are included in this rate theory model. An efficient numerical method of integrating the rate equations is presented. Example calculations for 4-MeV self-ion bombardment at 823 K are made, and the time and space dependences of loop growth and void swelling are discussed.

1.1.23 Point Defect Interactions and Growth of Dislocation Loops[23] — M. H. Yoo and J. O. Stiegler

A direct method of determining the effective measure of the interaction of point defects with dislocation loops is proposed. A system of partial differential rate equations for loop growth is formulated and solved numerically. An *in-situ* HVEM irradiation experiment was conducted to study growth kinetics of dislocation loops in nickel at 725 K. Systematic variations of the vacancy migration energy, E_v^m, and the preference factor of dislocation loops for self-interstitials, δ_i, reveal that E_v^m = 1.2 eV and δ_i = 0.06 together yield reasonable agreement between the theoretical model and experimental observations.

1.1.24 Effects of Short-Range Order on the Spectral Density Function for a One-Dimensional Amorphous Solid[10] — D. G. Hall[24] and J. S. Faulkner

The spectral density $A(q,E)$ is calculated exactly for a one-dimensional model of an amorphous solid. The model contains an adjustable short-range order parameter α, and $A(q,E)$ is calculated for several values of α. The harmonic-oscillator Hamiltonian appropriate to lattice vibrations and a tight-binding Hamiltonian describing

---

[22] Abstract of a paper presented at the San Diego Meeting of the American Physical Society, March 21–24, 1977, published as ORNL/TM-5789, (April 1977), and accepted for publication in *Journal of Nuclear Materials*.

[23] Abstract of a paper presented at the International Conference on Properties of Atomic Defects in Metals, held in Argonne, Ill. Oct. 18–22, 1976. The conference proceedings will be published in *Journal of Nuclear Materials*.

[24] Present address, Department of Physics, Southern Illinois University, Edwardsville.

in a simplified way either electrons or spin waves are studied for nearest-neighbor interactions. The calculated spectral densities are compared with the recent neutron-scattering measurements of Mook, Wakabayashi, and Pan.

1.2 X-RAY DIFFRACTION RESEARCH — H. L. Yakel and B. S. Borie

Research tasks of the X-Ray Diffraction Group through the past year have been diverse, fruitful, and stimulating. Our work has embraced a new theoretical approach to the old, poorly understood problems of extinction in x-ray scattering from imperfect crystals; a definitive use of synchrotron radiation to search for suspected superheavy elements; an attempt to unravel the "chemical crystallography" of an important rare earth oxide; and a continuing demonstration of the unique advantages and capabilities of our recently completed small-angle x-ray scattering camera. The following abstracts and brief descriptions of work in progress outline our program's principal thrusts.

1.2.1 A Search with Synchrotron Radiation for Superheavy Elements in Giant Halo Inclusions[25] — C. J. Sparks, Jr., S. Raman,[26] H. L. Yakel, R. V. Gentry,[27] M. O. Krause,[28] and E. Ricci[29]

Evidence for the existence of several superheavy elements (SHE) between $Z = 114$ and $Z = 127$ has been reported on the basis of proton microprobe excitation of x-ray spectra from monazite inclusions extracted from mica in which the inclusions had generated giant halo discolorations thought to arise from ~14-MeV α-particles. Weak peaks were observed in these spectra with energies and widths that did not correspond well with those expected from known K lines of 5th period elements. It was claimed that the $L\alpha_1$ line from $Z = 126$ was seen in five out of six inclusions studied. Concentrations were estimated to be as high as several hundred picograms for $Z = 124$ (100 pg $\approx 2 \times 10^{11}$ atoms for atomic mass ≈ 310) in one inclusion, raising expectations that a large number of nuclear spectroscopic studies could be carried

---

[25]Abstracted from the following: *Phys. Rev. Lett.* 38: 205 (1977); an invited paper given at the American Physical Society Meeting, Feb. 7–10, 1977, Chicago, Ill.; and American Physical Society Meeting, April 25–28, 1977, Washington, D.C.

[26]Physics Division.

[27]Visiting scientist at Oak Ridge National Laboratory from Columbia Union College, Takoma Park, Md., under NSF research grant DES74-234S.

[28]Chemistry Division.

[29]On internal sabbatical leave from Analytical Chemistry Division to Metals and Ceramics Division.

out. The very existence of primordial SHE, if confirmed, would necessitate drastic revisions of many existing ideas concerning nucleosynthesis and nuclear theory.

With proton excitation, possible confusion of SHE L x rays can occur with overlapping K x rays of 5th period elements, with γ rays produced by nuclear reactions, and with the radiative processes from cerium and lanthanum that could give lower energy radiation than the usual characteristic energy. In the case of $Z = 126$, interferences arise from Te K x rays and from a γ ray excited in the $^{140}Ce(p,n\gamma)$ reaction on cerium present in the inclusions. These uncertainties can be eliminated with a tunable monochromatic photon source, since the incident energy can be varied to bracket the absorption edge of interest. Though the K fluorescence energies may overlap some of the predicted $L\alpha_1$ energies of SHE, the K binding energies are about 4 keV below the SHE L_{III} edges, allowing a unique correlation of fluorescence energies with their absorption edges.

Electrons circulating in storage rings provide an intense photon fluence in a continuous energy spectrum into the x-ray region. An experiment was designed for the Stanford Synchrotron Radiation Project (SSRP),[30] which utilizes the photon flux from a storage ring (SPEAR) operated by the Stanford Linear Accelerator Center (SLAC). A key feature of the experiment was a hot-pressed (bent to a 0.10-m radius) pyrolytic graphite monochromator [$2d = 0.671$ nm (6.71 Å)] with 0.4° mosaic spread (FWHM) located 17 m from the source; this monochromator collected 2 mrad of radiation in the horizontal plane and half the total vertical divergence of the source. For 37.5-keV photons (300 eV FWHM), the focused flux contained about 4×10^{16} photons/s m^2 when SPEAR operated at an electron energy of 3.4 GeV and a current of about 20 mA. The fluorescence x rays were detected with a Si(Li) detector 16 mm diam by 5 mm deep mounted at 90 ± 15° to the incident beam and parallel to the plane of the synchrotron ring. As the synchrotron radiation is highly polarized with its electric vector in the plane of acceleration, the Rayleigh (elastic) and Compton (inelastic) scatter from the sample and mounting fiber are minimized at this angle.

No evidence was found for the existence of superheavy elements in the range of Z from 105 to 129, and, in particular, no evidence was found for $Z = 126$ at concentrations of about 5×10^9 atoms per inclusion or about 1–2 ppm by weight.

---

[30]Supported by the National Science Foundation under contract with Stanford University.

1.2.2 The Use of Intense Photon Fluxes from Storage Rings for Definitive Identification of Less than 10^{10} Atoms[31] — C. J. Sparks, H. L. Yakel, R. V. Gentry,[27] S. Raman,[26] D. Holcomb,[32] M. O. Krause,[28] A. Millet,[33] and E. Ricci[29]

An experiment using photon-induced excitation to aid in the search for superheavy elements was constructed for use at the Stanford Synchrotron Radiation Project.[30] The intense and broad energy spectrum of photons emitted by electrons circulating in storage rings permits selection by crystal monochromation of optimum photon energies for exciting the fluorescence of interest. In particular, the indicent energy can be tuned to just above and below the absorption edge of an element, allowing a unique correlation of fluorescent energies with the absorption energies. Though the fluorescent energies may overlap, there is no overlap of both the fluorescent energies and their absorption edges.

The calculated photon flux from the storage ring, SPEAR, in the energy region of 35 keV is combined with extrapolated cross sections, fluorescent yields, and radiative paths of the proposed superheavy elements to predict a detectability of less than 10^{10} atoms. Lower detectabilities are possible with SPEAR operating at electron energies in excess of the 3.4 GeV used in these experiments. Shown in Fig. 1.1 is the x-ray fluorescent signal obtained from $(4.6 \pm 1.7) \times 10^9$ cadmium atoms loaded into Dow cation exchange resin beads of about 75 μm diam. This spectrum was obtained with SPEAR operating at 3.64 GeV and 22 mA. The solid angle intercepted by the detector can be easily increased tenfold.

Design consideration for the x-ray optics and photon detection equipment will be discussed. Examination of eleven 50–100-μm-diam monazite inclusions that produced unusual radiation-damage effects (giant halos) in a mica matrix failed to give evidence for superheavy elements at this sensitivity level in any of the inclusions. The intense x-ray flux generated by storage rings will permit microanalysis of materials at concentration levels of parts per billion.

1.2.3 The Crystal Structure of Monoclinic Europia — H. L. Yakel

Collection of a diffracted intensity data set from a single crystal of monoclinic B-Eu_2O_3 in the normal laboratory atmosphere was suspended when it became apparent that the crystal was undergoing subtle changes as the experiment progressed. These changes were manifested by optical properties (the crystal appeared colorless rather than pink in transmission) and by small variations in lattice

---

[31] Abstract of paper presented at the Third Annual Stanford Synchrotron Radiation Project Users Group Meeting, Stanford Linear Accelerator Center, Stanford, Calif.; abstract in SSRP Report 76/11, Oct. 28–30, 1976.

[32] Plant and Equipment Division, retired.

[33] Instrumentation and Controls Division.

Fig. 1.1. X-Ray Fluorescence Detection of 4.6×10^9 Cadmium Atoms.

parameters and the magnitudes of certain diffraction maxima. We hypothesize that the crystal may be slowly reacting with an atmospheric component such as water or carbon dioxide.

To test this hypothesis, we have sealed B-Eu_2O_3 crystals into capillaries containing a short column of water and have observed their diffraction patterns over a period of several months. Two of three crystals exhibited an unmistakable triclinic distortion in which the angle between $\vec{b}$ and $\vec{c}$ remained 90°, but the angle between $\vec{b}$ and $\vec{a}$ increased to 90.04° ± 0.01°. The third crystal, more perfect than the other two and, unlike them, containing a monoclinic twin orientation, exhibited no distortion. The capillaries containing the triclinic crystals were unsealed, heated at 175°C for 18 hr to remove the water, and resealed in a helium-filled dry box. These crystals will be reexamined to assess any resultant changes in lattice symmetry and dimensions. Experiments with B-Eu_2O_3 crystals that have never been exposed to ambient atmospheres are also scheduled.

1.2.4 Crystal Structure of $LiTe_3$ — H. L. Yakel

Agreement of observed diffracted intensities from a crystal of $LiTe_3$ with those predicted by modulated three-dimensional (MS_3) group theory is qualitatively good enough to guarantee the essential correctness of the modulated structure.[34] The relative simplicity of the basic $LiTe_3$ structure and its modulation makes possible a meaningful test of the detailed quantitative applicability of MS_3 methods. To carry out such a test, we have selected suitably sized $LiTe_3$ crystals for careful quantitative measurements of diffracted intensities from which the crystal structure may be determined by conventional methods and the result compared with the MS_3 predictions.

1.2.5 Experimental Tests of EXAFS Using Alloys in Known States of Order[35] — B. S. Borie, O. B. Cavin, and H. L. Yakel

We have measured extended x-ray absorption fine structure (EXAFS) at K edges in elemental Cu, Ni, and Fe foils, the L_{III} edge in a gold foil, and the corresponding edges of these elements in foils of Cu_3Au and Ni_3Fe alloys in prescribed states of order.[36] Data are being interpreted by an analytic Fourier transform method and by a synthetic method based on transferability of back-scattering amplitudes and phases. Results to date fail to show significant changes in EXAFS patterns with order in the alloys studied.

1.2.6 Laves Phases of Uranium and 3d Transition Metals[37] — E. C. Beahm,[38] C. A. Culpepper,[38] and O. B. Cavin

Laves phases of uranium and 3d transition metals have been investigated theoretically and experimentally. Pauling's description of metal bonds was used to calculate bond numbers and d orbital participation in bonding. Limits to compound formation were found to be related to limits in d orbital hybridization. Simple equations are presented to calculate interatomic distances and composition limits of the Laves phases. Latice constants for Laves phases in the U-Cr-Fe, U-Cr-Co, U-Cr-Ni, and U-Cr-Fe-Ni systems are also presented and discussed.

---

[34]D. Y. Valentine, O. B. Cavin, and H. L. Yakel, "On the Crystal Structure of $LiTe_3$," *Acta Crystallographica*, in press.

[35]Work supported by the Exploratory Studies Program of the Oak Ridge National Laboratory.

[36]Experiments performed at the Stanford Synchrotron Radiation Project, which is supported by the National Science Foundation under contract with Stanford University.

[37]Abstract of *J. Less-Common Met.* 50: 57–71 (1976).

[38]Chemical Technology Division.

1.2.7 General Solution to the Darwin Transfer Equations with Absorption — B. S. Borie

The Darwin transfer equations, which are generally used to correct integrated intensity measurements for secondary extinction, have been solved without approximation. No assumptions concerning the absorption coefficient have been made, and our solution is applicable to crystals of any size and shape. Efforts are currently under way to find certain integration constants, which appear in our solution, from boundary conditions. Preliminary indications are that the constants may be found in a straightforward way.

Our result will allow us for the first time to plot real intensity distributions inside any crystal (whose mosaic character is compatible with the transfer equations) in both the incident and diffracted beams. We expect our result to cast light on the problem of correcting integrated intensity measurements for secondary extinction.

1.2.8 On the Observation of Forbidden Bragg Maxima for White Tin[39] — B. S. Borie

It is shown from symmetry considerations that nearly half of the recently reported forbidden diffraction maxima from white tin cannot be interpreted in terms of either anharmonic thermal motion or non-spherical atomic charge distributions.

1.2.9 One- and Two-Dimensional Position-Sensitive X-Ray and Neutron Detectors[40] — R. W. Hendricks

In this paper, position encoding techniques based both on electric analysis of signals for gas-filled ionization and proportional counters and on fluorescent screens coupled to image intensifiers and TV recording systems are discussed. Their principles of operation are illustrated, strengths and weaknesses are compared, and selected examples are given.

1.2.10 The ORNL 10-m Small-Angle X-Ray Scattering Camera[41] — R. W. Hendricks

A new small-angle x-ray scattering camera, which uses a rotating anode x-ray source, crystal monochromatization of the incident beam, pinhole collimation, and a two-dimensional position-sensitive proportional counter, has been developed. Because the sizes of the x-ray

---

[39]Abstract of paper submitted for publication to *Physica Status Solidi.*

[40]Abstract of *Trans. Am. Crystallogr. Assoc.* 12: 103–46 (1976).

[41]Abstract of paper submitted to *Journal of Applied Crystallography.*

focal spot, the sample, and the resolution element of the detector are each approximately 1 × 1 mm, the camera was designed so that the focal-spot-to-sample and sample-to-detector distances may each be varied in 0.5-m increments up to 5 m to provide a system resolution in the range 0.5 to 4.0 mrad. A large, general-purpose specimen chamber has been provided into which a wide variety of special-purpose specimen holders can be mounted. The detector has an active area of 200 × 200 mm and has up to 200 × 200 resolution elements. The data are recorded in the memory of a minicomputer by a high-speed interface, which uses a microprocessor to map the position of an incident photon into an absolute minicomputer memory address. With this interface, over 10^5 events per second can be recorded. The data recorded in the computer memory can be processed on-line by a variety of programs designed to enhance the user's interaction with the experiment. Among these are routines for background and detector sensitivity correction, contour and perspective plotting of the two-dimensional data, a variety of averaging schemes for determining circular averages and/or one-dimensional slices of the data, file management program to handle the large quantity of data produced by a two-dimensional detector, and an interactive package for communications with a central computing facility via a dedicated hardwired link. At the highest angular resolution (0.4 mrad) the flux incident on the specimen is 1.0×10^6 photons/s with the x-ray source operating at 45 kV and 100 mA. The performance of the instrument is demonstrated with several examples, among which are scattering patterns from voids in neutron-irradiated nickel, plastically deformed polyethylene, and collagen fibrils. Results from a kinetic study of the crystallization of polyethylene are also reported.

1.2.11 Research Applications of the ORNL 10-m Small-Angle X-Ray Scattering Camera — R. W. Hendricks, J. S. Lin, and R. D. Carlson

The ORNL 10-m small-angle x-ray scattering camera has now been in operation for approximately one year. During that time the instrument has proven its versatility and power through application to a wide variety of both ORNL- and university-sponsored research problems.

In cooperation with the Radiation Effects Group (K. Farrell, F. W. Wiffen), we have been examining voids in neutron-irradiated Ni, Al, Mo, and Nb. Void sizes and swelling obtained by SAXS agree well with electron microscopy results in all cases. In aluminum and nickel, data are obtained in less than 15 min per sample with Cu Kα radiation, while in molybdenum the measuring time is 1 to 3 hr because of the shorter x-ray wavelength (Mo Kα) used and the resulting lower efficiency of the detector (22%). In polycrystalline molybdenum samples with a void lattice, Debye-Scherrer lines from the lattice are clearly observed, thus giving an accurate void lattice parameter measurement. Similar measurements on neutron-irradiated molybdenum are currently in progress with a group from the University of Cincinnati (J. Moteff). Special problems arise with niobium because the irradiated samples emit Nb Kα and Nb Kβ radiation, which straddles the Mo Kα radiation used in our preliminary experiments. This problem will be eliminated through use of a β-filter and Ag Kα x rays.

In cooperation with the Ceramic Studies Group (C. S. Yust, L. A. Harris), we have undertaken an investigation of microporosity and microinclusions in an Illinois No. 6 coal by both SAXS and TEM. Such measurements allow us to determine the pore size spectrum, which is important for an understanding of coal gasification processes. Highly anisotropic void shapes have been observed in pyrocarbons in a collaborative study with W. H. Bragg of the University of California.

In a joint experiment with the Chemistry Division (E. L. Fuller, Jr.), we are investigating the total surface area of an alumina-supported cobalt molybdate catalyst. After annealing at 900°C, the surface area drops precipitously and intermediate phases form. Presumably there is an incipient melting and sintering. No such effect is observed on heat treatment of the naked support. Also in cooperation with the Chemistry Division (A. H. Narten, C. Musikas), we are studying the effect of varying pH on the coalescence (or "polymerization") in aqueous solutions of uranyl acetate. The size of the clusters changes significantly with only modest changes in pH.

Through a grant from the ORNL Exploratory Studies Program, we are investigating the potential of the instrument for biophysical research. In cooperation with the Biology Division (D. E. Olins), we are studying the structure of chromatin subunits (ν bodies or nucleosomes) and their organization in chromatin fibers. In an attempt to understand the mechanism of light stimulation of rhodopsin, we are undertaking an investigation of conformational changes in the purple membrane of *Halobacterium Halobium* with a group from the Medical School of the University of California at San Francisco (W. Stoeckenius). Finally, we are studying the growth of apatite crystallites in the developing teeth of infant rats. This work is in conjunction with scientists at Loyola University (Chicago) (M. E. Druyan).

An active program for the characterization of polymers in the solid state has been developed between our group and the Universities of Delaware, Denver, and Massachusetts, with an additional project being undertaken with the University of Cincinnati. S. K. Baczek and R. S. Stein (University of Massachusetts) have been utilizing the unique properties of the camera to measure asymmetry in the scattering curves of polyethylene as a function of plastic deformation. New theoretical advances in the analysis of the mechanism of deformation are being developed as a result of heretofore unavailable quantitative data. J. M. Schultz (University of Delaware) is measuring the kinetics of crystallization of polyethylene utilizing the unique high-speed data acquisition features of the camera. Here, a diffraction pattern of an isothermally solidifying polymer is recorded every 30 s. Such experiments were impossible before the development of this camera. These experiments could be performed in approximately 3 s, thus significantly increasing the range of undercoolings that could be studied, when the proposed upgrade of the camera with a 60-kW source is completed. P. Predecki (University of Denver) has been investigating very small changes in long-period spacing of polyoxymethylene as a function of heat treatment in his attempt to understand the mechanisms of crystallization of polymers. Here, large numbers of specimens have been measured in a short period of time. The data obtained did not require correction for

collimation effects as in traditional experiments because the new camera operates in point geometry.

Finally, in a program with the University of Florida (J. Lehman, R. W. Gould), techniques are being developed for the characterization of small (<1 μm) particulates of concern for environmental protection. We are particularly concerned with the determination of bimodal distributions of particle sizes.

1.2.12 Studies of Voids in Neutron-Irradiated Aluminum Single Crystals. III. Determination of Void Surface Properties[42] — R. W. Hendricks, J. Schelten,[43] and G. Lippman[43]

Anisotropic small-angle scattering has been measured with 0.8-nm neutrons from an aluminum single crystal containing 0.8 vol % octahedral voids created by exposure to a fluence of 1.7×10^{25} n/m^2 (>0.18 MeV) at 55°C. The scattering law in the ⟨111⟩ directions follows κ^{-2} [$\kappa = 4\pi(\sin\theta)/\lambda$] while in ⟨100⟩ it follows κ^{-4} after correction for the contribution from a small fraction (0.0014 vol %) of cubical voids. From the ratio of the intensity in these two directions, as determined in an experiment in which the data were recorded at a fixed scattering vector length while the crystal was rotated about [110], the mean truncation parameter of the octahedra was found to be 0.19 ± 0.02. From this value, the ratio of the specific surface free energy for these two planes is $\gamma_{100}/\gamma_{111} = 1.40 \pm 0.03$. The discrepancy between this value and the value 1.03 determined for aluminum containing helium bubbles by Nelson, Mazey, and Barnes is associated with contamination of the surfaces by transmutation-produced silicon.

1.2.13 Annealing Studies of Voids in Neutron-Irradiated Aluminum Single Crystals by Positron Annihilation[44] — V. W. Lindberg,[45] J. D. McGervey,[45] R. W. Hendricks, and W. Trifthäuser[43]

We have measured positron lifetimes and the angular correlation of annihilation radiation in neutron-irradiated high-purity aluminum single crystals, and have performed companion small-angle x-ray scattering experiments to determine the radius of gyration and volume fraction of radiation-induced voids. The lifetime data are consistent with a model in which positrons are trapped both in voids and in other defects, which are tentatively identified as vacancy clusters bound to transmutation-produced silicon. The lifetime of the latter defects increased from 230 to 430 ps as the voids annealed out (around 306°C), suggesting

---

[42]Abstract of paper submitted to *Philosophical Magazine*.

[43]Institut für Festkörperforschung, Kernforschungsanlage, Jülich, West Germany.

[44]Abstracted from paper to be published in *Philosophical Magazine*.

[45]Physics Department, Case Western Reserve University, Cleveland, Ohio.

that the clusters grow in size as voids disappear. The lifetime in voids remained constant at (550 ± 30) ps. Angular correlation results are consistent with the lifetime results. A magnetic quenching experiment showed less than 1% positronium formation in the voids. The results support the Hodges and Stott model of a surface state for a positron in a void.

1.2.14 X-Ray Excitation of Surface Plasmons on Spherical Voids in Metals[46] — T. L. Ferrel,[47] J. C. Ashley,[47] and R. W. Hendricks

The cross section for x-ray excitation of surface plasmons on a spherical void in an electron gas is derived by use of a hydrodynamical approximation. The result is compared with the cross sections for elastic scattering from the void and other inelastic processes such as scattering from bulk plasmons in order to provide information on the feasibility of detecting such surface plasmon excitations experimentally. Possible applications to the study of the mechanisms of void nucleation and growth are discussed.

1.2.15 Final Report of the International Project for the Calibration of Absolute Intensities in Small-Angle X-Ray Scattering[48] (Submitted to the International Union of Crystallography) -- R. W. Hendricks and L. B. Shaffer[49]

An international intercomparison project was undertaken to test the reproducibility and the comparative accuracy of the various absolute intensity calibration techniques in current use in small-angle x-ray scattering, with the participation of 15 investigators from eight different laboratories in six countries. In the project, the absolute differential x-ray scattering cross sections of standard samples of glassy carbon and polystyrene were calibrated by five different techniques at two different x-ray wavelengths. The results have been intercompared by use of a variety of statistical techniques. It is concluded that angularly dependent errors associated with determining the zero of angle, dead-time corrections, and collimation corrections are more important in accounting for discrepancies between laboratories than are differences in the absolute intensity calibration methods themselves.

---

[46] Abstract of *Philos. Mag.* 34: 929–35 (1976).

[47] Health Physics Division.

[48] Abstract from paper to be published in *Journal of Applied Crystallography.*

[49] Physics Department, Anderson College, Anderson, Ind.

1.2.16 High-Speed Memory Increment Hardware for the MODCOMP II[50] — J. C. Twichell[51] and R. W. Hendricks

A high-speed interface between a two-dimensional position-sensitive proportional counter and a general-purpose minicomputer is described. A very fast microprocessor is used for address mapping and custom input-output microcode is used for direct memory increment to achieve data rates in excess of 100 kHz.

1.2.17 Software to Augment the Capability of MODCOMP Computers Through Interaction with a Large Computing Center[50] — R. W. Hendricks, J. S. Lin, N. A. Betz,[52] and R. L. Stephenson[52]

The Oak Ridge National Laboratory has a central computing facility, which contains, among other equipment, an IBM 360/75, and IBM 360/91, three CALCOMP pen-and-ink plotters, and a CALCOMP CRT plotter. The IBM machines have shared peripherals and a common Computer Communications, Inc. CC-70 as a front-end processor for teleprocessing of remote batch entry terminals. As a part of the new 10-m small-angle x-ray scattering spectrometer, the Metals and Ceramics Division of the Laboratory has installed a MODCOMP II computer for control of the device and collection of large data arrays from a two-dimensional position-sensitive proportional counter. Because of the large quantity of data collected by our experiments and because some of the data processing is beyond the capability of the data acquisition machine, the MODCOMP has been hard-wired to the CC-70 as an IBM 2780 remote job entry terminal using the binary synchronous communication protocol. Communication is through a Model 4815 synchronous communications controller operating at 9600 baud over standard telephone lines. This situation provides the opportunity to augment the capabilities of the MODCOMP II by creating software that allows full utilization of the IBM resources. The present paper describes four such software packages designed to provide the MODCOMP II with access to the IBM 2314 disk drives, the high-speed line printers, and the CALCOMP plotters.

1.3 FUNDAMENTAL CERAMICS STUDIES — C. S. Yust

The objectives of this program are the investigation and elucidation of the fundamentals of high-temperature phenomena in ceramic solids. The topics of immediate interest are the deformation of ceramic systems,

---

[50] Abstract of paper presented at the Second Annual ModComp Users' Exchange, Fort Lauderdale, Fla., Dec. 5–6, 1976; to be published in the proceedings by Modular Computer Systems, Inc., Fort Lauderdale.

[51] Department of Nuclear Engineering, University of Wisconsin, Madison.

[52] Computer Sciences Division.

erosion processes in refractory oxides, and the stability of ceramic phases at high temperature. In addition, the types, sizes, and distribution of the microconstituents in coal are being studied by transmission electron and optical microscopy and small-angle x-ray scattering. Thermal properties of nuclear fuel materials have also been under investigation.

1.3.1 Erosion Processes in Ceramics — C. S. Yust

The study of the erosion process in ceramics has continued. The objective is a more complete understanding of subsurface damage mechanisms in well defined ceramic systems. A series of samples, including both single-phase and more complex microstructures, has been subjected to erosion in the Lawrence Berkeley Laboratory high-temperature erosion test device. Samples were tested at room temperature and at 500°C in an inert environment. The angle of impingement of the particles varied from 25 to 90°. The erosion damage is currently being analyzed by scanning and transmission electron microscopy. The initial scanning electron microscope results indicate that significant plastic deformation may be associated with the impact of a particle on alumina and mullite surfaces during room-temperature erosion. The initial transmission results on an alumina-silica composition support the indication of plastic deformation by the existence of extensive dislocation arrays in the matrix surrounding an impact pit.

1.3.2 Nuclear Fuel Properties[53] — R. L. Beatty

Apparatus has been constructed for both radial and axial heat flow thermal conductivity measurements on (U,Pu)C fuels. The radial flow apparatus allows variation of atmospheric pressure, temperature, and composition, and fuel particles have been measured in this system. Also, the effect of applied force on the conductivity of the Sphere-Pac fuel bed has been measured in the axial heat flow apparatus. We have developed equipment that simulates the temperature gradient encountered in a fuel pin for fuel-cladding compatibility tests. Although a heating arrangement for the fuel that does not alter its carbon activity is difficult to establish, a system has been devised that permits analysis of the carbon depletion of the fuel.

---

[53]This work was performed at the Swiss Federal Institute for Reactor Research during foreign assignment of R. L. Beatty.

1.3.3 Comparison of Pyrolytic Carbon Microstructures Derived from MAPP Gas and Propylene[54] — P. Krautwasser,[55] C. S. Yust, V. J. Tennery, and R. L. Beatty

The microstructure of pyrocarbon HTGR fuel particle coatings formed by pyrolysis of organic gases depends strongly on the deposition conditions. Microstructural variations induced by change of deposition gas have been studied by use of small-angle x-ray scattering, transmission electron microscopy, and plasma oxidation etching. The combined use of these techniques and others to define the microstructure is discussed.

1.3.4 A Study of Factors Affecting Elemental Analyses by STEM[54] — L. A. Harris, D. N. Braski, and C. S. Yust

The results of a study of the effect of sample holder materials on scanning transmission electron microscope elemental analyses is reported. Copper, beryllium, and graphite were the materials included. Data are presented on the contributions to the noise level and elemental analyses by x rays scattered from the holders. Special emphasis is placed on data obtained from the analysis of mineral inclusions in coal.

1.3.5 Electron Microscopy of Coal Constituents[56] — L. A. Harris, D. N. Braski, and C. S. Yust

A high-volatile bituminous coal (Hvab) has been studied by means of a 120-kV scanning transmission electron microscope (STEM) equipped with an energy dispersion unit for elemental analyses. Submicrometer minerals intimately associated with the organic matrix were located and identified by both elemental and electron-diffraction analyses performed on the same particle. Particles as small as 20 nm in diameter were analyzed. Elemental mapping across apparently homogeneous regions observed in the electron microscope image revealed mineralogical differences within these features.

---

[54]Abstract of a paper to be published in *Ceramic Microstructures '76'* (Proc. 6th Intern. Mater. Symposium, Berkeley, Calif., Aug. 24–27, 1976).

[55]Guest Scientist from Institut für Reaktorwerkstoffe, Kernforschungsanlage, Jülich, West Germany.

[56]Abstract of a paper to be published in *Microstructural Science*, Vol. 5 (Proc. Intern. Metallographic Soc., Seattle, Wash., July 1976).

1.3.6 The Use of Reflectivity Standards in an Image Analysis System[56] — L. A. Harris

The use of automated image analysis systems in coal petrography is being examined. This technique requires a volumetric analysis of the coal constituents as well as a reflectivity determination of the vitrinite maceral. Reflectivity standards normally used in determining the reflectance of vitrinite in coal samples for ranking purposes were correlated with threshold control settings on Quantimet models B and 720. The reflectivity was nearly linear in the threshold setting. The effects of variables such as wavelength, television image size, objective lens magnifications, and use of oil or air objectives were studied.

1.3.7 Quantitative Analyses of Pyrite in Coal by Optical Image Techniques[57] — L. A. Harris, E. T. Rose, L. DeRoos,[58] and J. Greene[58]

The feasibility of applying optical image analysis methods for volumetric analyses of pyrite in coal was studied. The results of analyses for total surface areas agree well with data obtained by chemical methods. Problems associated with the determinations are explored and error sources are discussed. Comparative analytical data are given for pyrite in three separate coals.

1.3.8 Direct Determination of Pyritic and Organic Sulfur by Combined Coal Petrography and Microprobe Analysis[59] — L. A. Harris, C. S. Yust, and R. S. Crouse

A method for determining organic and pyritic sulfur in coals by combined coal petrography and microprobe analyses (CPMA) was studied. The CPMA technique yielded results that agree well with chemical analyses of the same samples. In addition, this method reveals the distribution of the organic sulfur among the macerals.

1.3.9 Compatibility of Fuel, Fission Products, and Construction Materials — J. Brynestad[60] and S. L. Bennett

Tellurium is a fission product that causes intergranular embrittlement in some transition-metal-base construction materials. The stabilities of selected transition metal tellurides have been determined by vapor

---

[57] Abstract of paper to be published in *Economic Geology*.

[58] Products Certification Division, Oak Ridge Y-12 Plant.

[59] Abstract of a paper accepted for publication in *Fuel*.

[60] Now in Chemistry Division.

pressure measurements by the Knudsen effusion weight-loss technique. The experimental study of the Cr plus Cr_7Te_{8-x} system, the last of the series, has just been completed. The partial pressure of Te_2 (or Te) has been related to the experimentally measured total rate of mass loss along with the temperature, the effective orifice area, and the equilibrium constant for the dissociation of the dimer. Several experiments were performed over the temperature region 850 to 1140°C with effective orifice areas varying by a factor of 20. There were no changes, within experimental error, in the derived Te_2 (or Te) partial pressures, demonstrating that equilibrium had been achieved within the Knudsen cells. The composition of the phase boundary between Cr_7Te_{8-x} and (Cr_7Te_{8-x} + Cr) was determined over this temperature range. Values of S°_{298}, $H^\circ_T - H^\circ_{298}$, and $S^\circ_T - S^\circ_{298}$ for Cr_7Te_{8-x} will be estimated. The third-law ΔH°_{298} for the decomposition of this phase into Cr plus Te_2, based on these estimates and the experimental Te_2 pressures, will be compared with the ΔH°_{298} derived from the second-law treatment.

The measurement of the enthalpy of the β_2- to β_1-Ni_3Te_2 transformation and the measurement of the tellurium partial pressure as a function of composition over the single-phase Ni_3Te_{2-x} region now complete our study of the nickel-tellurium system.

1.4 PREPARATION AND SYNTHESIS OF HIGH-TEMPERATURE AND SPECIAL SERVICE MATERIALS — G. W. Clark

The growth of crystals and the directional solidification of eutectics of refractory materials constitute our central theme. We continue to devise and improve methods of crystal growth and directional solidification, to develop increased understanding of crystal growth processes and kinetics, and to provide materials needed in research. Crystals are grown by several methods: by internal zone growth, by temperature-gradient zone melting, from molten-salt solvents, from supercritical aqueous systems, by edge-defined film-fed growth, by the Bridgman method, and by the Verneuil method. During this report period, our crystals were shared for investigating electron spin resonance, optical and elastic properties, deformation, field emission, and electronic oscillator quality. We are investigating selected physical properties, both those related to the crystal growth process and those important for characterizing new compounds and eutectic structures. Of specific consideration is the use of metal oxide-metal eutectic composites as MHD electrode material and turbine components.

We have initiated an inquiry into the use of directionally solidified complex eutectic composites as special tool materials. A directionally solidified ceramic-metal eutectic composite may offer a better microstructure for use as tool material than the fine-grained composites commonly used in cutting and drilling. Properly chosen, such a ceramic-metal system might provide superior mechanical properties and better wear resistance.

1.4.1 Oxygen Partial Pressure Versus Phase Equilibria for Directional Solidification in the Cr-O-Mo System — J. D. Holder and G. W. Clark

Calculations made in 1976 predicted the oxygen partial pressure, P_{O_2} that would be required for equilibrium between the Cr_2O_3-Cr eutectic and its melts and the Cr_2O_3-Mo eutectic and its melt. In 1977 the calculations were further extended to predict equilibrium P_{O_2} for off-eutectic compositions and superheated melts of eutectic and off-eutectic compositions. The calculations suggest that the variation of P_{O_2} of Cr_2O_3-Mo melts with composition and temperature is sufficiently large to allow the high superheats usually required to directionally solidify off-eutectic compositions to produce eutectic-like structures.

Calculations for the Cr_2O_3-Cr eutectic system indicate that for a fixed gas mixture the melt can be superheated only a very few degrees before the metal component is oxidized or the oxide is reduced. In other words, because of the small superheat limit, the Cr_2O_3-Cr composite would be extremely difficult to grow by Internal Zone Growth and most open crucible techniques. These predictions are presently being experimentally verified.

The criteria developed for calculating required values of P_{O_2} for the directional solidification of metal-metal oxide eutectic composites should prove very useful in extending controlled solidification to other oxide-metal systems. This work also suggests the manner in which the same question can be posed for sulfide, oxysulfide, fluoride, chloride, and nitride systems should an interest develop in that direction.

1.4.2 $LaCrO_3$ and $YCrO_3$ Eutectics with W, Mo, and Cr — J. D. Holder, R. A. Hartzell,[61] and G. W. Clark

Several rare earth chromites have been identified as potential MHD electrode materials, particularly $LaCrO_3$. Since Cr_2O_3, La_2O_3, and Y_2O_3 were known to form eutectics with Mo and W, and Cr_2O_3 also forms a eutectic with Cr, we presupposed that $LaCrO_3$ and $YCrO_3$ would form eutectics with these metals. The P_{O_2}-oxide melt criterion for oxide-metal eutectic melts (discussed in Sect. 1.4.1) predicted chemically stable melts over a reasonable range of temperature and oxygen partial pressure for all six systems.

Gas mixtures of CO with CO_2 and H_2 with H_2O at 0.1 MPa (1 atm) total pressure were calculated to give the desired P_{O_2}-temperature range. Melting was achieved by radiofrequency heating hot-pressed pellets of the various mixtures in a cold crucible furnace. Eutectic-like structures were observed in the $LaCrO_3$-W, $LaCrO_3$-Mo, $LaCrO_3$-Cr, $YCrO_3$-W, $YCrO_3$-Mo, and $YCrO_3$-Cr systems. Melting points of Mo and W mixtures were near 1950°C and those of Cr mixtures near 1650°C. We believe this strongly indicated the presence of a eutectic in each system investigated.

---

[61] Graduate student at Carnegie-Mellon University, Pittsburgh, Pa., and summer participant at ORNL.

1.4.3 Directional Solidification by Internal Zone Growth of Cr_2O_3-Mo Eutectic Composites — J. D. Holder and G. W. Clark

In mid-1976 scale-up to 50-mm-diam samples was made to match the radiofrequency characteristics of Cr_2O_3-Mo mixtures to the Internal Zone Growth (IZG) technique for directional solidification. Late in 1976, the directional solidification of a 100-mm-long, 50-mm-diam sample was successfully accomplished. Unfortunately, thermal cracking in the composite grains prevented the mechanical and physical testing of these large samples. To reduce the thermal cracking tendencies as the eutectic composite grown from the melt, we returned to 20-mm-diam samples, which would allow a heat treatment of the solidified composite in the present IZG furnace.

The radiofrequency heating characteristics of a 20-mm-diam sample have made IZG very difficult. To circumvent this problem we decided to tailor the material to the IZG technique. The $LaCrO_3$-Mo and $La_{1-x}Sr_xCrO_3$-Mo systems are presently being investigated.

A new IZG furnace is being designed to allow for much larger post heaters and so increase the freedom to grow larger diameter samples.

1.4.4 Soret-Modified Eutectic Constitutional Supercooling Criterion — J. D. Holder

Extremely large thermal gradients are believed to exist at the solid-liquid interface during the directional solidification of oxide-metal eutectic composites by Internal Zone Growth.[62] Since heat flow can partially unmix chemical components in a homogeneous liquid phase by the Soret effect, the eutectic constitutional supercooling criterion of Mollard and Flemings[63] was rederived to include thermally induced mass flow. The Soret-modified criterion introduces a multiplication factor, which will raise or lower the required minimum ratio of thermal gradient to growth rate to avoid dendritic growth in off-eutectic compositions. The multiplication factor is a function of the Soret diffusion coefficient, chemical diffusion coefficient, liquidus slopes, eutectic composition, and bulk composition. The analysis indicates that for the systems of present interest in oxide-metal eutectic growth, the Soret effect will cause very little departure from the earlier criterion.

---

[62]J. E. Holder and G. W. Clark, "Directional Solidification by Internal Zone Melting of Cr_2O_3-Mo Composites," pp. 107–13 in *Conf. In-Situ Composites-II*, ed. by M. R. Jackson, H. L. Walter, F. D. Lemkey, and R. W. Hertzberg. Xerox Individualized Publishing, 1976.

[63]F. R. Mollard and M. C. Flemings, *Trans. Met. Soc. AIME.* 239: 1534–46 (1967).

1.4.5 Directional Solidification of WC-Co Melts — Felix Yen and G. W. Clark

The growth of WC-Co composites with directionally oriented carbide fibers has been initiated. This is a continuation of our overall effort at understanding complex metal-ceramic systems. Despite its wide applications as inserts and drill bits, not much has been reported on the phase equilibria of the WC-Co system. One of our first efforts is to establish the experimental conditions for stable carbide formation and to prevent the precipitation of metastable carbides with less ideal properties. The WC-Co melts are being contained in alumina crucibles in an Ar–4% H_2 atmosphere and solidified at slow rates. The relationship between the morphology of the composite, the growth conditions, and the composition will be determined. The mechanical properties will be assessed against those of sintered carbides. The improvement in properties by the addition of a third metal or carbide component is to be investigated.

1.4.6 Hard Metal-Ceramic Composites — Felix Yen and G. W. Clark

We are fabricating complex composites by hot-pressing and liquid-phase sintering. The objective is to understand the mechanism of densification and also the importance of the metallic component to the properties of the high-density composite. The metal-ceramic systems of interest consist of carbides and borides like WC, TiC, and TiB_2. The 19-mm-diam samples are being hot-pressed in a graphite die under an applied load of about 3.4 MPa (500 psi). Mechanical properties such as hardness, abrasion resistance, and bending strength are to be determined. Phase distribution and identification will be investigated with electron microscopy and x-ray diffraction.

1.4.7 Special Tool Materials — S. L. Bennett and G. W. Clark

The literature was searched for two-phase systems consisting of a suitable metal phase and a hard (or probably hard) boride phase. A number of systems were found of which Fe-(TiB_2,ZrB_2,HfB_2), Ni-Cr_5B_3, (V,Cr,Mo,W,Re)-ZrB_2, Fe-TaBeB, (Fe,VCo_3, VNi_3)-VN, ($TaNi_3$,$TaNi_2$,TaNi)-TaB, and others appear to be promising candidates.

We established that eutectics exist between the metals Fe, Co, and Ni and the corresponding ternary borides, Mo_2MB_2, and we have determined the approximate eutectic temperatures and compositions. All systems are compatible with alumina up to 1800°C. The Vickers microhardness of the ternary borides ranges from 2000 to 2600 kg/mm^2 (100-g loads), with the nickel-molybdenum boride being at the low end of the range. Directional solidification, by the Bridgman method, of these eutectic boride systems will begin immediately.

1.4.8 Hydrothermal Growth of Single-Crystal CdS — O. C. Kopp[64]

Acicular and prismatic single crystals of hexagonal CdS up to 2 mm long have been grown hydrothermally in type 304L stainless steel vessels. The largest crystals have been grown from 1 *N* and 2.5 *N* RbOH solvent at temperatures near 400°C and pressures near 100 MPa. Experimental evidence to date indicates that growth rates improve at higher temperatures and pressures; however, linear corrosion becomes excessive under those conditions. If the conditions for growing large single crystals of CdS hydrothermally can be attained, more perfect crystals of this important photoelectric material might be produced than is now possible by melt and vapor transport techniques at much higher temperatures.

1.4.9 Czochralski Growth of High-Purity Single-Crystal Fayalite (Fe_2SiO_4) — C. B. Finch and O. C. Kopp[64]

Czochralski growth of single-crystal fayalite has been accomplished by use of a gas-cooled seed, a moist Ar–4 vol % H_2 [P_{O_2} = 10 μPa (10^{-10} atm)] atmosphere, and a platinum crucible. The crystallization temperature was near 1200°C, and the crystals were grown at approximately 3 mm/hr. Fayalite is thought to be one of the important constituents of the Earth's mantle. The crystals produced here will be used for mechanical properties study at ORNL (by C. S. Yust), for shock propagation studies (by T. J. Ahrens of California Institute of Technology), and for creep studies (by S. Kirby of the National Center for Earthquake Research).

1.4.10 Edge-Defined, Film-Fed Growth of Mn_2SiO_4-MnO Eutectic Composites: Effect of Die-Top Geometry on Solidification Interface Shape[65] — C. B. Finch, J. D. Holder, G. W. Clark, and H. L. Yakel

The effect of die-top geometry (planar, convex, or concave) on solidification interface shape was investigated during edge-defined, film-fed growth (EFG) of Mn_2SiO_4-MnO eutectic composites. The composites were solidified as a function of growth rate (3 to 30 mm/hr) from melts of the initial compositions Mn_2SiO_4–15 and –29 mol % MnO. Banding effects attest that the solidification interfaces have contours that approach the die-top geometries used. An aligned microstructure of smaller than 1-μm-diam MnO rods in an Mn_2SiO_4 matrix was obtained at growth rates below 15 mm/hr. Discontinuities in rod growth at 1 to 5 μm intervals suggest mock lateral growth of the matrix. Independent of die-top geometry, an unbanded cellular microstructure predominated in boules grown at 20 mm/hr or more.

---

[64]Research participant from the Department of Geological Sciences, University of Tennessee, Knoxville.

[65]Abstract of *J. Cryst. Growth* 37: 245–52 (1977).

1.4.11 Crystal Growth of Calcium Oxide from the Molten Solvent LiF–20 mol % CaF_2 (ref. 66) — C. B. Finch, G. W. Clark and M. M. Abraham[67]

Calcium oxide single crystals up to 2 × 2 × 3 mm were grown from the molten solvent LiF-20 mol % CaF_2 in the temperature range 1200 to 1250°C. A thermal gradient technique (10°C/6 cm) with sealed platinum vessels was used for runs up to four weeks in duration. The best crystals are colorless, transparent rectangular parallelepipeds, with good {100} facial development. The crystals were identified by x-ray diffration, which indicated a lattice parameter of 481.00 ± 0.02 pm. The principal impurities in inclusion-free crystals are 1000 ppm F and 100 ppm Li. The technique was used to prepare CaO crystals intentionally doped with gadolinium.

1.4.12 Self-Luminescence of Several Fluorite-Structure Halides Doped with Curium or Berkelium[68] — C. B. Finch, R. L. Fellow,[69] and J. P. Young[70]

The self-luminescence emission spectra of several fluorite-structure halides doped with 0.1 cation % ^{244}Cm or ^{249}Bk were measured in the range 15×10^5 to 45×10^5/m (220 to 700 nm) between 295 and 600 K. The hosts studied included CaF_2, SrF_2, BaF_2, and $SrCl_2$ for Cm and BaF_2 and $SrCl_2$ for Bk. The room-temperature spectra of the Cm-doped samples all have relatively sharp peaks at approximately 16.5×10^5/m and broad, asymmetric bands with maxima near 35×10^5/m (fluorides) or 28×10^5/m ($SrCl_2$). The sharp peaks are attributed to the Cm dopant and are stable to at least 600 K, while the broad bands appear to be associated with host anion centers and disappear on sample heating. The room-temperature spectrum of Bk-doped BaF_2 also displayed an anion-related band at 35×10^5/m, while that of Bk-doped $SrCl_2$ has both an anion band at 28×10^5/m and a peak at 19×10^5/m (believed to be an additional host effect). The luminescence intensity of all samples decreased with room-temperature storage but could be partially restored by annealing.

1.4.13 Crystal Growth of Monoclinic Eu_2O_3 from Molten NaF[68] — S. L. Bennett, C. B. Finch, H. L. Yakel, J. Brynestad,[60] and G. W. Clark

High-purity monoclinic Eu_2O_3 single crystals were grown from the molten solvent NaF at temperatures between 1160 and 1200°C. The impetus

---

[66]Abstract of paper accepted for publication in *Journal of Crystal Growth*.

[67]Solid State Division.

[68]Abstract of paper submitted for publication.

[69]Department of Chemistry, University of Tennessee, Knoxville.

[70]Analytical Chemistry Division.

for crystal growth was convective mass transport over a 10 to 40°C solution temperature differential between Eu_2O_3 nutrient and self-forming nuclei. Platinum vessels were used in an argon atmosphere. Four-week runs produced transparent acicular crystals up to 0.2 × 0.2 × 5 mm with well-developed {101} and {$\bar{2}$01} prism faces. Representative samples were characterized by x-ray diffraction and optical methods. Mass spectrochemical analysis indicated a crystal purity exceeding 99.99%, with <3 ppm Na, 3 ppm F, and 1 ppm Pt as pertinent impurities.

1.5 STABILITIES OF MICROPHASES IN HIGH-TEMPERATURE STRUCTURAL MATERIALS — J. M. Leitnaker and G. M. Goodwin

We have initiated a program to study the stabilities of microphases, especially as influenced by the welding process. Initially, the program is designed to be descriptive of first the microstructure of the weld and then the relationship of microstructure to mechanical properties. We intend that the program cover both austenitic and ferritic materials, although most effort initially will be spent on austenitic welds. Finally, as our understanding grows, we hope to be able to model the welding process to indicate the influence of various parameters on the behavior of a given weld.

1.5.1 Investigation of Ferrite Content of Austenitic Welds — J. M. Leitnaker and D. P. Edmonds

That composition affects the amount of ferrite in welds has been known for some time. The Schaeffler[71] diagram describing the amount of ferrite and martensite as a function of chromium and nickel equivalents was published in the "40s". However, the Schaeffler diagram cannot accurately predict the amount of ferrite for a variety of welding parameters, as Table 1.1 makes clear for 16-8-2 weld metal in type 316 stainless steel. Examination by optical microscopy revealed variations in δ-ferrite within a particular weld as great as among the three welds listed in Table 1.1.

On aging at 650 and 730°C, ferrite numbers, as measured with a Magne-Gage, changed markedly. (The ferrite number is an approximate measure of the volume percent ferrite present.) For example, changes in ferrite number from about 2 to 22 were noted in a single heat. Other heats varied nearly as much; some varied only a little. Transmission electron microscopy revealed that $M_{23}C_6$ had precipitated around the α-ferrite phase and effectively removed the carbon from solution. The removal of carbon on aging reduced the "nickel equivalent" in the Schaeffler diagram and moved the sample into a region of both higher ferrite and martensite contents.

---

[71] A. L. Schaeffler, "Selection of Austenitic Electrodes for Welding Dissimilar Metals," *Welding J.* 20: 601-s–620-s (1947)

Table 1.1. Comparison of Measured Versus Calculated Ferrite Values (16-8-2 Welds)

Heat	Ferrite Number	
	Measured[a]	Calculated[b]
1	1.8–3.2	0
2	2.1	7
3	7.0–16.0	12

[a]With a Magne-Gage.

[b]By the Schaeffler formula. Similar discrepancies would be obtained by other equations.

The transition from γ to α appears from transmission electron microscopy to take place in two different ways: (1) by a martensitic transformation and (2) by a diffusional mechanism. The martensitic transformation is revealed by a heavily deformed region and was shown, by selected area diffraction, to be a mixture of $\gamma + \alpha$. The orientation relationship found between the two phases [$(211)_\gamma \parallel (311)_\gamma$] is typical of an austenite-martensite transformation. A region in which transformation on aging appeared to have taken place by diffusion was also found. However, the identification of ferrite was based on an electron diffraction pattern designed to produce desirable image constrast. This method is less than satisfactory for phase identification and must be regarded as tentative. Further examination of both as-welded and aged structures is under way.

1.5.2 Consequences of Composition Variations in δ-Ferrite of Welds — J. M. Leitnaker and J. Bentley

On aging at approximately 920 K, δ-ferrite regions in cast structures, of which welds are a special example, can transform to sigma phase. This behavior is well known, and internal cracking at the austenite-sigma phase interfaces is the principal mode of failure in these structures. (Internal cracking at the δ-ferrite-austenite phase interfaces does not, apparently, occur.) However, Stiegler et al.[72] have shown that within a given structure some δ-ferrite remains untransformed.

We analyzed a number of δ-ferrite regions in aged welds. These consisted of regions that had partially transformed and included some in which we could see no evidence of transformation. Analysis was by

[72]J. O. Stiegler, R. T. King, and G. M. Goodwin, "Effect of Residual Elements on Fracture Characteristics and Creep Ductility of Type 308 Stainless Steel Weld Metal," *J. Eng. Mater. Technol.* 97(3): 245–50 (July 1975).

x-ray fluorescent analysis (EDAX) on thinned electron microscopy samples. Results indicate that the precision in Cr/Fe atom ratios is within 0.01 at the 0.30 level. The Cr/Fe ratios in sigma phase varied between 0.50 and 0.84. The Cr/Fe ratio in the ferrite associated with a given sigma particle always showed a lower value than the Cr/Fe ratio in the sigma phase. The Cr/Fe ratios in the ferrite varied from 0.24 to 0.38. One ferrite region with no visible sigma showed a Cr/Fe ratio of 0.28. These data suggest that compositions vary between ferrite regions as well as within ferrite regions. Measurements on unaged simulated 16-8-2 welds revealed Cr/Fe ratios varying between 0.23 and 0.32.

These observations provide a partial explanation to the differences in transformation behavior noted by Stiegler et al. Transformation of ferrite to sigma could rationally be postulated to occur more rapidly with increased Cr content. In agreement with this postulation, we see significant variation in Cr content of ferrite regions. Note that the reason for Cr variation among the different ferrite regions is still unknown.

1.5.3 Investigation of Thermodynamic Parameters in Systems of Interest for Welding — D. J. Bradley, R. O. Williams, and J. M. Leitnaker

The influence of minor elements on the behavior of welds is especially significant. They appear to prevent or enhance σ-phase formation; to control, in certain instances, martensitic behavior; and to contribute strongly to mechanical property behavior. To model the behavior of welds, a quantitative understanding of the influence of these elements is necessary. We are attacking this problem in two ways: (1) we are measuring thermodynamic activities of carbon in iron- and nickel-base alloys, including the influence of common alloying elements and major impurities; and (2) we are putting the results in a formalism developed by Kohler.[73]

Activity coefficients for carbon in ten different nickel-base alloys were studied at three temperatures: 1170, 1370, and 1490 K. The results are given in Table 1.2. Addition of titanium decreases the activity coefficient of carbon in nickel, and chromium further decreases it; molybdenum, on the other hand, increases carbon's activity coefficient.

We have begun studying the activity of carbon in iron-base alloys at 1170 K. Chromium at the 2.25 wt % level decreases the activity coefficient of carbon in iron, while silicon at the 1 wt % level has the opposite effect. Molybdenum at the 1 wt % level slightly increases the activity coefficient. The data are not nearly so complete as for nickel-base alloys, but they hopefully will not need to be.

The Kohler formalism is being tested as a method of describing the the excess free energies of solution of all components of a multicomponent alloy. To the extent that such a description is possible, one could then write for each component

---

[73]F. Kohler, "Zur Berechnung der Thermodynamischen Daten einer Ternären Systems aus den Zugehörigen binären Systemen," *Monatsh. Chem.* 91: 738-40 (1960).

Table 1.2. Carbon Activity Coefficients as a Function of Temperatures

Content, at. %; Balance, Ni			Activity Coefficient[a] (γ_C)		
Ti	Mo	Cr	1170 K	1370 K	1490 K
2.5	0	0	120 ± 3	56.2 ± 1.3	37.9 ± 0.2
2.5	8	0	157[b]	70.7 ± 2.6	46.5 ± 1.5
2.5	0	8	124[b]	50.9 ± 0.9	33.1 ± 0.5
2.5	4	0	148[b]	65.7 ± 2.4	44.2 ± 0.8
2.5	0	4	125 ± 1	54.2 ± 0.9	35.5 ± 0.7
2.5	8	8		42.3[b]	
2.5	8	4		58.2 ± 2.4	35.0 ± 0.4
2.5	4	8		48.3 ± 2.4	31.1 ± 0.3
3.6	0	0	112 ± 2	51.1 ± 0.7	36.8 ± 0.5
Nickel 270			128 ± 2	59.9 ± 0.8	39.1 ± 0.7

[a]The standard state for carbon is pure graphite and the activity coefficient is calculated from the equation $A_C = \gamma_C X_C$, where A_C and X_C have their usual meaning, activity and mole fraction, respectively. To fix carbon activities, we used simultaneously equilibrated iron samples and the equation by J. Chipman, "Thermodynamics and Phase Diagram of the Fe-C System," *Metall. Trans.* 3: 55–64 (January 1972).

[b]The activity coefficient was determined at only one value of the activity.

$$A(\text{pure}) \doteq A(\text{soln in alloy})$$

and give the activity of element A as a function of temperature and composition.

The advantage of the Kohler formulation is — to the extent that the equations are obeyed — that one need do only a limited number of experiments. Using the data obtained we intend to investigate the error involved in using the assumption.

1.5.4 Thermodynamics of Precipitates in Materials of Welding Interest — J. M. Leitnaker and D. J. Bradley

The thermodynamic description of the constituents of an alloy is also important in describing the stability of precipitate phases. We are beginning to describe the composition of precipitates with more precision than heretofore. This is, of course, a first step in a quantitative description of the stability of a precipitate.

We have investigated MC-type precipitates in nickel-base alloys and have shown that both the metal and carbon contents can vary widely. In nickel-base alloys containing 3 at. % Mo and 2 at. % Ti, the TiC precipitate can contain up to 40 at. % MoC. The carbon content of the precipitate can vary depending on the aging temperature and time from $MC_{1.0}$ to about $MC_{0.7}$.

When titanium is not present (as a "stabilizer"), the equilibrium phase in Hastelloy N at service temperatures (below 800°C) is eta phase. We have shown that the composition of this phase is $M_{12}C$, with a high proportion (up to 25 at. %) of silicon. Apparently, the silicon stabilizes the eta-phase to a significant extent. Such partitioning of silicon is of critical importance in control of irradiation-induced swelling.

The eta phase can vary widely in carbon content. We also demonstrated that it can have the composition M_6C in 2 1/4 Cr-1 Mo steels, where the carbon activity is much higher than in the Hastelloy N. The phase can also accomodate larger amounts of silicon as M_6C.

2. DEFORMATION AND MECHANICAL PROPERTIES

2.1 PHYSICAL METALLURGY — R. A. Vandermeer

Materials science is a discipline premised on the view that important relationships obtain between the microstructure of a material and its properties. The Physical Metallurgy Group emphasizes discovering and characterizing these relationships with respect to deformation-related properties and identifying mechanisms. This year we summarize the results of such diverse studies as (1) phase transformations, deformation, and shape memory effects in uranium alloys of nuclear interest; (2) recrystallization of tantalum; (3) deformation-zone geometry and texture gradients in niobium; and (4) precipitation hardening and resistivity in dilute gold alloys in aluminum of very high purity.

2.1.1 Phase Transformations and Shape Memory Effects in Near-Monotectoid Uranium-Niobium Binary Alloys[1] — R. A. Vandermeer and J. C. Ogle

The formation of the equilibrium α-uranium (orthorhombic) and γ_2 (body-centered cubic) phases in uranium-niobium alloys near the monotectoid composition can be suppressed. If the alloys are cooled rapidly from the high-temperature γ_1 (bcc) phase field, metastable transition phases can form instead. Dilatometry has been used in this work to monitor such transformation events in alloys containing 12.5 to 16.4 at. % Nb during helium gas quenching from the γ_1 phase after a 1-hr stabilization anneal at 850°C. Interpretation of length change versus temperature data obtained on cooling together with room-temperature x-ray diffraction analysis of selected alloys allowed construction of the metastable phase diagram depicted in Fig. 2.1. In the lean niobium alloys the tranformation sequence on quenching is thought to proceed in two stages:

I. $\gamma_1 \rightarrow \gamma^{\circ}$ (tetragonal distortion of γ_1).

II. $\gamma^{\circ} \rightarrow \alpha''$ (monoclinic distortion of α-uranium).

Above about 15.5 at. % Nb only stage I is observed down to room temperature. Stage II may be classified as a thermoelastic martensite transformation, and M_s and M_f define the start and finish of that transition. For compositions above 14.2 at. % the M_f temperature may be below room temperature.

---

[1]Extended abstract of paper presented at the Metallurgy of Uranium-6 wt % Niobium Alloy Meeting, May 3–5, 1977, Los Alamos Scientific Laboratory, Los Alamos, N.M.

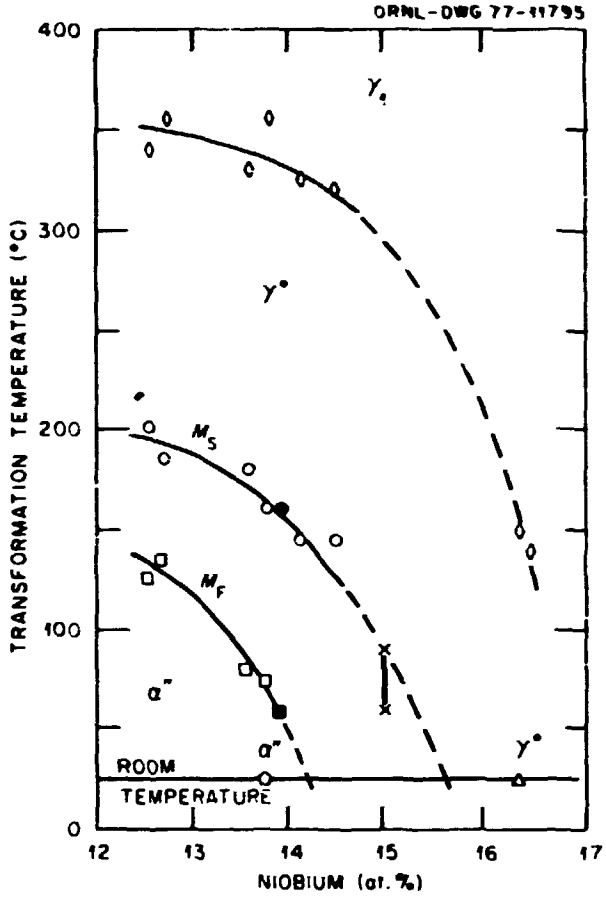

Fig. 2.1. Transformation Temperature Versus Niobium Content for Near-Monotectoid Uranium-Niobium Alloys. Crosses are from x-ray data of R. Jackson, RFP-1535, 1970.

Alloy compositions that transform to α'' exhibit shape memory effects. Figure 2.2 demonstrates this. A water-quenched rod stressed to a strain of 5.4% (along curve OA), upon unloading (AB) exhibited an "apparent plastic" strain of 4% (OB). Heating to 850°C (BC) caused much of that strain to be recovered, and after cooling to room temperature (CO) the alloy returned to its original length (i.e., net strain is zero). Such "heat-activated" strain recovery was virtually 100% for tensile strains up to about 7%. At higher strains an irreversible strain component was always present. The "heat-activated" shape memory is associated with the reverse transformation sequence

$$\alpha'' \text{ (strained)} \rightarrow \gamma^\circ \rightarrow \gamma_1 \ .$$

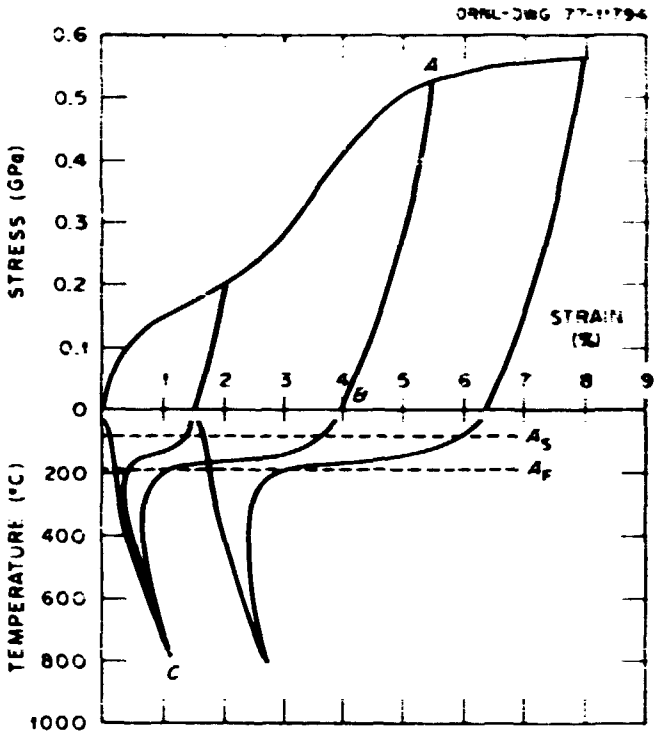

Fig. 2.2. Tensile Stress Versus Strain (Upper) and Strain Versus Temperature (Lower) for U–14 at. % Nb, Illustrating Shape Memory Behavior. Initially the alloy was quenched from 800°C. A_S and A_F represent the start and finish, repectively, of the $\alpha'' \rightarrow \gamma^{\circ}$ transformation.

2.1.2 Recrystallization of Rolled (110)[1$\bar{1}$0] Tantalum Single Crystals[2] — W. B. Snyder, Jr.[3] and R. A. Vandermeer

Very little information exists on the deformation and recrystallization behavior of body-centered cubic refractory metal single crystals.

The present investigation was a characterization of the recrystallization behavior of rolled (110)[1$\bar{1}$0]-oriented tantalum single crystals using optical metallography, microhardness, transmission electron microscopy, and x-ray diffraction. Upon rolling, the (110)[1$\bar{1}$0] crystals formed deformation bands of alternate orientations. Adjacent bands were separated by regions of mixed orientation called transition bands. Upon annealing, dislocation cells within the deformation bands served as recrystallization nuclei. The preferred orientation after recrystallization was observed to be identical to that of the deformed crystal. The rate of recrystallization depended on the character of deformation bands. Bands that were well defined optically and contained severe lattice curvature recrystallized more readily than bands that were less well defined and contained less lattice curvature.

---

[2]Abstract of paper presented at the 106th Annual Meeting of the Metallurgical Society of AIME, March 6–10, 1977, Atlanta, Ga.

[3]Development Division, Oak Ridge Y-12 Plant.

2.1.3 Deformation Zone Geometry and Texture Gradients in Cold-Rolled Niobium[4] — R. A. Vandermeer and J. B. Bernal[5]

Several niobium plates were cold-rolled at room temperature to a total reduction of 60%, with the geometry of the zone of deformation maintained constant for each plate. Pole figures were obtained by means of the Schulz x-ray reflection technique from various depths in the thickness direction for plates rolled with different Δ, the ratio of the mean height of the deformation zone to its contact length. Severe texture gradients were noted and characterized for $\Delta > 1$; a modified texture different from the normal texture was observed at intermediate through-the-thickness locations. Both lateral widening and microhardness gradients were also in evidence for this case. No previously proposed theoretical explanation could account for these results.

2.1.4 Precipitation Hardening and Resistivity in Dilute Aluminum-Gold Alloys of Very High Purity — R. A. Vandermeer, J. C. Ogle, and C. E. Zachary

In large superconducting magnets and in the proposed underground superconducting power transmission lines, ultrahigh-purity aluminum is a candidate material for the component serving to carry fault currents and to provide a path for the rated current should the superconductor temporarily go normal. If the aluminum could also mechanically support the superconductor assembly, certain design simplifications and weight savings might be realized. Unalloyed high-purity aluminum, though electrically suitable at the low temperatures, does not have sufficient strength. This research explored the possibility of manipulating the dispersant in a dilute, precipitation hardenable alloy whose solid solubility is extremely limited, in such a way as to strengthen aluminum while retaining a reasonably high conductivity.

A summary of the results of this investigation follows:

1. Zone-refined aluminum (residual resistivity ratio, RRR = 13,000) could be melted, cast, fabricated, heat-treated, and tested without encountering measureable contamination.
2. Precipitation was successfully monitored by microhardness, RRR, and transmission electron microscopy in four aluminum-gold alloys.
3. The RRR was a sensitive probe of the coalescence (coarsening) stage of precipitation in these alloys.
4. We could obtain RRRs from 1000 to 2500, but only after overaging to a point where the yield strength was just 30% higher than that of unalloyed zone-refined aluminum.
5. Under the conditions of maximum hardness, where the yield strength was estimated to be 100% higher than that of zone-refined aluminum, the RRR of the alloys was between 100 and 300.

---

[4]Abstract *Texture of Crystalline Solids* 2: 183–203 (1977).

[5]On assignment (1973–74) from Comisión Nacional de Energía Atómica, Buenos Aires, Argentina.

2.2 GRAIN BOUNDARY SEGREGATION AND EMBRITTLEMENT — C. L. White and R. E. Clausing

The purpose of this program is to study the mechanisms by which impurity segregation to grain boundaries affects the tendency of an alloy to fail intergranularly. From a theoretical standpoint impurity segregation to grain boundaries will affect the reversible work of fracture (surface and grain boundary energies); however, measured fracture energies are nearly always dominated by the irreversible plastic work done on the material adjacent to the crack path. Segregation of impurities must also affect the plastic work, but the mechanism for this is largely unknown at the present time.

2.2.1 Embrittlement in Iron-Base Alloys — C. L. White and R. E. Clausing

In order to study the mechanism of grain boundary embrittlement by impurity segregation, a series of Fe–3% Si alloys doped with 0, 300, 600, and 1200 wt ppm P was prepared. These alloys will be rolled to sheet and heat-treated to yield a large grained microstructure. Bicrystals will then be cut from the sheet for notched-bar tensile testing at liquid helium temperatures, where the plastic work terms can be minimized, to determine the fracture energy. Similar samples will be examined with Auger electron spectroscopy to determine the extent of phosphorus segregation to the grain boundaries. The first step in understanding the role of segregation in grain boundary embrittlement will be to correlate the fracture energy measurements with grain boundary phosphorus concentrations.

Experiments on the Fe–3% Si–1200 ppm P alloy are under way. Scanning electron microscopy indicates that this alloy fails intergranularly at 300 K as well as at 77 K. The ability to obtain intergranular fracture is, of course, essential for both fracture energy and grain boundary composition measurements. Auger electron spectroscopic analysis of a grain boundary fracture surface indicates that phosphorus is strongly segregated to the grain boundaries in this alloy, as we expected. Bicrystalline samples have been prepared, and preliminary fracture energy measurements are about to be made.

2.2.2 The Spectrum of Binding Energies Approach to Grain Boundary Segregation[6] — C. L. White and W. A. Coghlan

Experimental data on the temperature dependence of solute segregation to grain boundaries in polycrystalline metals does not appear to be adequately explained by a single binding energy between solute atoms and grain boundary sites. The extent of segregation in a given alloy appears to decrease more slowly with increasing temperature than is

---

[6]Abstract of paper accepted for publication in *Metallurgical Transactions A.*

consistent with a theory based on such a single binding energy. This behavior can be explained, however, if a spectrum of binding energies is assumed to exist. Such a binding energy spectrum presumably results from the site-to-site variation in the solute environment at the grain boundary. We have considered the elastic interaction between solute atoms and a tilt boundary as a model for low-angle boundaries and grain boundaries that deviate by a small angle from coincidence site bourdaries. Both the size mismatch (as characterized by the misfit parameter, δ and modulus effect mismatch (as characterized by bulk and shear elastic polarizabilities, α_K and α_G) have been included in the model. A typical distribution of binding energies is given in Fig. 2.3. The alternate shaded areas indicate the position of the sites relative to the boundary plane. Most of the high-energy binding sites lie within 2 atom distances of the boundary. Significant equilibrium segregation occurs for a boundary characterized by this spectrum of binding energies. The boundary solute concentration is shown in Fig. 2.4 for this case and also for other values of the elastic polarizabilities. The curve for $\alpha_G = \alpha_K = 0$ is the segregation predicted for a pure size misfit of 0.4 atomic volume.

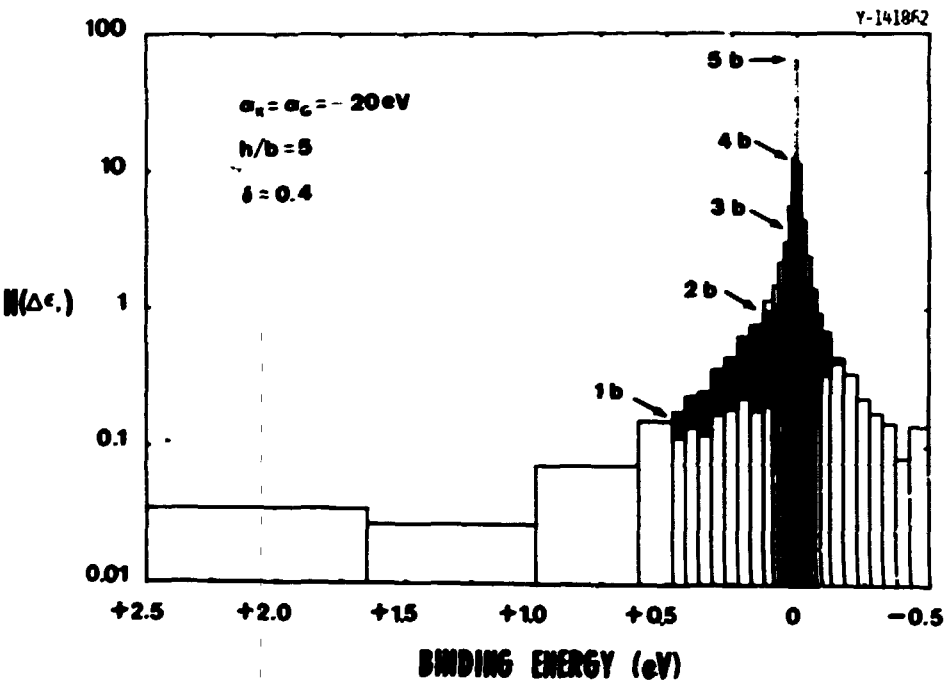

Fig. 2.3. The Binding Energy Spectrum for a Tilt Boundary Having $h/b = 5$ ($\theta = 11.7°$) for the Elastic Polarizabilities α_K and $\alpha_G = -20$ eV and the Size Misfit $\delta = 0.4$.

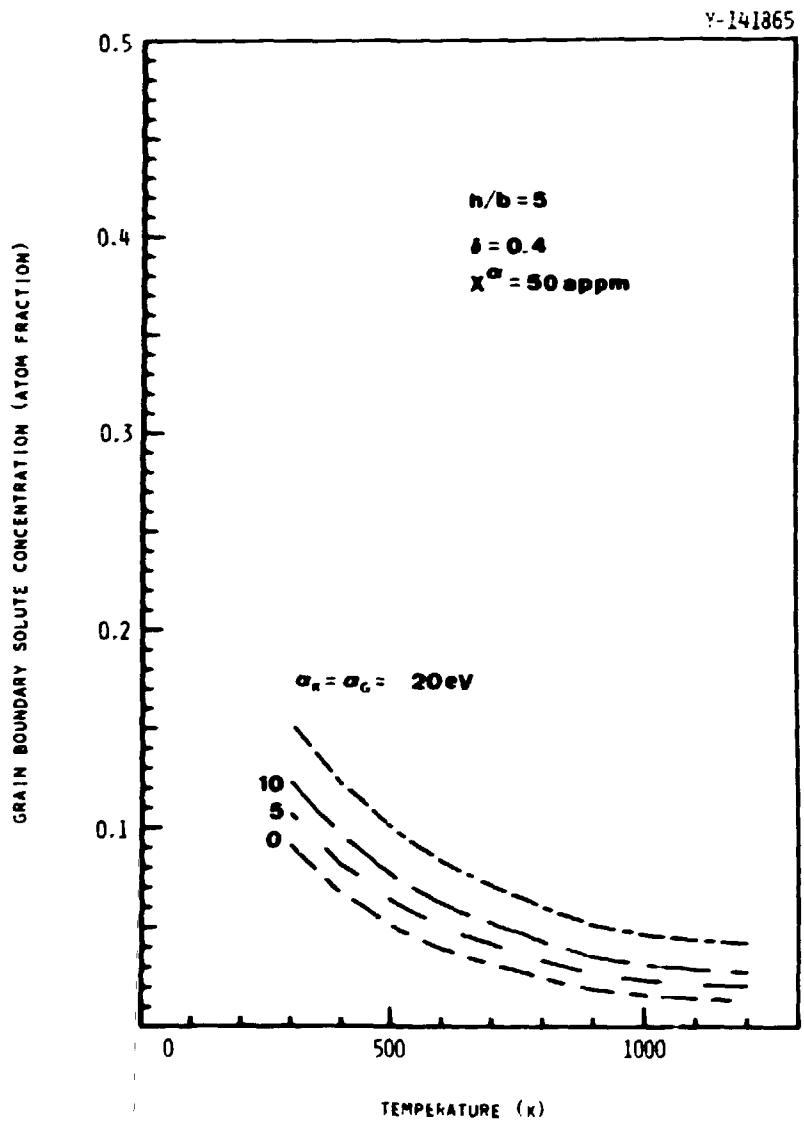

Fig. 2.4. Grain Boundary Solute Concentration as a Function of Temperature for h/b = 5, δ = 0.4 X^{α} = 50 at. ppm, and $\alpha_X = \alpha_G$ Ranging Between 0 and −20 eV.

BLANK PAGE

3. PHYSICAL PROPERTIES AND TRANSPORT PHENOMENA

3.1 MECHANISMS OF SURFACE AND SOLID STATE REACTIONS — J. V. Cathcart

This research involves studies of the fundamental mechanisms of oxidation and diffusion. Emphasis in the diffusion work is placed on understanding the influence on diffusion processes due to the interaction of the diffusing species with defects in the host lattice. The oxidation research is concentrated on alloy oxidation, with particular stress on sulfidation and reactions in mixed-gas environments. We attempt to use the new concepts developed in our diffusion work to clarify the atomistic details of material transport processes in oxide (sulfide) scales, and the ultimate goal of this effort to contribute to the development of a more satisfactory theory of alloy oxidation.

Research in a variety of areas has been carried out last year: (1) the reactions of iron-chromium alloys in mixed-gas environments, (2) anomalous fast diffusion processes, (3) interstitial and substitutional diffusion in oxides, (4) diffusion in metals, (5) reactions of ceramic-metal composites in oxidizing and sulfidizing environments, and (6) theoretical studies of diffusion and oxidation mechanisms. These research problems and, where possible, the materials studied were chosen because of their relevance to the needs of the general ERDA energy programs. The corrosion studies, for example, bear on a range of problems encountered in the Fossil Fuels Program, geothermal energy production, and the development of MHD units. Other projects relate to the tritium containment problem in fusion reactors, hydrogen embrittlement of metals, the handling of hydrogen in a hydrogen economy, and the development of new high-temperature materials.

3.1.1 Oxidation-Sulfidation of Metals in Mixed Gases — R. A. McKee, R. E. Druschel, and G. F. Petersen

As a part of a broad investigation of reactions of iron-base alloys with sulfur and in mixed oxygen-sulfur environments, a variety of experimental apparatuses and test methods has been developed that allow reaction kinetics to be determined, sulfur pressures to be measured accurately, and the defect structure of reaction products to be characterized in terms of their magnetic and electrical properties and through Hall-effect measurements. Because of the vigorous attack of sulfur on iron and low-alloy steels, special attention is being given to iron-sulfur compounds. The reaction of iron with sulfur is being investigated in two temperature ranges, 600 to 900°C and 250–500°C. At the higher temperatures reaction kinetics are being studied as a function of sulfur pressure, and Hall-effect, magnetic susceptibility, and electrical conductivity are being measured on the reaction products in order to characterize the electronic-ionic defect coupling in the sulfides.

Special importance is attached to the studies between 250 and 500°C because the pressure vessels in several coal conversion systems are

expected to operate near the midpoint of this range in an environment rich in sulfur. One of the anticipated reaction products, $Fe_{1-x}S$, is highly defective on its cation lattice; x may be as large as 0.18, and the growth rates of the sulfide scale are related to the defect concentration. In particular, the rate of cation diffusion is expected to be sensitive to vacancy ordering or interactions, both of which occur in this compound. At 320°C $Fe_{1-x}S$ goes through a magnetic transformation; below 320°C the compound is antiferromagnetic, and the cation spin states couple with the vacancy states, causing a pronounced vacancy ordering. Because this ordering will slow diffusion significantly, sulfidation kinetics of iron is being studied just above and just below 320°C in order to characterize the transformation fully.

3.1.1.1 Crystallographic Structure Determinations for Iron Sulfides — R. A. McKee and H. L. Yakel

In order to understand further the phenomenon of vacancy ordering in sulfides a program has been initiated in cooperation with the X-Ray Diffraction Group to study the properties of the high-temperature hexagonal form of pyrrhotite (FeS) by x-ray diffraction techniques. Single crystals of high-purity FeS have been synthesized, and preliminary structure work has been initiated. The aim of this work is to identify the stability parameters of the 320°C magnetic transformation in FeS and to characterize the influence of nontransition metal impurities on the transformation. If the transformation temperature could be raised, the resulting technological impact could be significant in terms of an increase in the sulfidation resistance of iron-base alloys.

3.1.2 Ceramic-Metal Composites — J. V. Cathcart and G. F. Petersen

In cooperation with the Fundamental Ceramics Group we have continued to investigate the corrosion resistance of ceramic-metal composites in high-temperature, mixed-gas environments. The severity of the attack of sulfur on Cr_2O_3-Mo composites was shown to vary with the sulfur pressure. At high sulfur potentials (pure H_2S at 1000°C) both the Cr_2O_3 matrix and the molybdenum fibers were heavily corroded. At $P_{S_2} \approx 0.1$ Pa, however, only the molybdenum was attacked. No corrosion was discernable in tests of MgO crystals in pure H_2S at 1000°C. Considerable effort was also expended in gathering thermodynamic data appropriate to the complex series of reactions possible for these composites, and in several instances stability diagrams were constructed.

3.1.3 Oxidation and Diffusion Theory — R. A. McKee

Two papers have been published and one has been submitted for review (see abstracts below) concerning the theory of diffusion for alloys in dissociative equilibrium. These papers relate to the correlation of tracer diffusion for both solute and solvent atoms in alloys for which interstitial vacancy interactions are responsible for the diffusion process. The mobilities of the solute in temperature gradients and electrical fields were calculated as well.

One of the most important contributions from these studies was the identification of a vacancy correlation factor for the infinitely dilute alloy in dissociative equilibrium. The vacancy correlation occurs because of the contribution of the interstitial-vacancy close pair to the diffusion process and the fact that the vacancy and interstitial must move in concert. This idea of vacancy correlation in dilute alloys has general as well as specific application to diffusion theory, a fact not previously recognized by other investigators. Current studies are aimed at a better understanding of the origin and the physical significance of vacancy correlation in alloys. This effort will provide the framework for a possible comprehensive restructuring of alloy diffusion theory and alloy oxidation theory.

For the latter of these, oxidation theory, modeling and calculations have been performed for the development of a new approach to the theory of alloy oxidation. This new approach differs from the classical Wagnerian theory of metal oxidation and will treat impurity-defect interactions in a growing oxide from an atomic rather than a phenomenological viewpoint and potentially will lead to a significantly enhanced understanding of alloy oxidation.

3.1.3.1 Solute and Solvent Diffusion for an Alloy in Dissociative Equilibrium[1] — R. A. McKee

Solute and solvent diffusion have been analyzed with the pair association theory for a dilute fcc alloy in which the solute is partitioned between the three states of unassociated substitutional solute atoms, interstitial-vacancy close pairs, and isolated interstitial solute atoms. Correlation factors are identified for solute and vacancy motion, and the relationship between the enhancement factor for solvent diffusion and the vacancy correlation factor attributable to solvent-vacancy exchanges in the presence of the interstitial solute-vacancy defect has been derived.

---

[1]Abstract of paper accepted for publication in *Physical Review*.

3.1.3.2 The Concentration Dependence of Solute Diffusion for an Alloy in Dissociative Equilibrium[2] — R. A. McKee

An analysis of solute pairing for an alloy in dissociative equilibrium permits an expression to be written for the concentration-dependent solute diffusion coefficient in a dilute fcc alloy. This expression explains recently reported measurements of Au diffusion in Au-Pb alloys, and Ag diffusion in Ag-Pb alloys. Furthermore, a unique result is predicted for the change in diffusivity in such alloys since the extremes of the dissociative equilibrium allow the solute pairs to form in distinctly different configurations. The conclusions are presented in terms of correlation factors, solute-solute binding energies, and the formation energy of interstitial-vacancy pairs.

3.1.3.3 Thermomigration in Alloys for which Substitutional-Vacancy and Interstitial-Vacancy Mechanisms are Operative[3] — R. A. McKee

The theoretical treatments of alloy diffusion in a temperature gradient by the substitutional-vacancy mechanism and by the interstitial-vacancy mechanism have been combined, and two types of thermomigration experiments, which differ in initial condition, have been analyzed. These experiments, as measurements of the impurity heat of transport, apparently cannot distinguish between the two mechanisms of diffusion. However, an expression for the lattice velocity in such a combined-state alloy is developed and will distinguish between the two mechanisms in a rather specific fashion.

3.1.3.4 Solute and Vacancy Diffusion of an Alloy in Dissociative Equilibrium[4] — R. A. McKee

The pair association theory has been used to analyze the kinetic characteristics of a dilute fcc alloy in dissociative equilibrium. Correlation factors, enhancement parameters, and defect mobilities are analyzed, and results of these calculations permit new considerations relating to diffusion mechanism in such an alloy. The results of these analyses may be compared directly with existing experimental measurements and suggest other specific experiments that can be used to look closer at the characteristics of solute-dissociative equilibrium.

---

[2]Abstract of paper submitted for publication in *Philosophical Magazine.*

[3]Abstract of *Philos. Mag.* 35: 715–26 (1977).

[4]Abstract of paper presented at the meeting of the American Physical Society, March 21–24, 1977.

3.1.4 Interstitial Diffusion

3.1.4.1 Tritium Diffusion in Oxides — R. A. Perkins, J. B. Bates,[5] and L C Manley, Jr.

The importance of oxide diffusion barriers in the containment of tritium in fusion reactors or in the prevention of hydrogen embrittlement of metals is well established. For this reason a study of the mechanism of hydrogen diffusion in oxides was undertaken. During the past year the diffusion of tritium into rutile (TiO_2) was measured parallel to the c axis in the temperature range 500 to 900°C. The diffusivity values were obtained directly from tritium concentration profiles. Infrared spectroscopy measurements provided information about the nature of the diffusing species. The diffusion results indicate that at least two diffusion mechanisms are operative in the lattice; one data set agrees with previously reported results of hydrogen diffusion in rutile, but the other data set is about four orders of magnitude lower. The infrared spectra of the faster diffusing species are discussed in the abstract given below.

3.1.4.2 Infrared Spectral Properties of Hydrogen, Deuterium, and Tritium in TiO_2 (ref. 6) — J. B. Bates[5] and R. A. Perkins

Infrared spectra of TiO_2 single crystals containing either hydrogen, deuterium, or tritium were measured at 300, 77, and 8 K. Bands observed at 3276, 2437, and 2065 cm^{-1} near 300 K are respectively assigned to OH^-, OD^-, and OT^- on the basis of a two-term anharmonic oscillator model of the hydrogenic species. The frequencies were also analyzed by use of a linear hydrogen bonded model with harmonic forces, but the correlation between frequencies and bandwidths was at variance with that of known hydrogen-bonded systems. The absorption strength per ion of OT^- was calculated at several levels of approximation, and the best value determined was $a_T = 9.24 \times 10^{-20}$ m. The harmonic and anharmonic mean-square displacements of OH^-, OD^-, and OT^- were calculated, and the differences between these quantities reflect the changes in the infrared bandwidths with reduced mass.

3.1.4.3 Oxygen Diffusion in Niobium and Niobium-Zirconium Alloys[7] — R. A. Perkins and R. A. Padgett, Jr.

The tracer diffusion of ^{18}O in pure niobium and niobium-zirconium alloys (≤1% Zr) has been measured from 550 to 1100°C. After the diffusion

---

[5]Solid State Division.

[6]Abstract of paper submitted for publication in *Physical Review.*

[7]Abstract of paper accepted for publication in *Acta Metallurgica.*

anneal, the specimens were bombarded with protons to cause the reaction $^{18}O(p,n)^{18}F$. The oxygen profile was then measured by autoradiographic techniques, which detected the ^{18}F. The temperature dependence of the oxygen diffusivity in pure niobium is

$$D = 4.55 \times 10^{-7} \exp(-25900/RT) m^2/sec \ .$$

Oxygen additions to the niobium (≤1.5 at. % O) did not significantly affect the oxygen diffusivity. As the zirconium content of the niobium increased the oxygen diffusivity decreased. As zirconium atoms are dissolved substitutionally onto the niobium lattice, they form trapping sites at which O-Zr clusters may be formed. The binding entropy, $\Delta S/k$, of the clusters was determined to be about −3.3.

3.1.4.4 The Diffusion of Oxygen in Oxygen-Stabilized α-Zirconium and -Zircaloy-4 (ref. 8) — R. A. Perkins

The diffusion of oxygen in α-Zircaloy-4 was measured at 1050, 1300, and 1450°C with ^{18}O used as the tracer species. The oxygen profile was determined by proton activation of the ^{18}O followed by autoradiography. The tracer diffusivity was appreciably lower than previously measured chemical diffusivity. However, the chemical diffusivity values obtained from the present data by use of the thermodynamic data for oxygen in α-zirconium compare well with those from previous studies. The concentration dependence of the oxygen diffusivity in α-zirconium is discussed, and the reliability of the results from other methods is considered.

3.1.5 Aliovalent Diffusion in Oxides — R. A. Perkins

The tracer diffusivity of Ti^{4+} in single-crystal NiO has been measured from 1000 to 1500°C in oxygen at 0.1 MPa (1 atm). The nickel self-diffusion is being measured also for comparison with the titanium data. The titanium diffusivity is approximately an order of magnitude greater than the nickel self-diffusion at 1000°C and three times greater at 1300°C. The activation energy measured for the nickel self-diffusion is about 263 kJ/mol and for the titanium 211 kJ/mol. A cell holder has been constructed to perform anneals at controlled oxygen pressures [0.1 to 10^5 Pa (10^{-6} to 1 atm)] to determine the pressure dependence of the titanium diffusivity to obtain the binding energy of titanium-vacancy complexes in NiO.

---

[8]Abstract of paper to be submitted to *Journal of Nuclear Materials*.

3.1.6 Anomalous Fast Diffusion Processes — P. T. Carlson, T. S. Lundy, and R. A. Padgett, Jr.

3.1.6.1 Diffusion of Interstitial Solute-Vacancy Pairs in Dilute Pb-Cd Alloys — P. T. Carlson and R. A. Padgett, Jr.

Attempts have been made to explain the anomalously fast diffusion of cadmium in lead in terms of the dissociative mechanism of diffusion, in which a substitutionally dissolved solute atom is thermally excited to an interstitial position. The degree of interaction between the resulting vacancy and the interstitial atom can appreciably affect the the diffusion rate of the solute and solvent atoms. The diffusion of cadmium tracer into Pb-Cd alloys ranging from 0 to 1.0 at. % Cd at 250°C has shown that the Cd diffusivity in the alloy relative to that in pure Pb decreases with increasing Cd content between 0 and 0.01 at. % Cd. As the Cd concentration increases above 0.01 at. % Cd, and Cd diffusivity increases in accordance with the expected behavior of solute diffusivity enhancement. This behavior is being interpreted in terms of the various forms of solute-solute and solute-defect interactions possible in the Pb-Cd system.

3.1.6.2 Diffusion in Pb-Ni Alloys — P. T. Carlson and R. A. Padgett, Jr.

Another investigation, which should also contribute to an understanding of the mechanisms of fast diffusion, has recently begun. It involves a study of the diffusion of Ni in Pb. In contrast to the Pb-Cd system, where the Cd atoms reside principally on substitutional sites, there is evidence that the Ni atoms occupy predominantly interstitial sites in Pb, with the bulk of these interstitials existing in interstitial-vacancy pairs. Because of the essentially interstitial character of the nickel, the solute diffusivity enhancement in the Pb-Ni system is expected to be small relative to that observed for Pb-Cd. Thus the diffusion behavior exhibited by the two sets of alloys will allow the two extremes of the dissociative diffusion mechanism to be compared.

3.1.6.3 Anomalously Fast Diffusion in Tungsten — T. S. Lundy and R. A. Padgett, Jr.

Atomic diffusion of the noble metals silver and gold is unusually rapid in several host lattices, including some that are bcc and some fcc. Considerable controversy exists regarding the most reasonable mechanism for this phenomenon, and we have begun an experimental program designed to examine the mechanistic details of this behavior. Specifically, we are concentrating on an in-depth look at atomic penetration profiles for the diffusion of silver and gold in tungsten. We will use the highly sensitive and reliable anodizing-and-stripping

technique that we previously developed for sectioning certain refractory metal specimens to define the penetration profiles highly precisely.

3.1.7 Intrinsic Diffusion and Vacancy Flow Effects in Vanadium-Titanium Alloys — P. T. Carlson

Previously obtained data were evaluated to obtain intrinsic diffusion coefficients and vacancy flow parameters in the vanadium-titanium system from 900 to 1600°C. The experimental results reflect a greater influence of the vacancy flow phenomenon on the intrinsic flux of each species than that predicted on the basis of the random alloy model. The principal assumption of the random alloy model is that all diffusing species find themselves in random environments, with no preferred sites for either atoms or vacancies. The observed discrepancies between theoretical and experimental values are examined in light of the existence of solute-vacancy complexes in titanium-rich alloys as well as the presence of solute-divacancy complexes at elevated temperatures. Both types of defect complexes result in highly correlated vacancy motion, and the effect of this deviation from the random alloy model on the vacancy flow theory is examined.

3.1.8 Short-Circuit Diffusion Phenomena — T. S. Lundy

3.1.8.1 Use of the Hart-Mortlock Equation to Interpret Tracer Diffusion Results[9] — T. S. Lundy

The Hart-Mortlock (HM) equation for estimation of dislocation and other short-circuit contributions to measured diffusion coefficients has been reexamined with focus on limitations due to theoretical assumptions and application of HM to experimental results. For certain "anomalous" solid-state systems, we conclude that HM is inadequate to reject short-circuit effects as the principal source of the anomalies. Improvements of the HM concept and experiments to help clarify the actual role of short-circuiting in the solid state diffusion process are suggested.

3.1.8.2 Have Short-Circuiting Diffusion Phenomena Been Short-Changed?[10] — T. S. Lundy

The significance of short-circuiting diffusion phonomena may have been seriously underestimated in recent measurements of diffusion

---

[9]Abstract of paper prepared for publication.

[10]Abstract of an oral presentation at the 1977 March Meeting of the American Physical Society.

in solids. The key points of background papers on these phenomena are presented and discussed, with emphasis on recent papers where the authors chose more exotic and perhaps less satisfactory explanations for their experimental results.

3.1.8.3 An Explanation for Diffusion in the Anomalous Body-Centered Cubic Metals[11] — T. S. Lundy

I propose that lattice diffusion in the anomalous bcc metals may have not yet been properly measured. Complex penetration profiles with significant short-circuiting influences coupled with techniques of measurement sensitive only for large penetration distances may have prevented previous experimenters from detecting the lattice diffusion portions of the profiles. More sensitive sectioning techniques, such as sputtering, should be combined with pre-diffusion anneals to minimize short circuiting and, therefore, examine this possibility. If the scenario is correct, lattice diffusion in these systems is not anomalous, only the previous experimental findings.

3.1.9 The Role of Stress Effects in the Oxidation Behavior of High-Temperature Alloys[12] — J. V. Cathcart

Inherent in the oxidation process for metals and alloys is the tendency for large stresses to develop in growing oxide layers. A variety of stress-generating mechanisms exist, involving such factors as the mode of diffusion, the oxide-to-metal volume ratio, and oxide morphology. These stresses may be relieved through creep or cracking of the oxide and by other mechanisms. Experimental evidence for these processes during the high-temperature oxidation of various metals and alloys is cited and, where data are available, similar results during sulfidation and in mixed gas environments are considered.

3.2 PHYSICAL PROPERTIES RESEARCH — D. L. McElroy

This effort obtains and analyzes accurate values of thermal conductivity, λ; electrical resistivity, ρ; specific heat, C_p, coefficient of thermal expansion, α; and Seebeck coefficient, S, for a variety of selected solids from 4.2 to 2600 K. Understanding the relations between these properties and their temperature dependence can provide useful insight about the solid, can often provide information for

---

[11] Abstract of paper in preparation.

[12] Abstract of paper presented at the fall 1976 meeting of the Electrochemical Society, Las Vegas, Nev., October 1976. To be published in the proceedings of the symposium on "Properties of High-Temperature Alloys."

systems where needed experimental data do not exist, and can suggest ways to improve and control properties. These material properties, particularly thermal conductivity, are important factors in the performance of all power generating systems.

3.2.1 Transport in Nonmetals

3.2.1.1 Thermal Conductivity of Cr_2O_3 — R. K. Williams and R. S. Graves

Preliminary measurements of the λ of hot-pressed Cr_2O_3 samples were obtained to aid in interpreting data on directionally solidified Cr_2O_3-Mo composites. Data on two samples, which were 96 and 98% of theoretical density and oriented in different directions, yielded consistent results, indicating that essentially random crystallite orientation was achieved. The results also show a change in temperature dependence near the Néel temperature, with the slope of the lattice thermal resistance, $1/\lambda_p$, decreasing by a factor of nearly 4. This behavior is not similar to the effects noted[13] in UO_2.

3.2.1.2 Lattice Thermal Conductivity in Electrically Insulating Crystals — J. P. Moore, R. K. Williams, and F. J. Weaver

Studies of the effects of mass ratio, absolute temperature, and Debye temperature on the λ of electrically insulating alkali halides continued. Measurements of λ on single-crystal CsBr and CsI showed negligible phonon scattering by impurities, grain boundaries, and voids in the polycrystalline specimens of the same compositions. A dry-box facility has been prepared and tested for machining the hygroscopic compounds RbF and CsF.

3.2.2 Physical Properties of Metals

3.2.2.1 Chromium — R. K. Williams, F. J. Weaver, and R. S. Graves

Our experimental data on high-purity Cr in the paramagnetic state[14] were analyzed in terms of significant parallel phonon and electron

---

[13] J. P. Moore and D. L. McElroy, "Thermal Conductivity of Nearly Stoichiometric Single-Crystal and Polycrystalline UO_2," *J. Am. Ceram. Soc.* 54(1): 40–46 (January 1971).

[14] J. P. Moore, R. K. Williams, and R. S. Graves, "Thermal Conductivity, Electrical Resistivity, and Seebeck Coefficient of High-Purity Chromium from 280 to 1000 K," *J. Appl. Phys.* 48(2): 610–17 (February 1977).

conductivities, but other investigators[15] have hypothesized that the phonon contribution is negligible. To aid in resolving this uncertainty, four samples of Cr alloys containing 0.5% Fe, 1% Fe, 5% Fe + 0.5% Mn, and 3% Mn + 3% V were obtained from annealed arc-cast ingots. The Néel temperatures (T_N) of the two binary Cr-Fe alloys are consistent with literature values,[16] and the Cr-Fe-Mn alloys have a T_N about 40 K higher than the corresponding binary Cr-Fe alloy. The T_N of the Cr-Mn-V alloy was only about 90 K, but this does indicate that a useful ternary Cr-Mn-V alloy could be produced because the addition of 3% V to Cr completely suppresses antiferromagnetism.[15] Other preliminary data indicate good sample homogeneity, and the room-temperature λ and ρ data show that phonon conduction is probably quite important in Cr.

3.2.2.2 Iron and Dilute Iron Alloys — R. K. Williams, D. W. Yarbrough,[17] and R. S. Graves

Additional results on dilute Fe-base alloys have been obtained, analyzed, and employed in explaining the behavior of 2 1/4 Cr-1 Mo steel, which was to be used in the CRBRP heat exchanger.[18] The data on Fe-Cr, Fe-Ni, Fe-Ti, Fe-Cr-Ni, and Fe-Cr-Mo alloys were used to define the phonon conductivity, λ_p, of pure iron[19,20] and to investigate the effects of the various solutes on λ_p. The solutes act in two ways, by scattering phonons and by producing small shifts in the electron-phonon thermal resistance of Fe (W_{ep}). The data show that Cr has only a small effect on λ_p, and most of the enhanced scattering in Mo-containing alloys can be attributed to the mass difference effect.

---

[15]M. A. Mitchell and J. F. Goff, "Effect of Molybdenum and Vanadium on the Lattice Thermal Conductivity and Lorenz Number of Chromium, *Phys. Rev. B* 12: 1858–67 (1975).

[16]S. Arajs and G. R. Dunmyre, "Electrical Resistivity of Chromium-Rich Chromium-Iron Alloys Between 40 and 320°K," *J. Appl. Phys.* 37: 1017–18 (1966).

[17]Consultant, Tennessee Technological University, Cookeville.

[18]C. R. Brinkman, R. K. Williams, R. L. Klueh, and T. L. Hebble, "Mechanical and Physical Properties of 2 1/4 Cr-1 Mo Steel in Support of Clinch River Breeder Reactor Plant Steam Generator Design," *Nucl. Technol.* 28: 490–505 (March 1976).

[19]J. W. Massey, T. K. Holder, D. W. Yarbrough, R. K. Williams, and J. P. Moore, "Iron and Dilute Iron Alloys," *Metals and Ceramics Div. Mater. Sci. Annu. Prog. Rep. June 30 1976*, ORNL-5182, p.44.

[20]T. K. Holder, *Thermal Conductivity, Electrical Resistivity and Seebeck Coefficient of High Purity Iron and Selected Iron Alloys from 90 K to 400 K*, ORNL/TM-5539 (June 1977).

Lattice strain scattering[21] plays a significant role in Fe-Ni and Fe-Ti alloys, but the analysis is complicated by shifts in W_{ep}. This difficulty could be resolved with data at lower temperatures. At present, the analysis indicates that the lattice strain scattering of phonons is only about one-fifth as large as the theoretical predictions.[21]

3.2.2.3 Electron-Phonon Scattering in Metals — R. K. Williams

The interaction of phonons with the conduction electrons, W_{ep}, limits the lattice thermal conductivity of metals at low and intermediate temperatures.[22] This parameter must therefore be defined if credible estimates of λ_p are needed; and, in addition, it may provide a useful tool for studying the electron-phonon interaction.[23] Literature data on Cu, Ag, Au,[23] Pt, and Pd[24] and our data on Fe, Mo, W, and Ta were combined by use of existing theory[22] to produce a semiempirical correlation, which should be useful in estimating W_{ep} values for alloys. The correlation, which may require further modification, involves the electronic specific heat constant, γ, and β, the linear temperature dependence of ρ:

$$W_{ep}(T = \infty) \approx 0.2\gamma\beta \ ,$$

where γ is in mJ/mol K^2 and β is in $\mu\Omega$ m/K.

The maximum deviation of the data is about a factor of 3, and this is probably near expectations because the results for transition metals do not exactly follow the theoretical formula[22] and the experimental uncertainties are large. Estimates based on this approach should still be useful because the $W_{ep}(T = \infty)$ values for the nine metals vary by a factor of about 175, and in some transition metals, such as Ta, the electron-phonon scattering appears to be much larger than the three-phonon umklapp resistance even at room temperature. The correlation can also be combined with the theoretical temperature dependence[22] to estimate W_{ep} at lower temperatures.

---

[21]B. Abeles, "Lattice Thermal Conductivity of Disordered Semiconductor Alloys at High Temperatures," *Phys. Rev.* 131: 1906–11 (1963).

[22]J. M. Ziman, *Electrons and Phonons*, p. 321, Oxford University Press, London, 1960.

[23]W.R.G. Kemp and P. G. Klemens, "The Lattice Thermal Conductivity of Alloys," *Aust. J. Phys.* 13: 247–254 (1960).

[24]R. Fletcher and D. Greig, "The Lattice Thermal Conductivity of Some Palladium and Platinum Alloys," *Philos. Mag.* 16: 303–315 (1967).

3.2.2.4 Niobium — J. P. Moore and R. S. Graves

A technique for measuring the residual resistivity ratio [RRR = $\rho(273\ K)/\rho(4.2\ K)$] of superconducting alloys was developed. The RRR of the commercially pure Nb, for which λ will be measured by the radial heat flow technique, was 36. This indicates an impurity level that is too low to have a measurable effect on the high-temperature λ. The best specimen of pure Nb obtained to date had an RRR of 330, but this value varied with heat treatment. The radial heat flow chamber for measuring λ of Nb and other materials at high temperature has been completed.

3.2.2.5 Some Transport and Thermomagnetic Properties of Pure Nickel and a Nickel-Base Thermocouple Alloy — J. P. Moore and R. S. Graves

It was recently shown[25] that the Ettingshausen-Nernst coefficient, Q, of Alumel (Ni–3% Mn–2% Al–1% Si–0.5% Co) must be much larger than literature values to explain the large thermocouple errors encountered when Alumel was used in magnetic fields. Confirmation of the errors in previous Q results is difficult since direct measurements of Q require experimental boundary conditions even more rigid than those required for measurements of λ. An existing technique for measuring λ was modified to permit direct measurements of Q, λ, ρ, S, Righi-Leduc coefficient, and Hall coefficient versus temperature.

The Q results are shown in Fig. 3.1 as a function of reduced temperature (T/Curie temperature) with values from a previous investigation[26] on Ni and implied Alumel results[25] for comparison. The present results show that the Q of Alumel is about 3 times that of pure Ni and is more than sufficient to cause the large errors observed in Chromel-vs-Alumel thermocouples below T_c of Alumel. The present results show that literature values[27] of Q were in error by factors of 1300 and 1100 for Ni and Alumel, respectively. There are several reasons for the low "implied" values for Alumel, and these have been discussed by Kollie et al.[25] The transport property data are being analyzed and compared to other data on Ni-base alloys.

---

[25]T. G. Kollie et al., "Large Thermocouple Errors Caused by Magnetic Fields," *Rev. Sci. Instrum.* 48(5): 0076–0086 (May 1977).

[26]A. W. Smith, "The Transverse Thermomagnetic Effect in Nickel and Cobalt," *Phys. Rev.* 33: 295–306 (1911).

[27]C. Loscoe and H. Mett, "Limitations in the Use of Thermocouples for Temperature Measurements in Magnetic Fields," pp. 283–87 in *Temperature, Its Measurement and Control in Science and Industry*, vol. 3, Part 2, ed. by A. I. Dahl, Reinhold, New York, 1962.

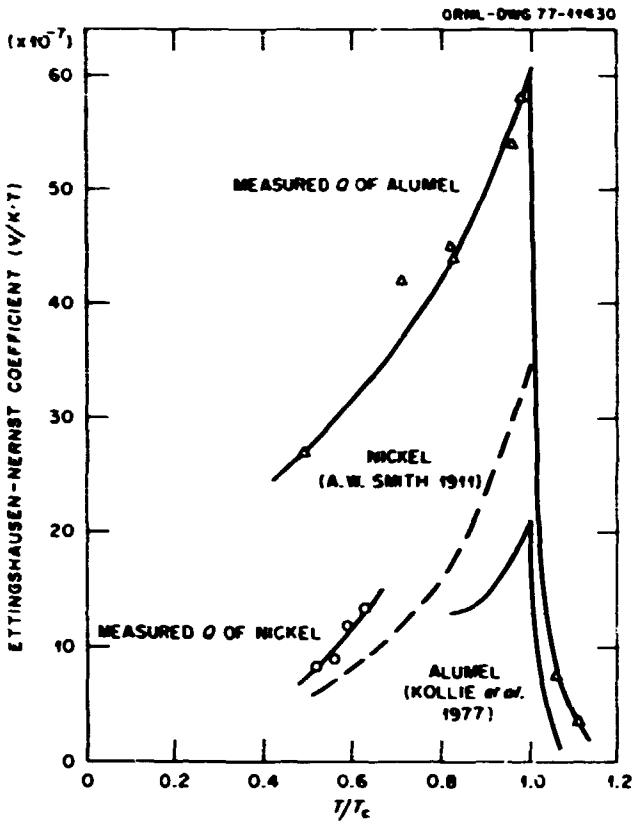

Fig. 3.1. The Ettingshausen-Nernst Coefficient for Nickel and Alumel as a Function of Reduced Temperature (T/T_c).

3.2.2.6 Thermal Expansion Coefficient of Nickel[28] — T. G. Kollie[29]

A fused-quartz dilatometer was used to measure the α of Ni between 300 and 1000 K. Measurements on National Bureau of Standards certified Cu and W standards with the dilatometer established the uncertainty in the α measurements on Ni as ±0.8% (±0.10 × 10^{-6}/K), except within ±2 K of the Curie temperature T_c, where the uncertainty was about ±1.6%. Results of 37 investigations of the expansion of Ni reported in the literature were anlayzed critically, resulting in a compilation of α of Ni from 0 to 1500 K. Theories of thermal expansion were employed to separate α into its paramagnetic α_p and magnetic α_m components. The calculated values of α_m near T_c were fitted to the power law equation $\alpha_m = A(t^{-a} - 1)a^{-1} + B$, which describes critical phonomenon near the critical temperature [$t = (T - T_c)/T_c$]. It was demonstrated

---

[28]Abstracted from T. G. Kollie, "Measurement of the Thermal Expansion Coefficient of Nickel from 300 to 1000 K and Determination of the Power Law Constants Near the Curie Temperature," accepted for publication in *Physical Review B*

[29]Present address, Development Division, Oak Ridge Y-12 Plant.

that the critical exponents above and below T_c, $\underline{a}$, and $\underline{a}'$, respectively, are the same as those derived from specific heat measurements and that $\underline{a} = \underline{a}' = -0.093$ (± 0.010) in agreement with scaling laws of critical phenomenon.

3.2.3 Related Projects

Other programs provide support for physical property determinations, which feed back and interact with work supported by the Division of Physical Research. Generally this related work has broadened the scope of our DPR effort, as indicated by the examples described below.

3.2.3.1 ASTM Comparative Heat Flow Technique — J. P. Moore

We use a comparative technique for measuring λ of small specimens over a limited temperature range. This technique is similar, in principle, to ASTM C 408-58. Although this general technique is infamous for its errors, many instruments of this type are being used to measure on materials of interest to energy production, such as salts (nuclear waste storage), composites (MHD), and coal. Since this technique has subtle error sources, we have chaired an ASTM committee to describe an improved technique, which would be subject to less error. Computer modeling studies have been combined with results from the literature to write a draft for a new standard technique. All our heat flow modeling has been switched over to the more powerful and flexible HEATING5 program.

3.2.3.2 High-Temperature Thermocouple Thermometry — R. K. Williams

Stable temperature sensors are required for all λ measurements, and thermocouple decalibration often causes serious errors in high-temperature λ measurements. Normal practice has been to use Al_2O_3-insulated Pt—10% Rh vs Pt thermocouples in direct contact with the specimen-furnace environment for measurements up to about 1300 K. A 1673 K 3.6 Ms drift test of a type B (Pt—30% Rh vs Pt—6% Rh) thermocouple in a reducing environment showed higher temperature measurements to be feasible if special precautions are taken. Decalibration rates as low as 10^{-5}K/s could be achieved. The decalibration is due to solution of aluminum in the thermoelements, and improvements may be attained by using another oxide insulation and including more protective thermocouple sleeving materials.

3.2.3.3 Thermal Expansion Measurements — D. L. McElroy and F. J. Weaver

Our pushrod dilatometer (Sect. 3.2.2.6), which is used to obtain α data from 300 to 1000 K, was modified and now obtains length data

with a standard deviation of less than 15 nm. The modified system was calibrated with an NBS fused-quartz standard and used to measure the irradiation-induced reduction of α on HTGR fuel rods, the α slope increase near 700 K due to disordering in Inconel 718, and the α behavior of an *ad hoc* graphite expansion standard and of a 2 1/4 Cr-1 Mo steel.

3.2.3.4 Insulation Evaluation — D. L. McElroy and S. H. Jury[30]

The energy conservation potential of industrial and building thermal insulations is well recognized; however the data base for heat transmission in thermal insulations is weak. An insulation evaluation project is in progress to improve knowledge and understanding of present products. Characterizations and thermal property tests are being conducted on high-temperature ceramic fiber insulations because adequate reference standards do not exist for thermal conductance measurements on thermal insulations; we helped an ASTM 16.30 Working Group address this problem, and recommended[31] a set of candidate materials to OSRM-NBS. Various ASTM thermal property test prescriptions are used to test insulations. We conducted heat flow calculations on the ASTM pipe tester using the HEATING5 program, and this revealed the merits of a much simplified design.

3.2.3.5 Isotropic Polycrystalline Graphite — J. P. Moore and R. S. Graves

The thermal conductivity of an isotropic polycrystalline graphite was measured from 80 to 400 K. This graphite may be issued by the National Bureau of Standards as a reference material, and these data will be used to establish λ at low temperatures.

3.3 SUPERCONDUCTING MATERIALS — D. M. Kroeger

We study the effects of metallurgical variables on the properties of superconducting materials. The superconducting property most structure sensitive appears to be current-carrying capacity in an applied magnetic field. It is affected by microstructural variables such as grain size, dislocation density and distribution, and morphology, composition, and volume fraction of second-phase particles. Meaningful correlation of structure and properties requires detailed knowledge

---

[30]Consultant, University of Tennessee, Knoxville.

[31]ASTM Subcommittee C16.30 "Reference Materials for Insulation Measurement Comparisons," Symposium on Advances in Heat Transmission Measurements on Thermal Insulation Materials and Systems, Philadelphia, Sept. 19–20, 1977.

of both. Consequently, some of our effort is devoted to obtaining basic metallurgical information on phase diagrams, transformation kinetics and products, and the microstructures that result from them in superconducting alloy systems. We correlate current-carrying capacity with the "model" microstructures.

Our laboratory has facilities to measure most superconducting properties of interest, such as critical current density, J_c, ac losses, superconducting-to-normal transition temperature, T_c, and upper critical field, H_{c_2}. We also measure low-temperature specific heat and effects of stress on superconducting properties.

Work this year has been primarily in three areas: (1) flux pinning in model materials, such as niobium bicrystals and niobium with radiation-induced voids, (2) studies of so-called advanced materials with high values of T_c and H_{c_2}, (3) mechanical properties of multifilamentary composite conductors and their relationship to the degradation of J_c under tensile stress and to the performance of large high-field magnets. This latter work is carried out in support of an applied program on stress effects in superconductors, which is funded in this group by the Superconducting Magnet Development Program in the Magnetic Fusion Energy Division, ORNL.

3.3.1 Fluxoid Pinning in Bulk Niobium by Voids Produced During Neutron Irradiation[32] — C. C. Koch, H. C. Freyhardt,[33] and J. O. Scarbrough

Fluxoid pinning due to voids has been studied in niobium irradiated at temperatures from 460 to 1080°C. The T_c decreased slightly and H_{c_2} increased with irradiation temperature, indicating possible oxygen contamination. The J_c vs H behavior was more complex, with maximum J_c values obtained in the samples irradiated at 790 and 940°C. With the measured superconducting parameters, and data on void size and distribution, our results were quantitatively compared with expressions for void pinning using the statistical theory of Labusch. Of particular interest in this study was the sample irradiated at 790°C, which has an ordered void superlattice.

---

[32]Abstracted from a paper presented at the 1976 Applied Superconductivity Conference and published in *IEEE Trans. Magnetics* MAG-13(1): 828–31 (January 1977).

[33]Institut für Metallphysik, Universität Göttingen, Gottingen, Germany.

3.3.2 Preparation and Superconducting Properties of Lithium Titanate[34] — U. Roy,[35] A. DasGupta, and C. C. Koch

The T_c of lithium titanate can be as high as 13.7 K and its H_{c2} (4.2 K) as high as 18 T, but reported critical current densities have been quite low. Values of the normal-state resistivity, the electronic specific heat coefficient, and T_c inserted into the Gorkov-Goodman expression yield too large a value for H_{c2}. Lithium titanate specimens were prepared by several methods and characterized by optical metallography, x-ray diffraction, critical temperature (T_c), and $J_c(B)$ measurements. Both the low J_c values and the discrepancy in the calculated value of H_{c2} are due to the presence of a previously unreported nonsuperconducting phase.

3.3.3 Temperature Increases in Superconducting Composites as a Result of Tensile Strains[36] — D. S. Easton, D. M. Kroeger, and A. Moazed[37]

Temperature increases were measured in both pure copper and superconducting Nb-Ti multifilamentary composites as functions of tensile stress and strain at 4.2 K. Thermoelastic behavior was found at room temperature but could not be detected at 4.2 K. Measurements were made under near-adiabatic conditions in vacuum. The composite conductors showed temperature rises at stress levels as low as 34.4 MPa (5000 psi). With initial strains of about 0.2%, ΔT increases of several degrees were found. Cyclic loading and unloading produced a linear increase in temperature with a slope dependent upon cycle frequency. This is in agreement with stress-strain curves of these composites, which exhibit hysteretic loops upon cyclic stressing. The areas of these loops represent thermal energy losses to the system. Temperature increases in pure copper were related only to the extent of plastic strain.

3.3.4 Stress-Induced Heating in Commercial Conductors and Its Possible Influence on Magnet Performance[38] — D. M. Kroeger, D. S. Easton, and A. Moazed[37]

Calorimetric measurements show that significant amounts of heat are generated when a multifilamentary composite conductor is stressed

---

[34]Abstracted from a paper presented at the 1976 Applied Superconductivity Conference and published in *IEEE Trans. Magnetics* MAG-13(1): 836–39 (January 1977).

[35]Solid State Division, presently at U.S. Patent Office, Washington, D.C.

[36]Abstracted from a paper presented at the Metallurgical Society of AIME Fall Meeting, Sept. 20–23, 1976, Niagara Falls, New York.

[37]University of Tennessee, Knoxville.

[38]Abstracted from a paper presented at the 1976 Applied Superconductivity Conference and published in *IEEE Trans. Magentics* MAG-13(1): 120–23 (January 1977).

in tension to levels expected in large, high-field magnet systems. When the stress on the conductor is repetitively cycled between zero and some maximum value, the amount of heat produced per cycle is constant after the first few cycles. Calorimetric determinations of heat injections are compared with the work done on the specimen as indicated by stress-strain curves. Stress-strain curves for a number of commercial conductors indicate that the properties of the matrix material determine to a large degree the magnitude of this effect.

3.3.5 Stress Effects on the Current Densities of Commercial Conductors at 4.2 K in Magnetic Fields[39] — D. S. Easton

Stress-strain curves at 4.2 K have been obtained for a wide variety of commercial multifilamentary (MF) composites with either Nb-Ti or Nb_3Sn filaments. The critical current density, J_c, was also measured as a function of tensile stress in magnetic fields to 7 T. Differences in stress-strain curves between conductors were primarily due to the type of matrix and superconductor-to-normal-material ratio. Tensile properties were close to those predicated by the rule of mixtures. The Nb-Ti conductors showed only small degradation in J_c with stress-strain (~15% at 2.0% strain), and this was recoverable to within 1 or 2% upon the release of stress. The J_c data on these composites was very reproducible. Both cabled and solid conductors containing Nb_3Sn filaments were studied. There was wide scatter in the J_c data, even for a particular conductor. Some samples showed immediate degradation with the onset of stress and did not exhibit any appreciable recovery, while the J_c of others increased at strains up to 0.2 to 0.3% before showing degradation. These latter samples also showed substantial recovery upon the release of stress.

3.3.6 Mechanical Behavior and Stress Effects in Hard Superconductors — A Review[40] — C. C. Koch and D. S. Easton

The mechanical properties of type II superconducting materials are reviewed as well as the effect of stress on their superconducting properties. The bcc alloys Nb-Ti and Nb-Zr exhibit good strength and extensive ductility at room temperature. Mechanical tests on these alloys at 4.2 K revealed serrated stress-strain curves, nonlinear elastic effects and reduced ductility. The nonlinear behavior is believed to be due to twinning and de-twinning or a reversible stress-induced martensitic tranformation. The brittle A-15 compound superconductors, such

---

[39] Abstracted from a paper presented at the Applied Superconductivity Conference, Stanford University, Calif., August 1976.

[40] Abstracted from an invited paper presented at the Metallurgical Society of AIME Fall Meeting in Niagara Falls, N.Y., Sept. 20–23, 1976, to be published in *Cryogenics*.

as Nb_3Sn and V_3Ga, exhibit unusual elastic properties and structural instabilities at cryogenic temperatures.

Multifilamentary composites consisting of superconducting filaments in a normal metal matrix are generally used for superconducting devices. The mechanical properties of alloy and compound composite tapes and composites of Nb(C,N) chemically vapor deposited on high-strength carbon fibers are presented. Hysteretic stress-strain behavior in the metal matrix composites produces significant heat generation, an effect that may lead to degradation in performance of high-field magnets. Measurements of the critical current density, J_c, under stress in a magnetic field are reported. Modest stress-reversible degradation in J_c was observed in Nb-Ti composites, while more serious degradation was found in Nb_3Sn samples.

The importance of mechanical behavior on device performance is discussed.

3.3.7 Distribution of Transport Currents in Type II Superconductors Investigated by Neutron Small Angle Scattering[41] — J. Schelten[42] and D. M. Kroeger

Neutron diffraction experiments have been performed on Nb-13% Ta specimens in order to obtain information about the distribution of transport currents in type II superconductors. In specimens with homogeneous flux pinning we demonstrated that a transport current was carried in the bulk, while in a specimen where surface pinning dominated the transport current was essentially carried on the surface. All experimental results could be explained by specific predictions of the critical state model.

3.3.8 Flux Pinning by Crystal Boundary in Niobium Bicrystals[43] — A. DasGupta, Y. T. Chou,[44] C. C. Koch, and D. M. Kroeger

To study flux pinning by crystal boundaries in type II superconductors, resistive critical current, I_c, was measured in cylindrical bicrystal samples of niobium, where the boundary is parallel to the cylinder axis. We measured I_c as a function of the applied magnetic field, H, and the angle, ϕ, between the field and the crystal boundary in as-grown, chemically polished, and surface oxidized (5 min at 400°C in air) states of the specimens. Very narrow peaks in $I_c(\phi)$ have been

---

[41] Abstracted from pp. 473–80 in *Proc. Conf. Neutron Scattering* (held in Gatlinburg, Tenn., June 6–10, 1976), Vol. 1, CONF-760601-P1.

[42] Institut für Festkörperforschung, Kernforschungsanlage, Jülich, West Germany.

[43] Abstracted from a paper presented at the American Physical Society Meeting in San Diego, Calif., March 21–24, 1977.

[44] Lehigh University, Bethlehem, Pa.

found at $\phi = 0$ with half-intensity width $\leq 1°$ and peak heights up to about 7 times the values at angles off the peak. The present experimental results provide the first direct evidence that the crystal boundary can carry large critical currents.

3.3.9 Work in Progress

3.3.9.1 Flux Pinning by Grain Boundaries — A. DasGupta, D. M. Kroeger, C. C. Koch, and Y. T. Chou[44]

It is generally accepted that flux is pinned in high-field A-15 structure superconductors primarily by grain boundaries. The initial work on niobium bicrystals has demonstrated that from such specimens one can determine unambiguously the basic interaction force between the flux line and grain boundary. Therefore, these measurements are being extended to A-15 materials. The measurements made so far have been on samples with tilt boundaries in which the anisotropy of H_{c2} should play no role. Since, in the case of twist boundaries, H_{c2} anisotropy should lead to pinning, this study will be extended to bicrystals containing such boundaries.

3.3.9.2 Flux Pinning by Small Perturbations of the Order Parameter — A. DasGupta and D. M. Kroeger

Following the first-order perturbational approach of Campbell and Evetts[45] to the Ginzburg-Landau free energy, variations of the upper critical field, H_{c_2}, and Ginzburg-Landau parameter, κ, have been considered and combined for a single-phase material. Upon optimizing, the interaction energy E_{int} between the fluxoid lattice and the pin yields three independent $E_{int}(b)$ solutions, where b is the reduced magnetic induction B/B_{c_2}. The elementary pinning force, f_p, scales with b; it shows a minimum at $b \approx 0.3$ and a maximum at $b \approx 0.65$. These calculations have been used to explain some important and hitherto unexplained experimental results from the literature.

3.3.9.3 Investigation of the Causes of Recoverable Degradation of J_c in Composite Conductors — D. M. Kroeger, D. S. Easton, J. O. Scarbrough, and A. DasGupta

Study of the effects of stress on the critical current density J_c in multifilamentary composite conductors consisting of fine filaments of Nb_3Sn in a bronze matrix has revealed that a portion of the reduction in J_c under tensile stress is recovered when the load is relieved.

---

[45] A. M. Campbell and J. E. Evetts, *Adv. Phys.* 21: 199 (1972).

It was also shown that tensile stress affects the critical temperature, T_c. An apparatus has been constructed to measure the upper critical field H_{c2} as a function of temperature under stress, and preliminary measurements have been made. These results are expected to contribute to understanding the mechanisms by which stress affects J_c, H_{c2}, and T_c.

3.3.9.4 Superconductivity in $LiTi_2O_4$ and $PbMo_6S_8$ — A. DasGupta, D. M. Kroeger, and U. Roy[35]

Work on $PbMo_6S_8$ has continued, with emphasis upon preparation techniques and the question of why only very low critical current densities have been observed in this material. The next step with $LiTi_2O_4$ will be an effort to prepare single-phase spinel material. Magnetization measurements have been performed on specimens of both materials.

3.3.9.5 Microstructural Studies of High-Field Superconductors — D. S. Easton, A. DasGupta, D. M. Kroeger, and R. E. Worsham[46]

A program to use x-ray diffraction and electron microscopy to study the microstructure, crystal structure, and possible phase transitions in A-15 and other high-field superconductors is in progress.

---

[46]Physics Division, ORNL.

4. RADIATION EFFECTS

J. O. Stiegler and K. Farrell

The Radiation Effects program has as its goal the understanding of changes in the physical and mechanical properties of metals and alloys resulting from elevated-temperature neutron irradiation. The focus of the work is on effects of composition and microstructure, with the aim of using these metallurgical variables to minimize or control the damage. Although the objective of the program is an understanding of the effects of neutron irradiation, simulation techniques that allow accelerated testing and evaluation of mechanisms are exploited. Both experimental and theoretical approaches are employed.

Work on this program complements the radiation effects activities in the ORNL Solid State Division, which are directed at describing the primary production of point defects by particle irradiation. The effort in the Metals and Ceramics Division is concerned with the organization of these defects into more complex configurations and with the properties of materials after large irradiation exposures. This work parallels applied programs in the Metals and Ceramics Division supported by the Breeder and Magnetic Fusion Reactor Programs but is aimed at uncovering mechanisms of damage by studying simple or model systems. In this report only work supported by the Division of Physical Research is described. Activities in the other programs are summarized in the progress reports for those programs.

4.1 EXPERIMENTAL STUDIES

4.1.1 Control of Radiation Damage Structure and Swelling in Aluminum by Alloying — K. Farrell and J. T. Houston

The role of alloying elements in the development of neutron damage structure and swelling in aluminum is being studied in dilute, binary solid-solution alloys based on high-purity aluminum. Specific alloying elements are Ag, Ca, Cr, Cu, Fe, In, Mg, Mn, Ni, Si, Sn, Ti, V, Zn, and Zr. Since most of these have low solid solubility in aluminum below 400 K, their concentration levels are maintained in the range of 100 at. ppm. We are investigating Zn and Mg, which have appreciable solubility, along with Cu, Si, and Mn at the 100 at. ppm level and at several higher levels. Specimens have been irradiated in HFIR at about 350 K to damage levels between 3×10^{-3} and 3 displacements per atom (dpa) to encompass the early stages of development of damage structure. Examination of the specimens by transmission electron microscopy is not yet complete, but the following general conclusions can be stated:

1. Not all the above alloying elements at the 100 at. ppm level significantly alter the microstructure and suppress swelling; Ag, Ca, Fe, In, Mg, Ni, Si, Sn, and Zn are seemingly ineffective. However,

before irradiation, the Fe, In, and Ni alloys contained coarse second-phase particles rich in the alloying element, so these particular alloys may have had very little alloying element in solid solution.

2. The elements Cr, Cu, Mn, Ti, V, and Zr suppress void formation, with Cu being effective at a level as low as 25 at. ppm. At levels of 1000 at. ppm or more, Mg and Si are effective void suppressants.

3. Where swelling is diminished, the average size of voids is not greatly changed, but the concentration of voids is reduced, implying that alloying elements have a larger effect on void nucleation than on void growth.

4. In all cases of void suppression, the development of dislocation structure is either delayed or is significantly different from that in the unalloyed reference aluminum; usually growth of dislocation loops into a general dislocation structure is retarded.

5. Radiation-induced precipitates are obvious at the highest fluence in the Cu, Si (1000 at. ppm), and Zn alloys. In the Cu and Si systems the concentrations, sizes, and spatial distribution of the precipitate particles are the same as those of loops at lower fluence; voids are sparse or absent. The Zn alloys show extensive radiation-induced precipitation but no obvious suppression of voids. In the Cr, Mn, Ti, V and Zr alloys, where void formation is diminished, tiny, unanalyzed clusters can just be resolved. Analysis and identification of the precipitate particles are complicated by particles of transmutation-produced silicon, whose nature seems to be affected diversely by different alloying elements.

An early assessment of the observations indicates that, while there is no sensible connection of swelling resistance with partial diffusion coefficients of the alloying elements, there may be a relationship with the degree of atomic misfit in the aluminum lattice; swelling is most strongly retarded by those alloying elements that have significant negative lattice misfit. Also, the swelling-resistant alloys are apparently those in which the solid solubility of the alloying element is low but finite at the irradiation temperature.

These observations suggest that suppression of void formation may be associated with binding between point defects and impurity atoms and/or retarded development of dislocation structure from radiation-induced segregation and precipitation of alloying elements at dislocation loops, which are major vacancy and interstitial sinks. The latter is itself a consequence of binding between point defects and impurities.

4.1.2 Solute Segregation in Stainless Steel Under Irradiation — Edward A. Kenik

Solute element additions can significantly influence the damage response of an alloy under irradiation (see Sect. 4.1.1, for example). A modified type 316 stainless steel, designated LS1A, has been developed and exhibits high resistance to swelling during ion bombardment. This alloy, containing additions of 1.0 wt % Si and 0.15 wt % Ti, swells 1/30 as much under nickel ion irradiation as does a nominal type 316 stainless steel. The evolution of dislocation portions of the damage

structure is modified by the silicon and titanium additions. Specifically, the stability of faulted dislocation loops in LSlA is quite high, and the growth of large loops is severely curtailed compared with steels containing lesser amounts of Si and Ti. At high exposures, radiation-induced precipitates of the same particle size and shape as the dislocation loops are observed. Since the growth of the dislocation and void substructures are strongly correlated, the swelling resistance of the alloy may be related to the behavior of the dislocation substructure.

Energy-dispersive x-ray microanalysis in an analytical electron microscope was employed to investigate the possibility of solute segregation of silicon or titanium to the faulted loops. This technique allows chemical analysis of volumes approaching 10 nm in diameter. Spot analyses were performed as a function of distance from both edge-on and face-on dislocation loops to determine the spatial distribution of alloying elements. The only indications of titanium in the alloy were blocky particles that appeared in both irradiated and unirradiated foils and were presumed to be carbides. High concentrations of silicon were detected in association with the fault plane of the Frank loop (Fig. 4.1). However, the distribution of excess silicon near the loop was not strongly localized at the fault plane, but was more like a spherical atmosphere surrounding the loop. The silicon concentration at the fault plane could not be measured directly, since the excited volume contained finite concentration gradients irrespective of the loop orientation. If some reasonable assumptions on the nature of the gradients are made, the silicon concentration can be estimated as 3.5 wt %. In addition, the radiation-induced precipitate particles were silicon-rich and were tentatively identified as possessing the $M_{23}C_6$ structure. From the similarities in composition, size, and shape between the faulted loops and the precipitates, we postulate that continued silicon segregation occurs at the dislocation loops until the second-phase precipitate particles are generated.

4.1.3 Phase Instability Studies — R. W. Carpenter, Edward A. Kenik, and M. H. Yoo

The understanding of phase instability in alloys undergoing energetic particle irradiation is essentially an extension of phase transformation theory into the region of large point defect concentration. Experimental neutron irradiation of aluminum-copper alloys containing coherent precipitates formed before irradiation has shown that silicon, formed by transmutation of a small amount of the aluminum in the alloy, precipitates at the interfaces between the initially coherent precipitate and the matrix.[1]

The silicon precipitate is crystalline, not amorphous. In addition, a smaller amount of silicon is precipitated on the surfaces of voids

---

[1]R. W. Carpenter and M. H. Yoo, paper presented at the 1977 AIME Annual Meeting, Atlanta, to be published.

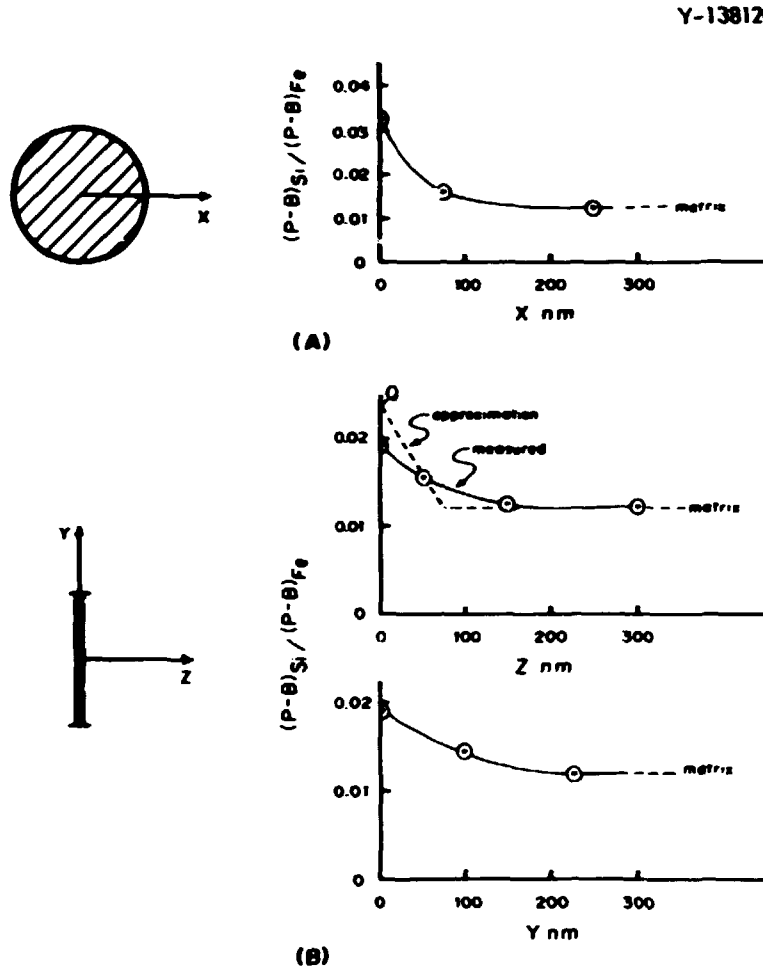

Fig. 4.1. Measured Silicon-to-Iron Count Ratio Profiles Typical for Faulted Dislocation Loop in LS1A Ion-Irradiated to 3 dpa at 900 K. (a) Burgers vector parallel to electron beam. (b) Burgers vector perpendicular to beam. Broken curve is linear approximation of actual silicon/iron profile.

and in the matrix of the same alloy. The solubility of silicon in aluminum is small, and this behavior could be interpreted as simply radiation-enhanced diffusion leading to silicon precipitation at the irradiation temperature, 325 K.

Experiments were conducted[2] on Ni–20 at. % Mo alloys with 4-MeV nickel ions and with 1-MeV electrons in the HVEM. A small amount of a new phase was formed and had a different lattice symmetry than any compounds known to form at the 20-at. % Mo composition. Analytical electron microscopy showed the composition of the new phase to be nearly 50 at. % Mo. The formation of such a phase cannot be explained

[2]R. W. Carpenter, E. A. Kenik, and R. J. Bayuzick, paper presented at the 1977 AIME Annual Meeting, Atlanta, to be published.

on the basis of equilibrium thermodynamics and radiation-enhanced diffusion, unless it is attributed to impurity contamination during irradiation and subsequent precipitation of a new phase. Our present evidence does not support this point of view.

The new phase may be considered a result of transport of molybdenum to sinks by diffusion of point defects, resulting in high local molybdenum concentrations,[3] or possibly a shift in thermodynamic equilibrium because a new pseudo "standard state" is defined when the alloy is in the displacive radiation field.[4] The new "standard state" would take into account the high steady-state point defect concentration. Alloys of Ni–20 at. % Mo exhibit metastable short-range order (SRO) before attaining long-range order (LRO), the equilibrium state. Both types of order are detectable by electron diffraction methods. Our radiation effects experiments showed that SRO is stable under ion irradiation, but LRO is the stable phase under 1-MeV electron irradiation; thus, the concept of phase stability is demonstrated further. The instability of LRO under nickel-ion irradiation is attributed to the "mixing" effect of displacement cascades formed during heavy particle irradiation. Cascades are not formed during 1-MeV electron irradiation.[4]

Further experimental work is being done on both alloy systems to develop a detailed description of the composition and crystallography of the phases formed under irradiation. The alloys being investigated are model systems. One of the primary reasons these particular alloy systems were chosen was their well-understood phase transformation behavior in the absence of irradiation. Some theoretical calculations to model the irradiation behavior of the aluminum-copper alloys have begun.[1]

4.1.4 Effects of Chemical Ordering and Coherent Precipitation on Void Nucleation During Irradiation — R. W. Carpenter, Edward A. Kenik, and M. H. Yoo

Last year we reported[5] that a number of model alloys containing a fine, densely dispersed coherent precipitate having tetragonal strain symmetry exhibited strong resistance to void nucleation during neutron or 1-MeV electron irradiation. This work was extended to include chemical ordering effects on void nucleation. The LRO phase in nickel-molybdenum alloys is tetragonal, and the strains associated with SRO may also be expected to be tetragonal. Nickel-molybdenum alloys

---

[3]N. Q. Lam et al., "Radiation-Induced Solute Segregation and Precipitation in Alloys," paper presented at the 1977 AIME Annual Meeting, Atlanta, to be published.

[4]S. I. Maydet and K. C. Russell, "Precipitate Stability Under Irradiation: Point Defect Effects," *J. Nucl. Mater.* 64: 101–14 (1977).

[5]R. W. Carpenter and J. C. Ogle, "Void Nucleation in Alloys," *Metals and Ceramics Div. Mater. Sci. Annu. Prog. Rep. June 30, 1976*, ORNL-5182, pp. 60–1.

containing SRO or small-domain-size LRO were irradiated over the temperature range 675 to 950 K with 1-MeV electrons or 4-MeV nickel ions at exposures up to 100 dpa; transmission electron microscopy showed no evidence for void nucleation. Other nickel-molybdenum alloys, in which no diffraction evidence for any type of order was found, did nucleate voids under identical irradiation conditions. The latter alloys were more resistant to void swelling than elemental nickel, but voids were clearly present at 100 dpa and a large amount of swelling occurred for exposures of about 200 dpa (nickel ion irradiation) at 900 K.

A further indication of the important influence of dense coherent precipitation on void swelling resulted from the continuing research of Gessel and Rowcliffe.[6] The void swelling response of Fe–21 at. % Ni–8 at. % Cr alloys was examined as a function of increasing aluminum additions. The irradiation conditions were 4-MeV nickel ions at 925 K, to an exposure of 170 dpa. The swelling dropped precipitously when the aluminum concentration reached 7.8 at. %. Our electron microscopy examination of identical specimens isothermally aged at the irradiation temperature showed the alloy to contain small coherent precipitate particles (~4-nm-diam). Diffraction patterns from these alloys show the precipitate to be ordered. The weak Bragg superlattice maxima are consistent with an $L1_2$ superlattice. In addition, weak diffuse maxima, whose origin may be lattice strains, are found near the fundamental Bragg maxima. This research is continuing.

4.1.5 Characterization of ^{244}Cm Oxide α Sources for Doping Irradiation Samples — N. H. Packan and W. A. Coghlan

During simulation of neutron radiation damage by heavy-ion bombardment the presence of gas atoms is desirable because helium that is produced by transmutation reactions plays an important role in nucleating voids and dislocation loops. The amount of helium that can be implanted into nickel foils by the alpha decay of a ^{244}Cm source has been determined by vacuum fusion implanted test foils. In addition to these bulk helium-concentration measurements, alpha-alpha scattering measurements were performed. This technique determines the concentration profile as a function of depth, thereby providing a much more sensitive test of our existing theoretical model for this process. These measurements confirm the uniform concentration region near the surface followed by the linearly decreasing region that is predicted by our model. However, the helium concentration values are not consistent with the vacuum fusion results. Much less helium is found in the samples measured by the alpha-alpha scattering. To see if the vacuum fusion results are consistent, we exposed

---

[6]G. Gessel and A. F. Rowcliffe, paper presented at the International Conference on "Radiation Effects in Breeder Reactor Structural Materials," Scottsdale, Ariz., 1977, to be published in the proceedings.

two nearly identical nickel foils to a source at room temperature to obtain expected values of 12 and 120 at. ppm He. The analyses found 12.8 and 131 at. appm. We are not yet able to explain the low concentration values found by alpha-alpha scattering.

4.2 THEORETICAL STUDIES

4.2.1 General Rate Theory Model of Void Swelling and Dislocation Loop Growth in Irradiated Metals — M. H. Yoo, L. K. Mansur, and W. A. Coghlan

We have initiated a program to develop a generalized rate theory model of void swelling and dislocation loop growth in metals under irradiation by fast neutrons or by high-energy charged particles. Based on the recent rate theory model[7] that takes into account both temporal and spatial (one-dimension) dependence of loop growth and void swelling, an efficient computer program will be written to include the following physical effects on void swelling: (1) cascade damage, (2) self-ion deposition, (3) solute trapping and segregation, (4) precipitate particles, (5) evolution of dislocation microstructures, (6) void coalescence, (7) applied stress, and (8) pulsed irradiation.

We will try to develop an improved numerical integration method for solving a system of rate equations. The present model will be applied to correlation studies of void swelling by self-ion and neutron irradiation, and also of void swelling data by step-height measurement and transmission electron microscopy.

4.2.2 Growth Kinetics and 'Preference Factor' of Frank Loops in Nickel During Electron Irradiation — M. H. Yoo and J. O. Stiegler

The growth kinetics of interstitial-type Frank loops in a thin foil of high-purity nickel at 725°K was measured during electron irradiation in a Hitachi high-voltage electron microscope operating at 650 keV. The experimental data were analyzed by use of the general rate theory model,[7] which takes into account both temporal and spatial dependence of loop growth.

The progressive growth of faulted loops was observed at 11 irradiation times ranging from 1 to 62 min, with electron exposures as high as 0.24 dpa. The foil thickness of 0.44 μm was determined stereomicroscopically. The depth positions of 35 loops were also determined.

---

[7]M. H. Yoo, *Dislocation Loop Growth and Void Swelling in Bounded Media by Charged Particle Damage*, ORNL/TM-5789 (April 1977); also accepted for publication in *Journal of Nuclear Materials*.

While the largest and the smallest loops among the 35 measured show the time exponents of $n = 0.9$ and 0.5, respectively, the mean loop radii yield $n = 0.6$. The time dependence agrees well between the measured mean radii and the calculated curves. In the depth position dependence the data points and the calculated curves agree qualitatively. Through systematic variations of the vacancy migration energy, E_v^m, and the preference factor of dislocations for self-interstitials, δ_i, we were able to determine that $E_v^m = 1.2$ eV and $\delta_i = 0.06$ by achieving reasonable consistency between the theoretical model and the experimental data.

4.2.3 Effect of Implanted Interstitials on Swelling During Self-Ion Bombardment — A. D. Brailsford[8] and L. K. Mansur

Bombardment of metals with energetic self-ions is widely used to simulate neutron irradiation. Differences in the resulting swelling may be due to the proximity of a free surface, differences in cascade structures and bombardment temperatures, greatly accelerated defect production rates, and implantation of ions in the specimen.[9] The effects of self-ion implantation are examined here.[10]

A higher production rate for interstitials than vacancies, $G_i = G_v(1 + \varepsilon)$, results from ion implantation. Here G_i and G_v are the net interstitial and vacancy production rates per unit volume and ε^{-1} is the net number of interstitials produced per ion implanted at a point. An expression has been derived for the resulting fractional reduction in swelling rate compared with the case of no implanted interstitials ($\varepsilon = 0$) in terms of material and irradiation parameters. Simplified limiting expressions are given for the extreme cases where most defects are lost by recombination or at sinks:

$$\frac{\delta(dV/d\Delta)}{(dV/d\Delta)_{\varepsilon = 0}} \approx -\left(\frac{Z_i^d + Z_v^d}{Z_i^d - Z_v^d}\right)\frac{\varepsilon\eta^{1/2}}{4} \quad \eta \gg 1 \quad \text{(recombination dominated)}, \qquad (1)$$

valid for $\varepsilon\eta^{1/2}/4\sqrt{2} \ll 1$, and

---

[8]Scientific Research Staff, Ford Motor Company, Dearborn, Mich.

[9]Many of these effects have been examined in the *Proceedings of the Workshop on Correlation of Neutron and Charged Particle Damage,* (held June 8–10, 1976, Oak Ridge, Tenn.), J. O. Stiegler, Comp., CONF-760673.

[10]A. D. Brailsford and L. K. Mansur, submitted to *Journal of Nuclear Materials,* contains a more detailed examination of this problem.

$$\frac{\delta(dV/d\Delta)}{(dV/d\Delta)_{\varepsilon = 0}} \approx -\varepsilon g^{-1}\left(Z_i^v Z_v^d + 4\pi Z_i^v Z_v^v r_v N_v / L\right) \quad \eta \ll 1 \text{ (sink dominated)} , \qquad (2)$$

where

V = void volume fraction;

Δ = G_v × time;

g = $Z_v^v Z_i^d - Z_i^v Z_v^d$, the bias;

$Z_{i,v}^{v,d}$ = capture efficiencies of voids and dislocations for interstitials and vacancies;

r_v and N_v = void radius and concentration;

L = dislocation density;

η = $4RG_v / \sum_j K_i^j \sum_j K_v^j$, which measures the recombination to sink loss rate;

$\sum_j K_{i,v}^j$ = $D_{i,v}(4\pi r_v N_v Z_{i,v}^v + Z_{i,v}^d L)$, the loss rates to sinks per interstitial, vacancy; and

$D_{i,v}$ = diffusion coefficient of interstitials, vacancies.

At low temperature [Eq. (1)] the fractional reduction increases with ε and G_v but decreases with T and $\sum K_{i,v}^j$. Using a typical ε of 3×10^{-4}, the results for a range of temperatures are given in Table 4.1. The results are sensitive to the value of E_v^m, the vacancy migration energy. The conservative value of 1 eV is used (using 1.4 eV, often quoted for nickel, more than doubles the value of fractional reduction shown for 450°C).

Table 4.1. Effect of Implanted Interstitials on Fractional Reduction in Swelling[a]

Irradiation Temperature (°C)	Recombination/Sink Loss Rate Parameter, η	Fractional Swelling Reduction $\delta(dV/d\Delta)/(dV/d\Delta)_{\varepsilon = 0}$
400	257	0.24
450	78	0.13
500	28	0.08
550	11	0.05
600	5	0.03

[a]Parameter values used in these computations are $\varepsilon = 3 \times 10^{-4}$, $Z_v^d = 1.0$, $Z_i^d = 1.01$, $D_v = 19 \exp(-E_v^m/kT)$mm/s, $E_v^m = 1$ eV, k = Boltzmann's constant, $R/\Omega D_i = 10^{20}/m^2$, $G\Omega = 10^{-3}$ defects/atom s, where $\Omega \equiv$ atomic volume.

Where sinks dominate, Eq. (2) applies. Taking the largest reasonable ε of 10^{-3} (ref. 10) and the smallest reasonable g of 10^{-2}, the reduction in swelling rate is less than about 20% if $4\pi Z_i^v Z_v^v r_v N_v / L$ is not much greater than unity. This latter condition is satisfied in many cases.[11] However, in unusual cases when L is very low but voids are present, saturation in swelling can be reached[10] at $V = (gL/\varepsilon)^3 / 3(4\pi N_v)^2$.

These results support the following conclusions:

1. Deposited interstitials decrease swelling at all temperatures.
2. Below the peak swelling temperature, the fractional reduction in swelling increases with decreasing temperature. The swelling at low temperatures, normalized to the peak swelling, is lower for self-ion bombardment than for neutron or electron irradiations.[12]
3. When sinks dominate, the fractional decrease in swelling is not sensitive to temperature. Also, under these conditions swelling will saturate at $V = (gL/\varepsilon)^3/3(4\pi N_v)^2$. This is normally such a high value as to be nonphysical. In rare cases where dislocation density becomes low because of recovery, as for example in pure nickel bombarded to high doses, the saturation swelling may be as low as 10%.

4.2.4 Assessment of the Theory of Void Growth — L. K. Mansur

A review and critical assessment of the theory of void growth have been completed. These are described in a paper[13] in the *Proceedings of the Workshop on Correlation of Neutron and Charged Particle Damage* held at the Oak Ridge National Laboratory in June 1976. Areas requiring further development are defined. The mathematical framework underlying numerical computations needed in modeling the behavior of voids and other elements in the microstructure is developed and analytic expressions are given for certain limiting cases.

Future improvement in capability to extrapolate and translate low-dose neutron data and high-dose charged particle data to predictions for high-dose neutron irradiations requires:

1. an understanding of the complex evolution of dislocation structure with dose and temperature, and
2. an understanding of the detailed mechanisms of impurity action.

---

[11] L. K. Mansur, K. Farrell, and J. O. Stiegler, "Comparison of Void Growth Kinetics in Irradiated Stainless Steels and Pure Metals," *Trans. Am. Nucl. Soc.* 21: 163–64 (1975).

[12] A similar effect due to *vacancy retention* in collapsed cascades is found in R. Bullough, B. L. Eyre, and K. Krishan, *Proc. Roy. Soc.* (London) A346: 81 (1975).

[13] L. K. Mansur, "Void Growth Kinetics: An Assessment of the Theory," pp. 61–109 in *Proc. Workshop Correlation Neutron Charged Particle Damage* (held at Oak Ridge National Laboratory, June 8–10, 1976), CONF-760673.

In particular, current models for the effects of impurity segregation to sinks on point defect capture efficiencies need to be combined with the conceptually separate effects of impurity trapping and impurity depletion due to segregation on point defect recombination in the matrix.

In frequent cases where void nucleation has ceased, where dislocation development with dose can be anticipated, and where the void growth rate at low-dose neutron or high-dose charged particle conditions are available, high-dose neutron swelling can be predicted sucessfully with the previously developed theory for the growth and coalescence of voids.

4.2.5 Influence of a Surface Coating on Void Formation — L. K. Mansur and W. G. Wolfer[14]

Impurities often alter radiation-induced swelling behavior of metals, and the mechanisms by which this might occur are under study. One mechanism by which segregation may affect swelling behavior is through the point-defect image interaction. The interaction between point defects and the coated void has recently been derived.[15] The purpose of this report is to summarize its effect on capture efficiencies of voids for point defects and ultimately on void nucleation and growth; a more detailed report is available.[16]

Bare voids exhibit a preference for interstitials over vacancies. However, for the coated void, the preference is reversed. This produces reductions in critical energy and critical size and accompanying substantial increases in void nucleation rate. In addition when the specific surface energy is decreased, an effect which usually occurs with segregation, the nucleation rate responds with extreme sensitivity, thus further favoring the coated void. Similarly, the growth rate of the coated void is enhanced and the growth kinetics are changed with respect to the bare void.

Void coatings are expected to occur widely on the basis of thermodynamic requirements for adsorption at surfaces as well as impurity drag due to radiation-induced point defect fluxes. Thus, these concepts may have some utility in suggesting interpretations of irradiation-induced swelling behavior in terms of properties of impurities in segregated layers. In addition, the possibility is raised that swelling could be reduced by introducing impurities that would trap segregants in the matrix or by forming precipitates.

---

[14]Department of Nuclear Engineering, University of Wisconsin, Madison.

[15]W. G. Wolfer and L. K. Mansur, *Phys. Status Solidi* 37(a): 211–22 (1976).

[16]L. K. Mansur and W. G. Wolfer, *Influence of a Surface Coating on Void Formation*, ORNL/TM-5670, in preparation.

4.3 FACILITY, EQUIPMENT, AND EXPERIMENT DEVELOPMENT

4.3.1 ORNL Heavy-Ion Bombardment Facility

4.3.1.1 The Dual-Ion Irradiation Facility — G. F. Wells,[17] M. B. Lewis, and N. H. Packan

A 0.4-MeV Van de Graaff ion accelerator is now operational in the 5-MV Ion Bombardment Laboratory. One beam line from the small accelerator connects with the new radiation damage chamber to permit helium or other light ions to be injected at 15° off normal incidence into specimens that are being simultaneously bombarded with heavy ions. A unique feature of the control system of the small accelerator is that it distributes the injected light ions uniformly throughout the volume of material that is being subjected to displacement damage by the heavy-ion beam. This distribution is achieved by ramping the energy of the light ions continuously and automatically over the range 0.2 to 0.4 MeV at 60-s intervals (20-s and 6-s cycles will be available later). Ramping is accomplished by a linear or "sawtooth" variation of the current in the analyzing magnet. This action causes the beam to strike a defining slit whose signal is received by the Van de Graaff energy stabilizing circuit, forcing the VdG energy to change such as to minimize the slit signal and maintain the initial beam direction. Light-ion beam intensities from 0.1 to 100 nA are available with uniformity of beam intensity maintained within ±10% over the entire energy range and ±3% over 80% of the energy range.

An additional feature is an auxiliary beam line in which the beam from the small accelerator can be switched to an ion scattering chamber. Here the beam, collimated to about 1 mm^2, impinges upon a target that can be oriented in one direction relative to the beam. Surface barrier detectors are mounted inside the scattering chamber to measure the precise energy of ions scattering from the target. Plans are being made to use this chamber to implant and measure gases in metal and other types of targets. Preliminary measurements of helium implanted in nickel are presently being carried out, and studies have been initiated with R. A. Perkins, Surface and Solid State Reaction Group, to measure oxygen diffusion profiles in vanadium by a nuclear reaction method.

4.3.1.2 General Facility Improvements — N. H. Packan, R. A. Buhl, M. B. Lewis, and G. F. Wells[17]

As part of a general facility upgrading, a new damage chamber was installed and put into operation during the reporting period. With it, up to six separate specimen modules, each containing as many as nine

---

[17]Physics Division.

3-mm-diam disk specimens, can be ion bombarded before reloading specimens. Cross-checked temperature monitoring is provided by thermocouples and infrared pyrometry. The apparatus has demonstrated an extraordinary stability in holding the selected temperature within 1°C over multihour bombardment runs. Auxiliary equipment on the chamber includes a residual gas analyzer and a mask drive mechanism, whose main function is to assess the beam spatial uniformity with an array of small apertures. The mask can also be used to uncover progressively the middle and upper rows of the 3 × 3 specimen array during a single bombardment, thus obtaining up to three different damage levels in one run. The new chamber is rough-pumped by liquid nitrogen sorption pumps; high vacuum [low 10^{-5} Pa (10^{-7} torr) range] is maintained with a 1 m^3/s cryopump.

In other facility modifications, the beam line section between the final focusing lens and the new radiation damage chamber was replaced with larger diameter electropolished stainless steel tubing having ultrahigh-vacuum joints and is now pumped to 10^{-6} Pa (10^{-8} torr) by a second cryopump. The ion source on the 5-MV Van de Graaff has been modified so that three different beam species can be selected at the control console. The system has been tested in extracting beams of $^{58}Ni^{+}$, $^{51}V^{+}$, and $^{4}He^{2+}$ by remote control.

4.3.1.3 Initial Damage Simulation Experiments in the Dual-Ion Irradiation Facility — K. Farrell and N. H. Packan

Late in this reporting period a 400-keV Van de Graaff accelerator was attached to the 5 MeV Van de Graaff machine to permit simultaneous injection of light ions into the damaged region of specimens undergoing heavy-ion displacement damage. This allows some critical experiments to resolve questions on the role and effects of gases on displacement damage. We have performed the irradiations for two such experiments. The first is concerned with the effects of helium on void formation in pure nickel; here we are comparing the behavior of helium injected at room temperature with that of helium injected simultaneously with heavy ion damage at elevated temperature to see which more closely resembles the damage structures in neutron-irradiated nickel. This is an extension of an on-going program correlating rapid ion damage with neutron damage. The second experiment is a new one aimed at one of the most critical questions facing materials performance in the first wall of a magnetic fusion reactor: What will be the effect(s) of the high He/dpa ratio? In a fusion device undergoing bombardment with 14-MeV neutrons the ratio of the helium production rate to the displacement damage rate will be about 20 at. ppm/dpa, roughly 100 times that in fast-fission reactors. At present the only way to reproduce these ratios is with a dual ion beam facility. Therefore, we have taken a high-purity stainless steel, known to be highly sensitive to swelling, and have bombarded it to two He/dpa ratios, 0.2 and 20, at several dpa levels up to 70 and at temperatures of 850, 900, and 950 K. The peak swelling temperature with cold-preinjected helium is 900 K. We have included some cold-preinjected specimens and have bombarded them with nickel ions at 900 K to compare the effects of pre- and simultaneously injected helium. The microstructures of these specimens will be studied shortly.

4.3.1.4 Operations — M. B. Lewis, M. B. Inman, and F. K. McGowan[17]

During the past year the 5-MV Ion Bombardment Facility was used to make 73 nickel ion bombardment experiments varying from 1 to 300 dpa/bombardment. Damage rates were frequently about 35 dpa/hr, equivalent to a fluence of approximately 5×10^{26} n/m^2 (>0.1 MeV). Experiments were performed with groups from Westinghouse, General Electric, and the ORNL Solid State Division as well as by Metals and Ceramics Division personnel in the breeder reactor alloy development and materials science research groups.

4.3.2 Simulation of Neutron Irradiation Creep — T. C. Reiley, P. G. Jung,[18] R. L. Auble,[17] and M. G. Duncan[19]

During this year the major accomplishment was the completion of our apparatus, which uses a beam of light ions (60-MeV alpha particles from the Oak Ridge Cyclotron, ORIC) to simulate neutron irradiation creep. This construction was finished by the latter part of December, in time for the last cyclotron experiment of this reporting period. (ORIC will resume operations in the mid-summer, 1977, allowing further experiments.) Figure 4.2 shows the apparatus and Fig. 4.3 shows a schematic of the system.

Two cyclotron experiments were performed. The first was concerned primarily with beam handling and characterization. An ionization monitoring device was also tested as a secondary measure of beam currents. The second experiment, in December, was performed to monitor the function of several components of the system, including the data acquistition system and modified version of the temperature control system. The results from this experiment[20] indicated that the specimen temperature during operation at full beam could be controlled to about 0.005 K, and that the thermal transients associated with complete beam loss were negligible after about 0.2 s. An infrared pyrometer, which scanned the specimen during irradiation, showed an acceptable temperature gradient in the specimen (~±10 K). Several components of the apparatus have been modified on the basis of operating experience; these include the load application system, the standard resistor (used to reference the specimen resistance), and a multiplexing device to allow greater data flow capabilities. The apparatus is now ready for irradiation creep experiments.

Several support investigations were initiated. One, the thermal creep testing of thin specimens to determine the effects of specimen thickness (25–200 μm) and environment (vacuum vs helium) on creep rate,

---

[18]Visiting Scientist from KFA, Jülich, West Germany.

[19]Consultant, University of Tennessee.

[20]M. G. Duncan, *Precision Rectifier Detectors for AC Resistance Bridge Measurements with Application to Temperature Control Systems for Irradiation Creep Experiments*, ORNL/TM-5715 (May 1977).

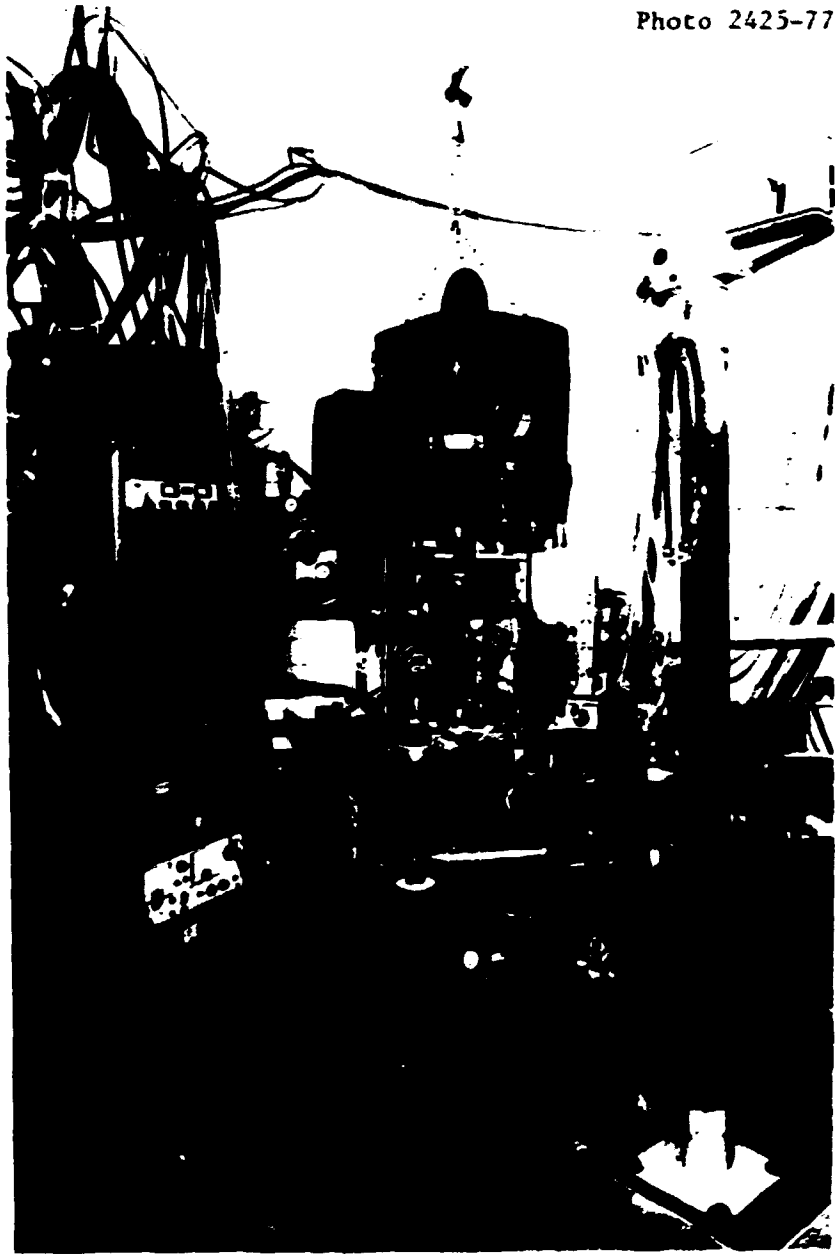

Fig. 4.2. Irradiation Creep Apparatus in Place at the Oak Ridge Isochronous Cyclotron.

a. SPECIMEN, GRIPS, PULLRODS
b. LIQUID NITROGEN-FILLED COOLING BLOCK
c. WATER COOLED PLATES AND SUPPORTS
d. BEAM MASK AND ION COUNTER
e. INFRA-RED PYROMETER (MOVABLE)
f. MOTOR-DRIVEN LOADING DEVICE
g. HELIUM CIRCULATOR AND AMBIENT TEMPERATURE CONTROLLER
h. TO OXYGEN METER AND GAS PURIFIER
i. BEAM LINE
j. CONTAINMENT VESSEL
k. HELIUM INLET
l. FARADAY CUP PORT
m. TO COLD TRAP AND DIFFUSION PUMP

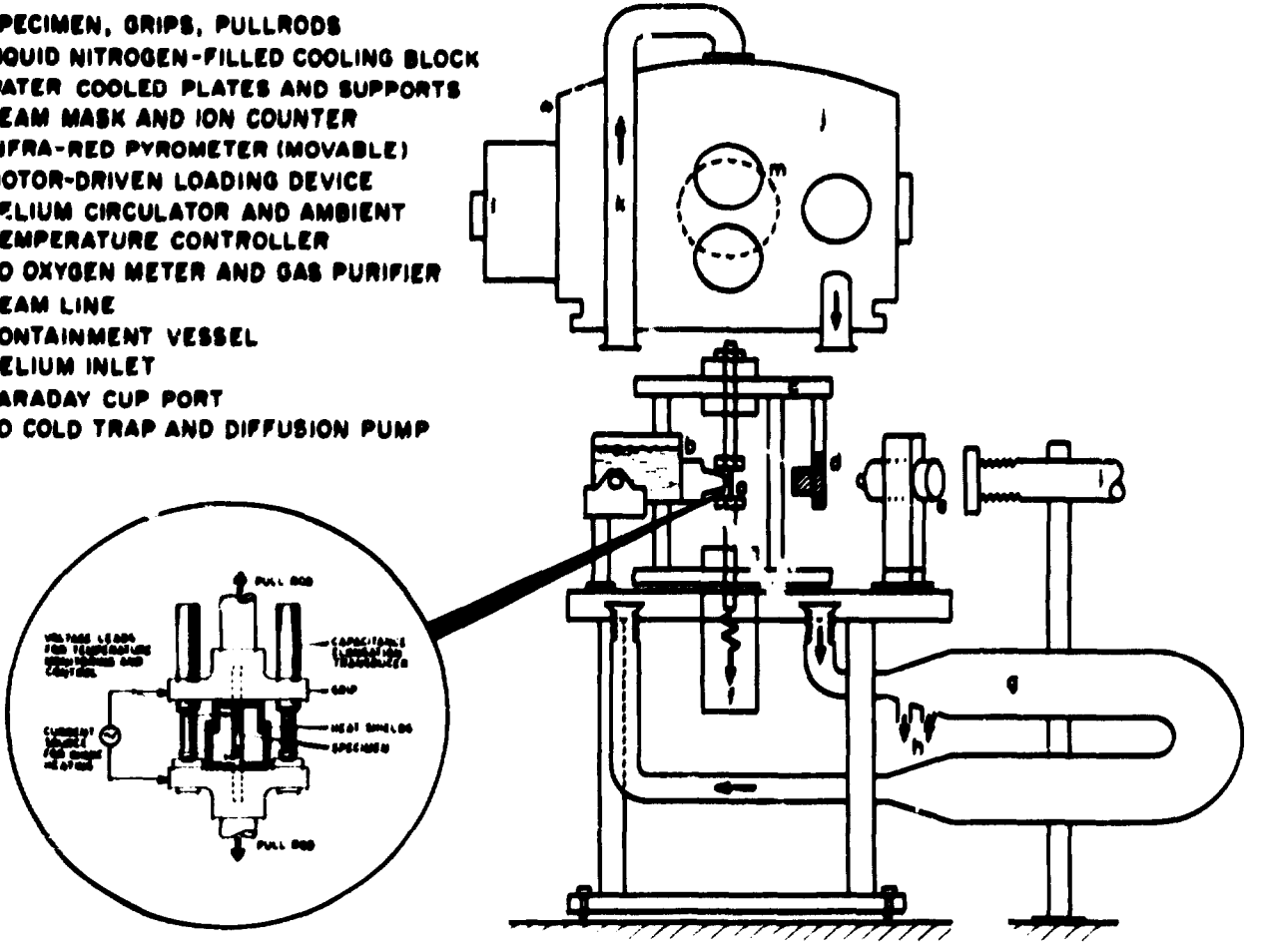

Fig. 4.3. Schematic Illustration of Components of Irradiation Creep Apparatus.

has progressed[21] to the point where we have demonstrated for type 316 stainless steel at 813 K that bulk properties can be duplicated in vacuum or helium with specimens as thin as 25 μm. This is essential for the irradiation creep simulation experiments, in which thin specimens (75–125 μm) will be used. An important part of this effort was the modification of an existing creep machine to accept thin, spring-loaded specimens. Another supporting project has begun in which we compare, from first principles, the factors that differ in the displacement process between neutron and light-ion irradiation and also affect the irradiation creep rate.

There is evidence[22,23] that, according to the calculated dpa rates, light ions are about 10 times as effective in enhancing the irradiation creep rate as are fast neutrons.

Other support work includes the development of a microprocessor-controlled system to monitor thermal creep experiments in the irradiation creep apparatus. This is to allow thermal creep experiments to proceed when the cyclotron is not available. Also, irradiation creep specimens were completed and sent to the EBR-II for preirradiation (to a fluence of 2×10^{26} to $4 \times 10^{26}/m^2$, >0.1 MeV) for later testing in the apparatus. Specimens of structural, developmental, and pure materials are being irradiated.

4.3.3 Analytical Electron Microscopy (AEM)

4.3.3.1 Optimum Operating Modes for an Analytical Electron Microscope — R. W. Carpenter, J. Bentley, and Edward A. Kenik

A comprehensive experimental investigation of all static and scanning beam imaging and diffraction modes of a modern AEM was made during the past year[24,25] to determine the optimum operating modes for analysis of

---

[21]T. C. Reiley and P. G. Jung, "The Simulation of Irradiation Creep," presented at the International Conference on Radiation Effects in Breeder Reactor Structural Materials, Scottsdale, Arizona, June 1977; to be published in the proceedings.

[22]J. L. Straalsund, Hanford Engineering Development Laboratory, private communication.

[23]R. J. McElroy, AERE, Harwell, UK, private communication.

[24]R. W. Carpenter, J. Bentley, and E. A. Kenik, "Analytical Electron Microscopy Investigation of Structural and Spatial Composition Variation in Lamellar Multiphase Alloys," pp. 411–22 in *Scanning Electron Microscopy*, Vol. I (Proc. Workshop Analytical Electron Microscopy), IIT Research Institute, Chicago, March 1977.

[25]R. W. Carpenter, "Application of Transmission Scanning Electron Diffraction to Alloy Phase Transformations," (Summary) pp. 398–99 in *34th Ann. Proc. Electron Microscopy Soc. Amer.*, (Miami Beach), G. W. Bailey, ed., Claitor's Publishing Division, Baton Rouge, 1976.

lattice defects and local composition variations in crystalline alloy specimens.

A lamellar two-phase alloy with the composition Cu-4 wt % Ti was used to investigate most of the operating modes of the instrument. The microstructure was composed of thin plates of an ordered Cu-Ti intermetallic phase formed by isothermal precipitation in the fcc matrix. The interfaces are flat and sharp on {111} matrix planes and formed ideal objects to examine the response of the energy-dispersive x-ray and scanning transmission (STEM) imaging systems. A typical example of normal transmission imaging in diffraction contrast is shown in Fig. 4.4, for which the specimen was tilted to reveal the dislocation structure in the incoherent precipitate-matrix interface. This imaging mode was found to be the best and fastest for analysis of geometric lattice defects. Scanning imaging modes were found to be superior for use during chemical analysis of different small regions in the microstructure for two reasons. First, when an area is selected for chemical analysis in STEM and the electron-probe scan is stopped on the chosen area for measurement of the emitted characteristic x-ray spectrum, maximum spatial resolution is possible because the incident electron probe diameter can be reduced to about 2 nm in this imaging mode. Second, the surface topography of the specimen area in which chemical analyses are performed can be directly examined in the secondary electron imaging mode. Local variations in thickness can result in erroneous chemical

Fig. 4.4. Bright-Field Diffraction-Contrast Transmission Electron Micrograph. Note interfacial dislocations in interface between matrix and lamellar intermetallic compound. Scale marker = 0.1 μm.

analyses. An example of both these imaging modes is shown in Fig. 4.5 for the lamallar two-phase Cu-4 wt % Ti alloy. The two phases were polished differentially during thinning to electron transparency, with the ordered phase polishing more slowly. The surface relief between the ordered plates and matrix was found to be ~20 nm from SEM stereo pairs.

Typical microchemical analysis results from the same specimen are shown in Fig. 4.6. Figure 4.6(a) shows an STEM image of lamellar plates, and Fig. 4.6(b) a Ti Kα line scan corresponding to the line A-B, in Fig. 4.6(a). The two contrast features marked T in Fig. 4.6(a) are twin boundaries in the copper-rich matrix, not lamellar precipitate. Note the one-to-one correspondence between regions of large amplitude on the Ti Kα line scan and the ordered lamellar precipitates, and the indication of slight titanium segregation to twin boundaries in Fig. 4.6(b). The width of the thinnest nearly edge-on lamellar plates in Fig. 4.6(a) is about 60 nm, and the foil thickness is about 150 nm. One can see that the x-ray line scan has more than adequate resolution to delineate these regions of high titanium concentration.

Energy-dispersive x-ray spectra taken from a single lamellar precipitate and from an adjacent matrix area are shown in Fig. 4.7. These spectra were taken with the microscope operating in the STEM mode with a stationary probe. The composition of the ordered lamellar precipitate is 20.3 ± 2.0 at. % Ti, corresponding to nearly Cu_4Ti. Further details on x-ray analysis are given in Sect. 4.3.3.2.

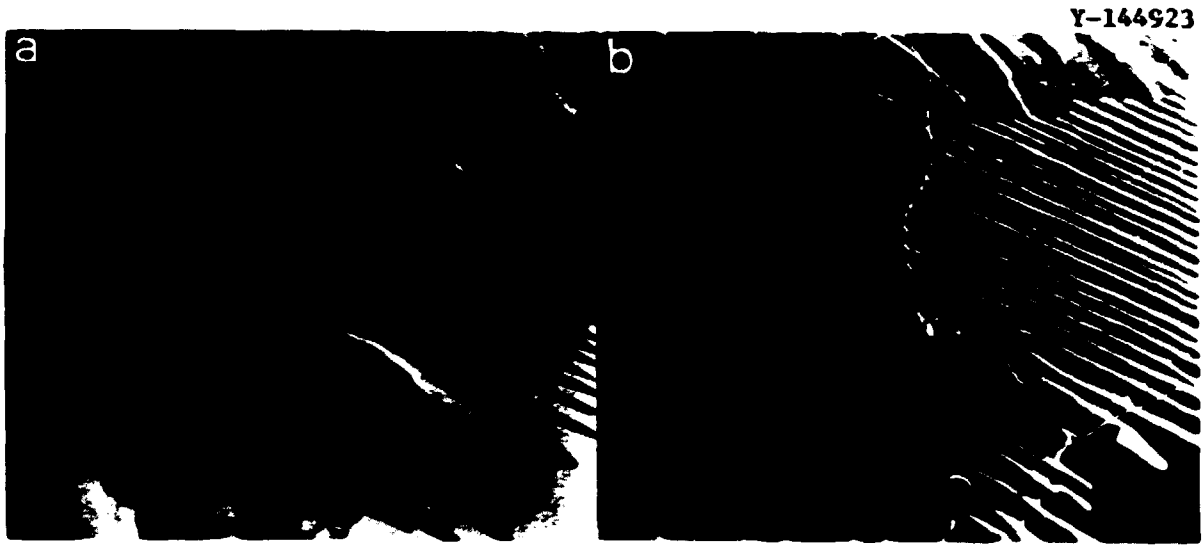

Fig. 4.5. Scanning Images of Lamellar Two-Phase Alloy. (a) Scanning transmission image showing several grains; (b) SEM secondary electron image of specimen surface, same area as (a). Note the obvious projection of ordered plates above the matrix surface. Scale marker = 1 μm.

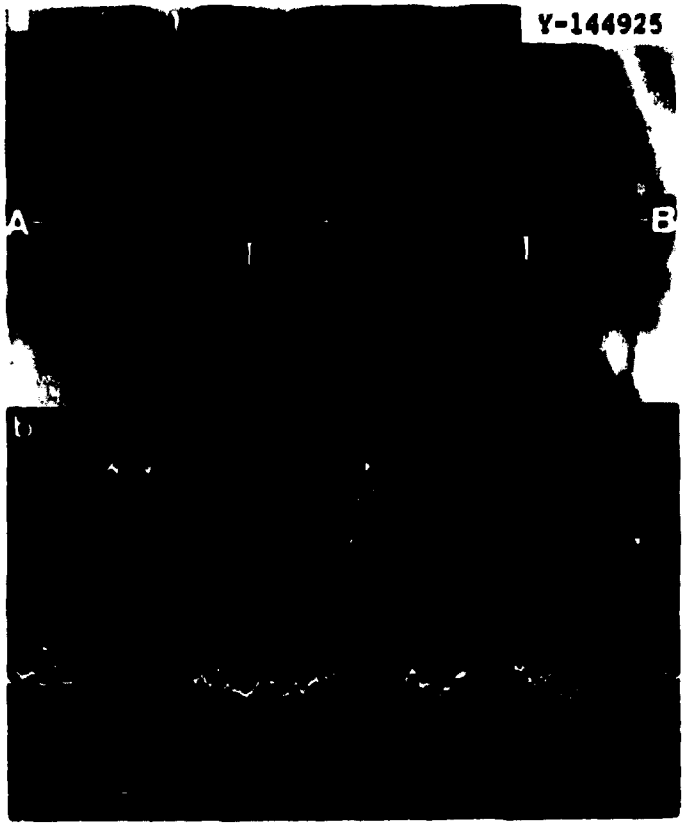

Fig. 4.6. Lamellar Microstructure. (a) STEM image. (b) Ti Kα x-ray line profile along line AB shown in (a). Scan time = 100 s, rate meter line constant = 1 s. Scale marker = 200 nm. T marks twinned matrix.

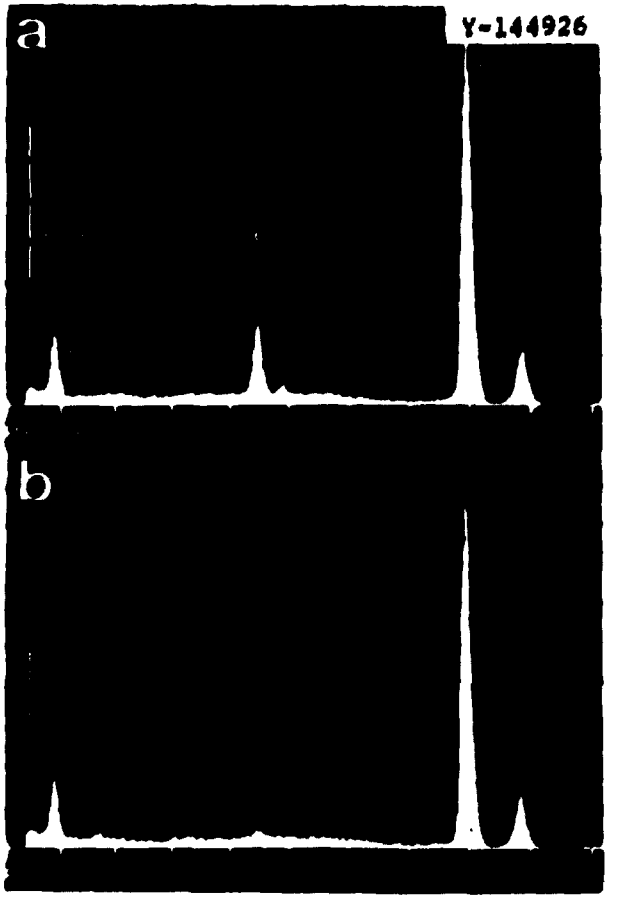

Fig. 4.7. Energy-Dispersive X-Ray Spectra from Ordered Precipitate Plate of Width About 60 nm. (b) From adjacent matrix region of about 150 nm width.

Several different electron diffraction methods were investigated. They all could produce excellent-quality electron diffraction patterns from selected areas above about 600 nm diam (selected area diffraction) down to about 10 nm diam (micro-micro diffraction) from a single ordered plate. Large-angle convergent-beam diffraction patterns and small-angle electron diffraction patterns can also be produced easily. A unique feature of this analytical electron microscope is the capability for measurement of electron intensity in diffraction patterns or images, using Grigson scanning coils and a photomultiplier detection system. An example of the method is shown in Fig. 4.8, which is the (020) matrix maximum with two diffuse satellite peaks from a Cu-4 wt % Ti alloy, aged to form a modulated structure. Vertical deflection of the horizontal traces is proportional to the diffracted intensity distribution in reciprocal space. The curved lines around the intensity maxima are isointensity contours. The angular displacement of the satellite peaks from the (020) Bragg peak is quite small, but they are still well resolved, showing that excellent angular resolution can be obtained with this method.

This instrument is proving indispensable in the study of phase stability in irradiated alloys, which is described in Sect. 4.1.3.

Fig. 4.8. Transmission Scanning Electron Diffraction (TSED) Pattern Taken at Large Camera Length on (020) Bragg Maximum of Spinodally Decomposed Cu-4 wt % Ti Alloy. $\alpha = 4.7 \times 10^{-4}$ rad.

4.3.3.2 Energy-Dispersive X-Ray Analysis in an AEM — Edward A. Kenik and J. Bentley

A simple method for thin foil analysis in an analytical electron microscope (AEM) is based on the ratio of x-ray peak intensities. If the specimen is sufficiently thin that x-ray absorption and fluorescence in the foil can be ignored, the ratio of the concentrations is given by:

$$C_1/C_2 = KI_1/I_2 \ ,$$

where C_i is the concentration, I_i is the peak intensity, and K represents the relative total system efficiency for production and detection. This constant can be evaluated from relative intensity measurements of a large number of alloys or compounds from which a calibration curve can be constructed. An alternative and often simpler method, when the base alloy composition is known, is to perform a large area scan at a suitable foil thickness and calculate K from the observed intensity ratio.

There is some controversy[26,27] about the importance of x-ray absorption in thin foils, and several published methods for calculation of the effect are incorrect. The magnitude of the absorption correction can be calculated[27] from

$$I_{ab}/I_o = \frac{\sin \psi}{\mu t \cos \phi} \left[1 - \exp(-\mu t \cos \phi / \sin \psi)\right] \ ,$$

where I_{ab} and I_o are the detected intensities with and without absorption, μ is the absorption coefficient, t is the foil thickness, ψ is the x-ray take-off angle, and ϕ is the angle between the foil normal and the beam direction. In practice a number of effects cause complications, which must be recognized before this simple procedure for analysis can be performed. The first is the presence of "system peaks" (signals arising from constituent elements of the specimen environment). The origin of these extraneous x rays is the fluorescence of the nonspecimen components by scattered electrons or by x rays produced in the specimen or elsewhere in the microscope. An obvious solution is the use of low-atomic-number materials in the specimen environment, particularly the specimen holder. The design and construction of a beryllium specimen holder is detailed below.

The second complicating effect is x-ray-induced fluorescence of the specimen, which leads to x-ray intensities different from those characteristic of electron excitation and thus results in incorrect intensity ratios, as well as poor spatial resolution for analysis.[28] If x-ray intensities for a homogeneous alloy, such as Ni–20 at. % Mo, are plotted

---

[26]J. Bentley and E. A. Kenik, "Energy Dispersive X-Ray Measurements of Thin Metal Foils," pp. 426–27 in *34th Ann. Proc. Electron Microscopy Soc. Amer.*, G. W. Bailey, ed., Clartor's Publishing Division, New Orleans, 1976.

[27]J. Bentley and E. A. Kenik, "Reply to 'Comments on Energy Dispersive X-ray Measurements on Thin Metal Foils,'" *Scr. Metall.* 11: 261–63 (1977).

[28]E. A. Kenik and J. Bentley, "Influence of X-Ray Induced Fluorescence on Energy Dispersive X-Ray Analysis of Thin Foils," accepted for publication in 35th Annual Proceedings of Electron Microscopy of America, Boston, Massachusetts, 1977.

as a function of foil thickness, two effects are noted (Fig. 4.9). A finite x-ray spectrum is obtained even when the specimen is not intercepting the electron beam, a so-called "in-hole" spectrum since the beam passes through a hole in the specimen. In addition, the intensity ratio depends on foil thickness. Identification of the origin of the "in-hole" spectrum is based on the behavior of the spectrum with different filament emission current and condenser apertures. The "in-hole" count rate is essentially independent of probe current when changes are produced by different apertures at constant filament emission but depends strongly on filament emission current for constant probe current. Such dependences are inconsistent with the "in-hole" spectrum arising from electron "tails" and indicate x-ray-induced fluorescence of the specimen. These uncollimated x-rays are energy analyzed by scattering them off a Mylar film into the spectrometer while the electrons pass through a hole in the Mylar film. The "in-hole" spectrum so obtained contains x-ray signals from the specimen holder and scattered lead and molybdenum x rays from the illumination system.

The observed dependence of x-ray intensity ratio on foil thickness arises from the finite "in-hole" counts, which are larger for higher energy x-rays, and is consistent with x-ray-induced fluorescence. This effect can be corrected by subtracting the "in-hole" counts from the integrated intensities and recalculating the ratios.

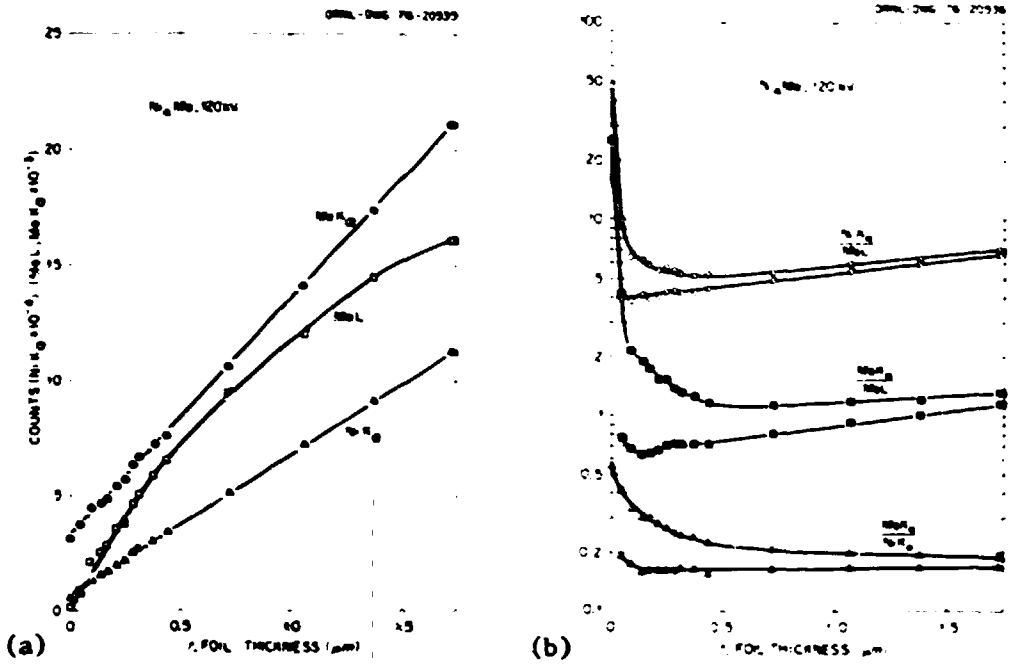

Fig. 4.9. Effects of X-ray Fluorescence in Ni–20 at. % Mo alloy. (a) Integrated counts versus foil thickness, t. (b) Ratios of integrated intensities. For each ratio the upper curve shows uncorrected data, and the lower curve shows data corrected by subtraction of x-ray-induced fluorescence.

Another x-ray-induced fluorescence effect is associated with x rays generated in the specimen holder, either by backscattered electrons trapped in the objective lens field or by x rays from the illumination system. X rays from the holder induce fluorescence of the specimens, resulting in incorrect intensity ratios for analysis. For the Ni–20 at. % Mo alloy, the Mo-Ni Kα ratio was determined to be 0.155 in a bronze holder and 0.183 in a beryllium holder. The excess nickel counts for the bronze holder arise from fluorescence of the nickel induced by the Cu Kβ x rays. The use of low-Z specimen holders thus has two advantages: the removal of extraneous "system peaks" and the minimization of this effect.

Several modifications to the existing AEM have been made to minimize the spurious effects described above and simplify microchemical analysis.

1. Simultaneous structural and EDS analysis of a crystalline specimen requires the use of a double tilt holder in order to achieve desired diffraction conditions for specimen imaging and to achieve the optimum x-ray take-off angle. The holder material should not contribute any "system peaks" to complicate the spectrum or to cause anomalous fluorescence of the specimen. The design should allow a wide range of tilt angles, while avoiding shadowing of either the electron beam or the detector. A modification of the standard double tilt holder was designed and built of beryllium. System peaks, primarily copper and tin, were reduced by greater than 90%.

2. X rays generated in the condenser assembly contribute to the x-ray-induced fluorescence of the specimen, the associated degradation of spatial resolution, and to the generation of "system peaks." These x rays are generated by the deceleration of electrons by the condenser aperture material. To absorb a larger portion of these x rays, the fixed and movable condenser apertures, 100- and 25-μm molybdenum, respectively, were changed to 0.51-mm platinum. A fourfold reduction in both the x-ray flux from the condenser assembly and the in-hole spectrum was achieved.

3. It is often desirable to be able to measure the electron probe current incident upon the specimen. To achieve this a small Faraday cup was designed and built for installation in the viewing chamber of the AEM. The cup has a grounded shield and is complete with a grid for suppression of secondary electrons. Phosphor on the upper surface of the shield and the location of the cup on the beam stop aid in rapid and accurate positioning (or complete removal) relative to the beam. As well as measuring probe currents for normalization in x-ray analyses, the Faraday cup also allows absolute diffracted intensity measurement.

4.3.4 High-Voltage Electron Microscopy — R. W. Carpenter and Edward A. Kenik

During the past year the HVEM was used as a research tool to study phase instability and void nucleation, primarily in nickel-base binary alloys and nickel. This work is still in progress; current results are described in Sects. 4.1.3 and 4.1.4. Modifications to the column vacuum system to improve high-temperature performance are described below. A brief progress report on the conversion to side-entry specimen stage is also given.

4.3.4.1 Modification of the Vacuum System

Residual gases in the column of a high-voltage electron microscope cause undesirable chemical reactions with specimens under observation, especially when a hot stage is used and the specimen is maintained at elevated temperature during observation. A hot stage is usually used for high-temperature deformation, void swelling radiation damage, and phase transformation experiments. We have observed surface contamination of many specimens during high-temperature void swelling experiments from such chemical reactions, when the pressure at the specimen region was in the mid-10^{-4}-Pa (10^{-6} torr) range. The largest contributors to undesirable chemical reactions in the residual column vacuum were analyzed with a mass spectrometer and found to be oxygen and water vapor. As a first step to reduce the problem, the HVEM column was completely disassembled, and the vacuum seals were renewed in all critical regions. Additional pumping capacity in the form of a high-capacity low-backstreaming diffusion pump was added to the column. This reduced the specimen region pressure to 50 μPa (4×10^{-7} torr). Further improvements were obtained by fitting an additional liquid nitrogen cryopump between the camera chamber and the specimen chamber and by fitting a helium cryopump in the specimen chamber. After these additional modifications the pressure was measured with a nude ionization gage in the specimen chamber and found to be 11 μPa (8×10^{-8} torr). This is the lowest specimen chamber pressure ever reported for a conventional HVEM. The column on any HVEM is very large, and leaks in the vacuum system are very difficult to locate. Obviously, maintaining an operating pressure of 11 μPa (8×10^{-8} torr) requires continuous monitoring of the system for leaks. Plans are presently being made for permanent installation on the column of a mass spectrometer for this purpose.

4.3.4.2 Modification of the Stage to Side-Entry Configuration

Last year we reported that side-entry conversion for the existing HVEM was feasible. The specifications for the conversion were written and a contract for the conversion was let to Gatan, Inc. The necessary equipment for the conversion is now being installed in the microscope. Further equipment installation will occur later in the year. The modification should be complete near the end of the calendar year.

4.4 COOPERATIVE STUDIES WITH UNIVERSITIES AND OTHER RESEARCH ORGANIZATIONS – K. Farrell

A number of our studies on radiation damage are being made with the cooperation of personnel at other research establishments. Usually this involves examination of specimens provided to the investigator from ORNL experiments.

At the University of Cincinnati, J. Moteff and a Ph.D. student, J. Stubbins, have completed their examination of various grades of

molybdenum neutron irradiated at temperatures in the range 490 to 1170 K, and are preparing a series of reports on the findings.

Specimens of zirconium and Zircaloy have been studied by D. Northwood at Chalk River Nuclear Laboratories, Canada. Very few voids were found; the data are now being assessed for publication.

A. Jostsons at the Lucas Heights Laboratory, Australia, has completed his portion of work on the fluence dependence of damage in pure aluminum and dilute aluminum-silicon and aluminum-indium alloys. Little or no effects of the alloying elements were observed at the 100 at. ppm level. Examination of various grades of neutron-irradiated zirconium and titanium is proceeding.

R. L. McConville of the University of Illinois Center for Electron Microscopy is studying neutron damage in magnesium-aluminum alloys.

Neutron-irradiated specimens of pure Al, Al-Si, and Al-Mg have been sent to J. D. McGervey, Case Western Reserve University, to expand his positron annihilation experiments with R. W. Hendricks.

A program of positron annihilation studies of dilute binary nickel-base alloys has just begun with C. L. Snead, Jr., of Brookhaven National Laboratory. We hope to determine vacancy formation energies and vacancy-alloying element binding energies in unirradiated alloys. Specimens from these alloys are also being irradiated with neutrons to see if there is any systematic change in structure that can be correlated with the positron annihilation data.

J. Narayan, ORNL Solid State Division, has used the ion bombardment facility to study low-temperature defect structures in stainless steel single crystals and to study damage in MgO.

APPENDIX

1. STAFF ASSIGNMENTS

R. L. Beatty from Fundamental Ceramics Studies to Swiss Federal Institute for Reactor Research (EIR), Wurenlingen, Switzerland; July 1976–July 1977.

D. N. Braski from Radiation Effects and Microstructural Analysis Group to Institut für Festkörperforschung, Kernforschungsanlage, Jülich, FRG; September 1976–August 1977.

C. C. Koch from Superconducting Materials to ORNL Central Management Offices; October 1976.

J. S. Faulkner from Theoretical Research to Visiting Professor, H. H. Wills Physics Laboratory, University of Bristol, England; September 1976–September 1977.

C. B. Finch from Crystal Physics to Institut de Physique Nucléaire, d'Orsay, France; May 1977–September 1977.

T. G. Godfrey from Physical Properties Group to ORNL Fossil Energy Program assigned to Pittsburgh Energy Research Center; September 1976–September 1977.

2. GUEST ASSIGNMENTS

P. Jung, Institut für Festkörperforschung, Kernforschungsanlage, Jülich, FRG; June 1976–July 1977.

H. P. Krautwasser, Institut für Reaktorwerkstoffe, Kernforschungsanlage, Jülich, FRG; May 1975–November 1976.

H. C. Freyhardt, Institut für Metallphysik, Universität Göttingen, Germany; August–September 1976.

B. L. Gyorffy, H. H. Wills Physics Laboratory, University of Bristol, England, to Theoretical Research; July–September 1976.

E. Ricci, ORNL Analytical Chemistry Division, internal sabbatical leave to X-Ray Diffraction Research; October 1976–September 1977.

M. G. Duncan, doctoral student from University of Tennessee; June 1976–March 1977.

H. M. Loretto, University of Birmingham, England, to Radiation Effects Program; Summer 1977.

Joseph Mansur, Cornell University; Summer 1977.

Thomas Klimowicz, Massachusetts Institute of Technology; Summer 1977.

D. C. Reiter, Thiel College; Summer 1977.

D. J. Bradley, Oak Ridge Associated Universities doctoral student from University of Michigan; June 1976–August 1977.

3. STAFF CHANGES

J. Brynestad from Fundamental Ceramics Studies to Chemistry Division; October 1976.

C. F. Yen from Massachusetts Institute of Technology to Fundamental Ceramics Studies; February 1977.

James Bentley from University of Birmingham, England, to Radiation Effects; January 1977.

G. M. Stocks from University of Bristol to Theoretical Research; December 1976.

W. Oliver from University of Tennessee to Stabilities of Microphases; March 1977.

R. D. Carlson from University of Tennessee, Oak Ridge Graduate School of Biomedical Sciences, to Small-Angle X-Ray Scattering Studies; September 1976.

4. ORNL-UT JOINT APPOINTMENTS FOR ACADEMIC YEAR 1976-1977

B. S. Borie, Professor, Metallurgical Engineering.

C. J. McHargue, Professor, Metallurgical Engineering.

R. A. Vandermeer, Associate Professor, Metallurgical Engineering.

R. W. Carpenter, Assistant Professor, Metallurgical Engineering.

W. A. Coghlan, Assistant Professor, Metallurgical Engineering.

5. PRESENTATIONS AT TECHNICAL MEETINGS

Compiled by Julia L. Bishop

"Carbon 76" International Carbon Conference, Baden-Baden, West Germany, June 28–July 2, 1976

P. Krautwasser, H. Nickel,* and C. S. Yust, "Influence of Heat Treatments on the Microstructure of Pyrocarbon Coatings"

P. Krautwasser, H. Nickel,* and C. S. Yust, "The Influence of Annealing on the Microstructure of Pyrocarbon Coatings"

9th International Metallographic Society Meeting, Seattle, Washington, July 25–28, 1976

L. A. Harris, "The Use of Reflectivity Standards in an Image Analysis System"

L. A. Harris,* D. N. Braski, and C. S. Yust, "Electron Microscopy of Coal Constituents"

34th Annual Meeting of the Electron Microscopy Society of America, Miami Beach, Florida, August 9–13, 1976

J. Bentley* and E. A. Kenik, "Energy Dispersive X-Ray Measurements of Thin Metal Foils"

D. N. Braski, "High Resolution SEM Fractography of Te-Embrittled Hastelloy-N"

R. W. Carpenter, "Application of Transmission Scanning Electron Diffraction to Alloy Phase Transformations"

P. S. Sklad and J. Bentley,* "Changes in the Distribution and Morphology of γ' Precipitate in Neutron Irradiated PE-16"

Summer Meeting of the American Crystallographic Association, Evanston, Illinois, August 10–13, 1976

R. W. Hendricks, "Recent Experimental Results from the ORNL 10 meter Small-Angle X-Ray Scattering Spectrometer"

P. Krautwasser* and R. W. Hendricks, "Application of SAXS for Characterization of Pyrocarbon Coatings"

J. S. Lin,* E. L. Fuller, Jr., and R. W. Hendricks, "Studies of Catalysts: Cobalt-Molybdate"

L. B. Shaffer* and R. W. Hendricks, "Report of the IUCr Commission on Crystallographic Apparatus International Project for the Calibration of Absolute Intensities in Small-Angle X-Ray Scattering"

R. H. Stinson, T. Kurg,* P. R. Sweeney, and R. W. Hendricks, "A Study of the Structure of Collagen Fibrils by Small-Angle X-Ray Scattering"

---

*Speaker.

Applied Superconductivity Conference, Stanford University, Palo Alto, California, August 17–20, 1976

D. S. Easton, "Stress Effects on the Current Densities of Commercial Conductors at 4.2 K in Magnetic Fields"

C. C. Koch* and H. C. Freyhardt, "Fluxoid Pinning in Bulk Niobium by Voids Produced During Neutron Irradiation"

D. M. Kroeger,* D. S. Easton, and A. Moazed, "Stress-Induced Heating in Commercial Conductors and Its Possible Influence on Magnet Performance"

U. Roy, A. DasGupta,* and C. C. Koch, "Preparation and Superconducting Properties of $LiTi_2O_4$"

Sixth International Materials Symposium, University of California, Berkeley, California, August 24–27, 1976

L. A. Harris,* D. N. Braski, and C. S. Yust, "A Study of Factors Affecting Elemental Analyses by STEM"

H. P. Krautwasser, R. L. Beatty, V. J. Tennery, and C. S. Yust,* Comparison of Pyrolytic Carbon Microstructures Derived from MAPP-Gas and Propylene"

International Conference on Positron Annihilation, Helsingor, Denmark, August 1976

V. W. Lindberg, J. D. McGervey,* and R. W. Hendricks, "Positron Lifetimes in Voids and Other Defects in Neutron-Irradiated Aluminum"

Sixth European Congress on Electron Microscopy, Jerusalem, September 12–17, 1976

G. S. Bauer* and R. W. Carpenter, "Hydrogen Induced Twinning in Thin Nickel Foils"

TMS-AIME Fall Meeting, Niagara Falls, New York, September 20–23, 1976

R. W. Carpenter, "Structural Transformation During Oxide Precipitation in Refractory Metal Alloys"

D. S. Easton,* D. M. Kroeger, and A. Moazed, "Temperature Increases in Superconducting Composites as a Result of Tensile Strain"

A. DasGupta,* U. Roy, and C. C. Koch, "Superconductivity in $LiTi_2O_4$"

C. C. Koch* and D. S. Easton, "Mechanical Behavior and Stress Effects in Superconductors – A Review"

C. J. McHargue* and J. L. Scott, "Materials Requirement for Fusion Reactors"

R. A. Perkins* and R. A. Padgett, Jr., "Oxygen Diffusion in Niobium and Niobium-Zirconium Alloys"

R. A. Perkins, "Oxidation Diffusion in β-Zircaloy"

C. L. White, "A Spectrum of Sites Approach to Grain Boundary Segregation"

Electrochemical Society Fall Meeting, Las Vegas, Nevada, October 17-22, 1976

J. V. Cathcart, "The Role of Stress Effects in the Oxidation Behavior of High-Temperature Alloys"

International Conference on Properties of Atomic Defects in Metals, Argonne National Laboratory, Argonne, Illinois, October 18-22, 1976

R. W. Hendricks, "A Model for the Mechanism of Void Formation in Neutron Irradiated High-Purity Aluminum"

V. W. Lindberg, J. D. McGervey, and R. W. Hendricks,* "Positron Lifetimes in Voids and Other Defects in Neutron Irradiated Aluminum"

L. K. Mansur* and W. G. Wolfer, "Influence of a Surface Coating on Void Formation"

M. H. Yoo* and J. O. Stiegler, "Point Defect Interactions and Growth of Dislocation Loops"

American Chemical Society Southeastern Regional Meeting, Gatlinburg, Tennessee, October 27-29, 1976

J. S. Lin,* E. L. Fuller, Jr., and R. W. Hendricks, "Small-Angle X-Ray Scattering: Cobalt-Molybdate Catalyst"

C. J. Sparks, Jr., "Quantitative, Multi-Element X-Ray Fluorescence Analysis" (Invited Paper)

Geological Society of America Annual Meeting, Denver, Colorado, November 8-11, 1976

L. A. Harris* and C. S. Yust, "A Study of the Submicron Minerals in Coal"

Modcomp Users Meeting, Fort Lauderdale, Florida, December 6-8, 1976

R. W. Hendricks, J. S. Lin, N. A. Betz, and R. L. Stephenson,* "Software to Augment the Capability of Modcomp Computers Through Interaction with a Large Computing Center"

R. W. Hendricks and J. C. Twichell, "High-Speed Memory Increment Hardware for the Modcomp II" (presented by R. L. Stephenson)

American Crystallographic Association Meeting, Asilomar, California, February 21-25, 1977

H. L. Yakel* and L. A. Harris, "Can Crystallographers Convert to Coal?"

AIME Annual Meeting, Atlanta, Georgia, March 6–10, 1977

D. J. Bradley, J. M. Leitnaker,* and F. H. Horn, "The Precipitation of Carbon in Nickel and Nickel-Titanium Alloys"

R. W. Carpenter* and G. S. Bauer, "Hydrogen-Induced Deformation in Nickel Foils"

R. W. Carpenter* and M. H. Yoo, "The Effects of Semicoherent Precipitation on Segregation and Void Swelling in Neutron-Irradiated Al-Cu Alloys"

R. W. Carpenter, E. A. Kenik,* and R. J. Bayuzick, "The Effect of Irradiation on Void Swelling and Chemical Order in Ni-Mo, Ni-V, and Ni-Ti Alloys"

A. DasGupta,* Y. T. Chou, C. C. Koch, and D. M. Kroeger, "Role of Grain Boundaries in Supporting Large Critical Currents"

D. S. Easton, "Stress Effects in a Variety of Nb_3Sn Superconducting Composites"

J. M. Leitnaker,* D. J. Bradley, and D. N. Braski, "The Composition of Some Cubic Precipitates in Ni-Base Alloys"

M. H. Yoo, "Void Swelling in Bounded Media by Charged Particle Damage"

1977 March Meeting, American Physical Society, San Diego, California, March 21–24, 1977

S. K. Baczek,* R. S. Stein, R. D. Carlson, and R. W. Hendricks, "Deformation Studies of Polyethylene Using Small-Angle X-Ray Scattering"

W. H. Butler* and P. B. Allen, "Electronic Contribution to the Phonon Lidewidth in Nb"

A. DasGupta,* Y. T. Chou, C. C. Koch, and D. M. Kroeger, "Flux Pinning by Crystal Boundary in Niobium Bicrystals"

D. R. Lloyd, C. M. Quinn, N. V. Richardson, R. Jordan, G. M. Stocks,* B. L. Gyorffy, and W. E. Temmerman, "Angle-Resolved Photoemission Spectra from a Disordered CuNi Alloy"

T. S. Lundy, "Have Short-Circuiting Diffusion Phenomena Been Short-Changed?"

R. A. McKee, "Solute and Vacancy Diffusion for an Alloy in Dissociative Equilibrium"

G. S. Painter, "Surface Studies of Chemisorptive Bonding"

G. M. Stocks,* B. L. Gyorffy, W. E. Temmerman, E. S. Guiliano, and R. Ruggeri, "The Coherent Potential Approximation for Nonoverlapping Muffin-Tin Potentials: Applications to Disordered CuNi and MoNb Alloys"

M. H. Yoo, "Dislocation Loop Growth and Void Swelling in Bounded Media by Charged Particle Damage"

Workshop on Analytical Scanning Transmission Electron Microscopy at the IITRI Scanning Electron Microscopy 1977 Meeting, Chicago, Illinois, March 27–April 1, 1977

R. W. Carpenter,* J. Bentley, and E. A. Kenik, "Analytical Electron Microscopy Investigations of Structural and Spatial Composition Variation in Lamellar Multiphase Alloys"

79th Annual Meeting of the American Ceramic Society, Chicago, Illinois, April 23–28, 1977

L. A. Harris,* C. S. Yust, G. C. Wei, and V. J. Tennery, "The Use of Electron Microscopy in Slag Analyses"

Seventh Annual International Symposium on Electronic Structure of Metals and Alloys, Gaubig, East Germany, April 18–22, 1977

J. S. Faulkner, "Electronic States in Disordered Solids"

Uranium Alloy Meeting, Los Alamos Scientific Laboratory, Los Alamos, New Mexico, May 3–5, 1977

R. A. Vandermeer* and J. C. Ogle, "Phase Transformations and and Shape Memory Effects in Near Monotectoid Uranium-Niobium Binary Alloys"

Second International Congress on Hydrogen in Metals, Paris, France, June 6–11, 1977

G. S. Bauer* and R. W. Carpenter, "Hydrogen-Induced Twinning in Thin Nickel Foils"

AIME International Conference on Radiation Effects in Breeder Reactor Structural Materials, Scottsdale, Arizona, June 20–23, 1977

D. G. Doran,* G. R. Odette, R. L. Simons, and L. K. Mansur, "Damage Correlation in Theory and Practice"

T. C. Reiley* and P. G. Jung, "The Simulation of Irradiation Creep"

W. G. Wolfer,* L. K. Mansur, and J. A. Sprague, "Theory of Swelling and Irradiation Creep"

1977 Annual Meeting of the American Nuclear Society, New York, June 12–16, 1977

A. D. Brailsford and L. K. Mansur,* "Effect of Implanted Interstitials on Swelling During Self-Ion Bombardment"

N. H. Packan, J. O. Stiegler, and K. Farrell,* "Correlation of Neutron and Nickel-Ion Damage in Pure Nickel"

6. PUBLICATIONS

Compiled by Meredith R. Hill

G. S. Bauer and R. W. Carpenter, "Hydrogen Induced Twinning in Thin Nickel Foils," paper 2B12 in *2nd Int. Conf. Hydrogen in Metals, Paris, June 6–11, 1977*, French Society for Metals, Paris.

G. S. Bauer and R. W. Carpenter, "Formation of Deformation Twins in Nickel Foils by Hydrogen Induced Dissociation of Dislocations," pp. 584–86 in *Electron Microscopy, 6th European Conf., Jerusalem, 1976*, TAL International Publishers, Jerusalem.

E. C. Beahm, C. A. Culpepper, and O. B. Cavin, "Laves Phases of Uranium and 3d Transition Metals," *J. Less-Common Met.* 50: 57–71 (1976).

J. Bentley and E. A. Kenik, "Energy Dispersive X-Ray Measurements of Thin Metal Foils," (Summary) pp. 426–27 in *34th Ann. Proc. Electron Microscopy Soc. Amer.*, G. W. Bailey, ed., Clator's Publishing Division, Baton Rouge, 1976.

J. Bentley and E. A. Kenik, "Reply to 'Comments on Energy Dispersive X-Ray Measurements on Thin Metal Foils,'" *Scr. Metall.* 11: 261–63 (1977.)

H. K. Birnbaum, M. L. Grossbeck, and M. Amano, "Hydride Precipitation in Nb and Some Properties of NbH," *J. Less-Common Met.* 49(1-2): 357 (1976).

E. E. Bloom, J. M. Leitnaker, and J. O. Stiegler, "Effect of Neutron Irradiation on the Microstructure and Properties of Titanium-Stabilized Type 316 Stainless Steels," *Nucl. Technol.* 31: 232–43 (November 1976).

A. D. Brailsford and L. K. Mansur, "Effect of Implanted Interstitials on Swelling During Self-Ion Bombardment," (Summary) *Trans. Am. Nucl. Soc.* 26(TANSAO 26): 178–79 (June 1977).

D. N. Braski, "High Resolution SEM Fractography of Te-Embrittled Hastelloy-N," pp. 458–59 in *34th Ann. Proc. Electron Microscopy Soc. Amer.*, G. W. Bailey, ed., Clator's Publishing Division, Baton Rouge, 1976.

W. H. Butler and P. B. Allen, "Gap Anistropy and T_c Enhancement: General Theory, and Calculations for Nb, Using Fermi Surface Harmonics," pp. 73–120 in *Super Conductivity in d- and f- Band Metals*, D. H. Douglas, ed., Plenum, New York, 1976.

W. H. Butler, "One-Dimensional Model for Transition Metals and Their Alloys," *Phys. Rev. B* 14(2): 468–78 (July 1976).

W. H. Butler, J. J. Olsen, and J. S. Faulkner, "Electron-Phonon Interaction in Cubic Systems: Application to Niobium," *Phys. Rev. B* 14(9): 3823–36 (Nov. 1, 1976).

W. H. Butler, "Electron-Phonon Coupling in the Transition Metals: Electronic Aspects," *Phys. Rev. B* 15(11): 5267–82 (June 1977).

R. W. Carpenter, "Application of Transmission Scanning Electron Diffraction to Alloy Phase Transformation," (Summary) pp. 398–99 in *34th Ann. Proc. Electron Microscopy Soc. Amer.*, G. W. Bailey, ed., Clator's Publishing Division, Baton Rouge, 1976.

R. W. Carpenter and J. C. Ogle, "The Effect of Solute Content and Precipitate Distribution on Fast Neutron Damage in Aluminum-Copper Alloys," pp. 1203–12 in *Fundamental Aspects of Radiation Damage in Metals* (Proc. Int. Conf. Gatlinburg, Oct. 6–10, 1975), CONF-751006-P2, Vol. II.

R. W. Carpenter, J. Bentley, and E. A. Kenik, "Analytical Electron Microscopy Investigation of Structural and Spatial Composition Variation in Lamellar Multiphase Alloys," pp. 411–22 in *Scanning Electron Microscopy*, Vol. I (Proc. Workshop Analytical Electron Microscopy), IIT Research Institute, Chicago, March 1977.

R. W. Carpenter and E. A. Kenik, "Stability of Chemical Order in Ni$_4$Mo Alloy Under Fast Electron Irradiation," pp. 48–49 in *35th Ann. Proc. Electron Microscopy Soc. Amer.*, G. W. Bailey, ed., Clator's Publishing Division, Baton Rouge, 1977.

J. G. Cook, J. F. Moore, T. Matsumura, and M. P. Van der Meer, "Thermal and Electrical Conductivity of Aluminum," pp. 65–71 in *Thermal Conductivity*, Vol. 14 Plenum, New York, 1976.

M. G. Duncan, *Precision Rectifier Detectors for AC Resistance Bridge Measurements with Application to Temperature Control Systems for Irradiation Creep Experiments*, ORNL/TM-5715 (May 1977).

D. S. Easton, D. M. Kroeger, and A. Moazed, "Thermomechanical Heat Generation in Copper and a Nb-Ti Superconducting Composite," *Appl. Phys. Lett.* 29(6): 382–84 (Sept. 15, 1976).

D. S. Easton and R. E. Schwall, *Performance of Multifilamentary Nb_3Sn Under Mechanical Load*, ORNL/TM-5653 (November 1976).

D. S. Easton and C. C. Koch, "Mechanical Properties of Superconducting Nb-Ti Composites," pp. 453–62 in *Advances in Cryogenic Engineering*, Vol. 22, K. D. Timmerhaus et al., eds., Plenum, New York, 1977.

K. Farrell, "3.7 Radiation Damage," pp. 325–27 in *Conf. Proc. Low Activation Materials Assessment for Fusion Reactors*, Spec. Rep. EPRI-ER-328-SR, Electric Power Research Institute, March 1977.

K. Farrell, J. Bentley, and D. N. Braski, "Direct Observation of Radiation-Induced Coated Cavities," *Scr. Metall.* 11: 243–48 (1977).

J. S. Faulkner, "Electronic States in Disordered Alloys II: Results from Real Solids," *Intern. J. Quant. Chem.* 10: 405 (1976).

J. S. Faulkner, "The Fermi Surface of Technetium from a Constant-Energy-Search Korringa-Kohn-Rostoker Band-Theory Calculation," *Phys. Rev. B* 16(2): 736–40 (July 1977).

T. L. Ferrell, J. C. Ashley, and R. W. Hendricks, "X-Ray Excitation of Surface Plasmons on Spherical Voids in Metals," *Philos. Mag.* 34(6): 929–35 (1976).

C. B. Finch, J. D. Holder, G. W. Clark, and H. L. Yakel, "Edge-Defined, Film-Fed Growth of Mn_2SiO_4–MnO Eutectic Composites: Effect of Die-Top Geometry on Solidification Interface Shape," *J. Cryst. Growth* 37: 245–52 (1977).

G. Gahr, M. L. Grossbeck, and H. K. Birnbaum, "Hydrogen Embrittlement of Nb I–Macroscopic Behavior at Low Temperatures," *Acta Metall.* 25(2): 125–34 (February 1977).

M. L. Grossbeck, P. Williams, C. A. Evans, Jr., and H. K. Birnbaum, "Application of Ion Probe Analysis to Studies of Hydrogen Behavior in Solids," *Phys. Status Solidi (a)* 34: 197 (1976).

M. L. Grossbeck and H. K. Birnbaum, "Low Temperature Hydrogen Embrittlement of Niobium II–Microscopic Observations," *Acta Metall.* 25(2): 135–47 (February 1977).

D. G. Hall, *Spectral Density Functions for Disordered Systems*, ORNL-5184 (November 1976).

D. G. Hall, "The Quasicrystalline Approximation: Comparison of the Spectral Density with Exact Results," *Solid State Commun.* 20(5): 509–12 (1976).

D. G. Hall and J. S. Faulkner, "Spectral Density Functions for Amorphous Solids," pp. 800–06 in *Proc. Conf. Neutron Scattering Vol. II*, CONF-760601-P2 (1976).

D. G. Hall and J. S. Faulkner, "The Effects of Short-Range Order on the Spectral Density Function for a One-Dimensional Amorphous Solid," *Phys. Rev. B* 15(12): 5850–57 (June 1977).

L. A. Harris, T. Rose, L. DeRoos, and J. Greene, "Quantitative Analyses of Pyrite in Coal by Optical Image Techniques," *Econ. Geol.* 72(4): 695–97 (June–July 1977).

L. A. Harris, D. N. Braski, and C. S. Yust, "Electron Microscopy of Coal Constituents," pp. 351–57 in *Microstructural Science Volume 5*, J. D. Braun, H. W. Arrowsmith, and J. L. McCall, eds., Elsevier, New York, 1977.

L. A. Harris, "The Use of Reflectivity Standards in an Image Analysis System," pp. 303–09 in *Microstructural Science Volume 5*, J. D. Braun, H. W. Arrowsmith, and J. L. McCall, eds., Elsevier, New York, 1977.

R. W. Hendricks, "One- and Two-Dimensional Position-Sensitive X-Ray and Neutron Detectors," *Trans. Am. Crystallogr. Assoc.* 12: 103–46 (1976).

R. W. Hendricks, J. S. Lin, N. A. Betz, and R. L. Stephenson, "Software to Augment the Capability of MODCOMP Computers Through Interaction with a Large Computing Center," *Proc. 2nd Annu. MUSE Meeting Dec. 5–6, 1976, Fort Lauderdale, Florida*, Modular Computer Systems, Inc. 1650 West McNab Road, Fort Lauderdale, Florida 33309.

T. K. Holder, *Thermal Conductivity, Electrical Resistivity, and Seebeck Coefficient of High Purity Iron and Selected Iron Alloys from 90 to 400 K*, ORNL/TM-5539 (June 1977).

P. J. Jennings, G. S. Painter, and R. O. Jones, "Local Densities of States and Bonding Properties of 3d Transition Metal Clusters," *Surf. Sci.* 60: 255–71 (1976).

W. G. Johnston, N. H. Packan, and F. A. Smidt, Jr., "Summary of Workshop Discussion," pp. 313–47 in *Proc. Workshop on Correlations of Neutron and Charged Particle Damage held at Oak Ridge National Laboratory, June 8–10, 1976*, CONF-760673.

E. A. Kenik, "Solute Segregation in Stainless Steel Under Irradiation," pp. 46–7 in *35th Ann. Proc. Electron Microscopy Soc. Amer.*, G. W. Bailey, ed., Clator's Publishing Division, Baton Rouge, 1977.

E. A. Kenik and J. Bentley, "Influence of X-Ray Induced Fluorescence on Energy Dispersive X-Ray Analysis of Thin Foils," pp. 328–29 in *35th Ann. Proc. Electron Microscopy Soc. Amer.* G. W. Bailey, ed., Clator's Publishing Division, Baton Rouge, 1977.

C. C. Koch, H. C. Freyhardt, and J. O. Scarbrough, "Fluxoid Pinning in Bulk Niobium by Voids Produced During Neutron Irradiation," *IEEE Trans. Magnetics* MAG-13(1): 828–39 (January 1977).

D. M. Kroeger and J. Schelten, "Bending of Flux Lines by Transport Currents in Type-II Superconductors Measured by Neutron Diffraction," *J. Low-Temp. Phys.* 34(3/4): 369–81 (1976).

D. M. Kroeger, D. S. Easton, and A. Moazed, "Stress-Induced Heating in Commercial Conductors and Its Possible Influence on Magnet Performance," *IEEE Trans. Magnetics* MAG-13(1): 120–23 (January 1977).

P. L. Leath, "Cluster Shape and Critical Exponents Near Percolation Threshold," *Phys. Rev. Lett.* 36: 921 (1976).

L. K. Mansur, "Void Growth Kinetics: An Assessment of the Theory," pp. 61–109 in *Proc. Workshop on Correlations of Neutron and Charged Particle Damage held at Oak Ridge National Laboratory, June 8–10, 1976*, CONF-760673.

R. A. McKee, "Thermomigration in Alloys for Which Substitutional-Vacancy and Interstitial-Vacancy Mechanisms are Operative," *Philos. Mag.* 35(3): 715–26 (March 1977).

R. A. McKee, "Solute and Solvent Diffusion for an Alloy in Dissociative Equilibrium" *Phys. Rev. B* 15(12): 5612–17 (June 1977).

J. P. Moore, R. S. Graves, M. B. Herskovitz, K. R. Carr, and R. A. Vandermeer, "Nicrosil II and Nisil Thermocouple Alloys: Physical Properties and Behavior During Thermal Cycling to 1200 K," pp. 259–66 in *Thermal Conductivity*, Vol. 14, Plenum, New York, 1976.

J. P. Moore, R. K. Williams, and R. S. Graves, "Thermal Conductivity, Electrical Resistivity, and Seebeck Coefficient of High-Purity Chromium from 280 to 1000 K," *J. Appl. Phys.* 48(2): 610–17 (February 1977).

J. P. Moore, R. S. Graves, and W. P. Eatherly, "Thermal Conductivity and Electrical Resistivity of Simulated Fuel Elements," pp. 396–97 in *13th Biann. Carbon Conf. Extended Abstracts and Program* (July 18–22, 1977, University of California), American Carbon Society.

N. H. Packan, J. O. Stiegler, and K. Farrell, "Correlation of Neutron and Nickel-Ion Damage in Pure Nickel," (Summary) *Trans. Am. Nucl. Soc.* 26(TANSAO 26): 190–91 (June 1977).

G. S. Painter, R. O. Jones, and P. J. Jennings, "Bonding Properties of Stepped Transition Metal Surfaces," pp. 136–49 in *The Electron Factor in Catalysis on Metals, Nat. Bur. Stand. Spec. Publ.* 475, L. H. Bennett, ed., U.S. National Bureau of Standards, Washington, D.C., 1977.

K. Petersen, N. Thrane, G. Trumpy, and R. W. Hendricks, "Position Annihilation Study of Voids in a Neutron Irradiated Aluminum Single Crystal," *Appl. Phys.* 10: 85–90 (1976).

U. Roy, A. DasGupta, and C. C. Koch, "Preparation and Superconducting Properties of Lithium Titanate," *IEEE Trans. Magnetics* MAG-13(1): 836–39 (January 1977).

U. Roy, R. K. Williams, W. E. Brundage, and F. J. Weaver, "Electrical Resistivities of Some Spinel Ferrites," *J. Am. Ceram. Soc.* 60(1–2): 88–9 (January–February 1977).

J. Schelten and D. M. Kroeger, "Distribution of Transport Currents in Type-II Superconductors Investigated by Neutron Small Angle Scattering, pp. 473–80 in *Proc. Conf. Neutron Scattering Vol. I*, CONF-760601-P1 (1976).

C. L. Snead, Jr., A. N. Goland, and F. W. Wiffen, "Tracing the Evolution of Bubbles in Helium-Injected Aluminum by Means of Positron Annihilation," *J. Nucl. Mater.* 64: 195–205 (1977).

C. J. Sparks, Jr., "Quantitative X-Ray Fluorescent Analysis Using Fundamental Parameters," pp. 19–52 in *Advances in X-Ray Analysis*, Vol. 19, R. W. Gould et al., eds., Kendall/Hunt Publishing Company, Dubuque, Iowa, 1976.

C. J. Sparks, Jr., S. Raman, H. L. Yakel, R. V. Gentry, and M. O. Krause, "Search with Synchrotron Radiation for Superheavy Elements in Giant-Halo Inclusions," *Phys. Rev. Lett.* 38(5): 205–8 (Jan. 31, 1977).

J. C. Twichell and R. W. Hendricks, "High Speed Memory Increment Hardware for MODCOMP II," *Proc. 2nd Annu. MUSE Meeting, Dec. 5–6, 1974, Fort Lauderdale, Florida*, Modular Computer Systems, Inc., 1650 West McNab Road, Fort Lauderdale, Florida 33309.

D. Y. Valentine, O. B. Cavin, and H. L. Yakel, "On the Crystal Structure of $LiTe_3$," *Acta Cryst.* B33: 1389–96 (1977).

R. A. Vandermeer and J. B. Bernal, "Deformation Zone Geometry and Texture Gradients in Cold-Rolled Niobium," pp. 183–203 in *Texture of Crystalline Solids*, Gordon and Breach, London, 1977.

C. L. White and D. F. Stein, "On the Upper Limit to Equilibrium Segregation at a Grain Boundary," *Scr. Metall.* 11: 613–16 (1977).

F. W. Wiffen, "The Microstructure and Swelling of Neutron Irradiated Tantalum," *J. Nucl. Mater.* 67: 119–30 (1977).

P. Williams, C. A. Evans, Jr., M. L. Grossbeck, and H. K. Birnbaum, "Ion Microprobe Analysis for Niobium Hydride in Hydrogen Embrittled Niobium," *Anal. Chem.* 48: 964 (1976).

W. G. Wolfer, "Segregation of Point Defects by Internal Stress Fields," pp. 812–19 in *Fundamental Aspects of Radiation Damage in Metals* (Proc. Int. Conf. Gatlinburg, Oct. 6–10, 1975) CONF-751006-P2, Vol. II.

W. G. Wolfer and M. Ashkin, "Diffusion of Vacancies and Interstitials to Edge Dislocations," *J. Appl. Phys.* 47(3): 791–800 (March 1976).

W. G. Wolfer and T. C. Reiley, *The Use of Pressurized Eccentric Tubes to Study the Effect of Hydrostatic Stress on Swelling*, ORNL/TM-5780 (May 1977).

W. G. Wolfer and L. K. Mansur, "The Mechanical Interaction of Point Defects with Spherical Surface Layers," *Phys. Status Solidi A* 37(1): 211–32 (September 1976).

M. H. Yoo, W. H. Butler, and L. K. Mansur, "Defect Annealing and Clustering in the Elastic Interaction Force Field," pp. 804–11 in *Fundamental Aspects of Radiation Damage in Metals* (Proc. Int. Conf. Gatlinburg, Oct. 6–10, 1975) CONF-751006-P2, Vol. II.

M. H. Yoo and L. K. Mansur, "Distributions of Point Defects in Bounded Media Under Irradiation," *J. Nucl. Mater.* 62: 282–92 (1976).

M. H. Yoo and W. H. Butler, "Steady-State Diffusion of Point Defects in the Interaction Force Field," *Phys. Status Solidi (b)* 77: 181–93 (1976).

M. H. Yoo, *Dislocation Loop Growth and Void Swelling in Bounded Media by Charged Particle Damage*, ORNL/TM-5789 (April 1977).

G. J. Yurek, J. V. Cathcart, and R. E. Pawel, "Microstructures of the Scales Formed on Zircaloy-4 in Steam at Elevated Temperatures," *Oxid. Met.* 10(4): 255–76 (1976).

C. S. Yust, V. J. Tennery, H. P. Krautwasser, and R. L. Beatty, "Structural Characterization of HTGR Pyrocarbon Fuel Particle Coatings," *J. Am. Ceram. Soc.* 69(5-6): 268–74 (1977).

Publications Pending

J. B. Bates and R. A. Perkins, "Infrared Spectral Properties of Hydrogen, Deuterium, and Tritium in TiO_2," submitted to *Physical Review*.

J. L. Bennett, C. B. Finch, H. L. Yakel, J. Brynestad, and G. W. Clark, "Crystal Growth of Monoclinic Eu_2O_3 from Molten NaF," submitted to the *Journal of Crystal Growth*.

B. S. Borie, "On the Observation of Forbidden Bragg Maxima for White Tin," submitted to *Physica Status Solidi*.

A. D. Brailsford and L. K. Mansur, "Effect of Self-Ion Injection in Simulated Studies of Void Swelling," to be published in *Journal of Nuclear Materials*.

W. H. Butler, "Momentum Dependence of the Electron-Phonon Interaction in Nb," cleared for *Journal of Physics* J or F.

R. W. Carpenter and G. S. Bauer, "Electron-Optical Investigations of Hydrogen-Induced Deformation in Nickel Single-Crystal Foils," submitted to *Acta Metallurgica*.

R. E. Clausing, L. C. Emerson, L. Heatherly, and R. J. Colchin, "Wall Conditioning Studies for ORMAK and ISX," to be published in the proceedings of the International Symposium on Plasma Wall Interaction, Jülich, West Germany, October 18–22, 1976.

W. A. Coghlan and M. H. Yoo, "Modeling the Growth of a Finite Interstitial Loop Under Irradiation," (Summary) to be published in the Transactions of the American Nuclear Society, Winter Meeting, 1977.

D. G. Doran, G. R. Odette, R. L. Simons, and L. K. Mansur, "Damage Correlation in Theory and Practice," to be published in the proceedings of the International Conference on Radiation Effects in Breeder Reactor Structural Materials, Scottsdale, Arizona, June 20–23, 1977.

J. S. Faulkner, "Scattering Theory and Cluster Calculations," submitted to *Journal of Physics (English)*.

J. S. Faulkner, "The Theory of Excitations in Disordered Solids," submitted to *International Journal of Quantum Chemistry*.

C. B. Finch, G. W. Clark, and M. M. Abraham, "Crystal Growth of Calcium Oxide from the Molten Solvent LiF–20 mole % CaF_2," accepted for publication in *Journal of Crystal Growth*.

C. B. Finch, R. L. Fellows, and J. P. Young, "Self-Luminescence of Several Fluorite-Structure Halides Doped with Curium or Berkelium," submitted to *Journal of Luminescence*.

T. A. Gabriel, B. L. Bishop, and F. W. Wiffen, "Calculated Irradiation Performance of Materials Using a Fusion Reactor First-Wall Neutron Spectrum," submitted to *Nuclear Technology*.

E. S. Giuliano, R. Ruggeri, B. L. Gyorffy, and G. M. Stocks, "Is the Rigid Band Model Valid for Mo_cNb_{1-c} Alloys?" to be published in *Journal of Physics F*.

B. Gordon, W. Temmerman, B. L. Gyorffy, and G. M. Stocks, "Fermi Surface of Concentrated Paramagnetic Cu_cNi_{1-c} Alloys," to be published in *Journal of Physics F*.

B. L. Gyorffy, G. M. Stocks, W. M. Temmerman, R. Jordan, D. R. Lloyd, C. M. Quinn, and N. V. Richardson, "Angle Resolved Photoemissions from a 001 Surface of Single Crystal $Ni_{23}Cu_{77}$ Random Substitutional Alloy," submitted to *Physical Review*.

L. A. Harris, D. N. Braski, and C. S. Yust, "A Study of Factors Affecting Elemental Analyses by STEM," to be published in Proceedings of 6th International Materials Symposium, University of California, August 24–27, 1976, *Ceramic Microstructures '76*.

L. A. Harris, D. N. Braski, and C. S. Yust, "Electron Microscopy of Coal Constituents," to be published in Proceedings of International Metallographic Society, Seattle, Washington, July 1976, *Microstructural Science 5*.

L. A. Harris, C. S. Yust, and R. S. Crouse, "Direct Determination of Pyritic and Organic Sulfur by Combined Coal Petrography and Microprobe Analysis (CPMA) – A Feasibility Study," accepted for publication in *Fuel*.

L. A. Harris, "The Use of Reflectivity Standards in an Image Analysis System," to be published in Proceedings of International Metallographic Society, Seattle, Washington, July 1976, *Microstructural Science 5*.

R. W. Hendricks, The ORNL 10-Meter Small-Angle X-Ray Scattering Camera," to be published in *Journal of Applied Crystallography*.

R. W. Hendricks, J. Schelten, and G. Lippman, "Studies of Voids in Neutron-Irradiation Aluminum Single Crystals. III. Determination of Void Surface Properties," to be published in *Philosophical Magazine*.

R. W. Hendricks and L. B. Shaffer, "Final Report of the International Project for the Calibration of Absolute Intensities in Small-Angle X-Ray Scattering," to be published in *Journal of Applied Crystallography*.

J. D. Holder, R. A. Hartzell, and G. W. Clark, "$LaCrO_3$ and $YCrO_3$ Eutectics with W, Mo, and Cr," submitted to *Journal of the American Ceramic Society*.

E. A. Kenik, "Simulation of Radiation Damage and Stability in Type 316 Stainless Steel," to be published in the *Transactions of the American Nuclear Society*, Winter Meeting 1977.

C. C. Koch and D. S. Easton, "Mechanical Behavior and Stress Effects in Superconductors — A Review," to be published in the proceedings of the Fall AIME Meeting, Niagara Falls, New York, September 20–23, 1976.

T. G. Kollie, "Measurement of the Thermal Expansion Coefficient of Nickel from 300 to 1000 K and Determination of the Power Law Constants Near the Curie Temperature," submitted to *Physical Review B*.

H. P. Krautwasser, R. L. Beatty, V. J. Tennery, and C. S. Yust, "Comparison of Pyrolytic Carbon Microstructures Derived from MAPP-Gas and Propylene," to be published in the proceedings of 6th International Materials Symposium, University of California, August 24–27, 1976, *Ceramics Microstructures '76*.

J. M. Leitnaker, G. A. Potter, D. J. Bradley, . . C. Franklin, and W. R. Laing, "The Composition of Eta Carbide in Hastelloy N After Aging 10,000 hr at 815°C," submitted to *Metallurgical Transactions*.

J. M. Leitnaker and J. Bentley, "Precipitate Phases in Type 321 Stainless Steel After 17 Years at ~600°C," submitted to *Metallurgical Transactions*.

V. W. Lindberg, J. D. McGervey, R. W. Hendricks, and W. Triftshäuser, "Annealing Studies of Voids in Neutron Irradiated Aluminum Single Crystals by Positron Annihilation," to be published in *Philosophical Magazine*.

K. G. Lynn, C. L. Snead, Jr., A. L. Goland, Robert Grynszpan, and F. W. Wiffen, "Positron-Annihilation Investigation of High-Temperature Neutron-Irradiated Molybdenum," submitted to *Physics Letters*.

L. K. Mansur and W. G. Wolfer, "Influence of a Surface Coating on Void Formation," to be published in the proceedings of the International Conference on Properties of Atomic Defects in Metals," Argonne National Laboratory, October 18–22, 1976.

L. K. Mansur, M. H. Yoo, and W. A. Coghlan, "The Effect of Impurities on Void Nucleation and Growth," to be published in the *Transactions of the American Nuclear Society*, Winter Meeting 1977.

J. D. McGervey, V. W. Lindberg, and R. W. Hendricks, "Positron Lifetimes in Voids and Other Defects in Annealed, Neutron-Irradiated Aluminum," to be published in *Journal of Nuclear Materials*.

R. A. McKee, "The Concentration Dependence of Solute Diffusion for an Alloy in Dissociative Equilibrium," submitted to *Philosophical Magazine*.

C. J. McHargue and J. L. Scott, "Materials Requirements for Fusion Reactors," submitted to *Metallurgical Transactions*.

G. S. Painter, "Bonding of Oxygen on Aluminum: Relation Between Energy Band and Cluster Models," submitted to *Physical Review*.

R. E. Pawel, R. A. Perkins, R. A. McKee, J. V. Cathcart, G. J. Yurek, and R. E. Druschel, "The Diffusion of Oxygen in Beta-Zircaloy and the High Temperature Zircaloy-Steam Reaction," to be published in *Zirconium in the Nuclear Industry, Special Technical Publication 633*, American Society for Testing and Materials.

R. A. Perkins, "The Diffusion of Oxygen in Oxygen Stabilized Alpha-Zirconium and Alpha-Zircaloy-4," submitted to *Journal of Nuclear Materials*.

R. A. Perkins, "Oxygen Diffusion in Beta-Zircaloy," to be published in *Journal of Nuclear Materials*.

R. A. Perkins and R. A. Padgett, Jr., "Oxygen Diffusion in Niobium and Niobium-Zirconium Alloys," submitted to *Acta Metallurgica*.

T. C. Reiley and P. G. Jung, "The Simulation of Irradiation Creep," to be published in the proceedings of the International Conference on Radiation Effects in Breeder Reactor Structural Materials, Scottsdale, Arizona, June 19–23, 1977.

A. F. Rowcliffe, "Alloy," to be published in *Encyclopedia of Science and Technology*, McGraw Hill, New York.

G. M. Stocks, B. L. Gyorffy, E. S. Giuliano, and R. Ruggeri, "The Coherent Potential Approximation for Nonoverlapping Muffin-Tin Potentials: Paramagnetic Ni_xCu_{1-x}," to be published in *Journal of Physics F*, Vol. 7 (1977).

C. L. White and W. A. Coghlan, "The Spectrum of Binding Energies Approach to Grain Boundary Segregation," to be published in *Metallurgical Transactions*.

C. L. White and D. F. Stein, "Sulfur Segregation to Grain Boundaries in Ni_3Al and $Ni_3(Al,Ti)$ Alloys," submitted to *Metallurgical Transactions*.

C. L. White and D. F. Stein, "On the Upper Limit to Equilibrium Segregation at a Grain Boundary," accepted for publication in *Scripta Metallurgica*.

W. G. Wolfer, L. K. Mansur, and J. A. Sprague, "Theory of Swelling and Irradiation Creep," to be published in the proceedings of the International Conference on Radiation Effects in Breeder Reactor Structural Materials, Scottsdale, Arizona, June 19–23, 1977.

M. H. Yoo and L. K. Mansur, "General Rate Theory Model of Void Swelling in Irradiated Metals," to be published in the *Transactions of the American Nuclear Society*, Winter Meeting 1977.

M. H. Yoo and J. O. Stiegler, "Growth Kinetics and Preference Factor of Frank Loops in Nickel During Electron Irradiation," submitted to *Philosophical Magazine*.

M. H. Yoo, "Dislocation Loop Growth and Void Swelling in Bounded Media by Charged Particle Damage," submitted to *Journal of Nuclear Materials*.

M. H. Yoo and J. O. Stiegler, "Point Defect Interactions and Growth of Dislocation Loops," submitted to *Journal of Nuclear Materials*.

C. S. Yust and V. J. Tennery, "Optical and Electron Microscopy of Vapor Deposited Silicon Carbide Coatings of HTGR Fuel Particles, submitted to *Journal of the American Ceramic Society*.

Patent

E. E. Bloom, J. M. Leitnaker, J. O. Stiegler, and A. F. Rowcliffe, *Austenitic Stainless Steel Alloys Having Improved Resistance to Fast Neutron-Induced Swelling* (to U.S. Energy Research and Administration and Development) U.S. Patent 4,011,133. March 8, 1977.

Thesis

Michael Gary Duncan, "Precision Rectifier Detectors for AC Resistance Bridge Measurements with Application to Temperature Control Systems for Irradiation Creep Experiments," Ph.D. Thesis, the University of Tennessee. Published as ORNL/TM-5715 (May 1977).